Fermi National Accelerator Laboratory

FERMILAB-PUB-93/004-T

BNL-48631

January 1993

RARE AND RADIATIVE KAON DECAYS*

L. Littenberg[a] and G. Valencia[b]

[a] *Physics Department*

Brookhaven National Laboratory

Upton, NY 11973

[b] *Theoretical Physics*

Fermi National Accelerator Laboratory

Batavia, IL 60510

Abstract

We review the status of theory and experiment of very rare and forbidden kaon decays. We then review the radiative non-leptonic decays, and the associated Dalitz pair modes. We pay particular attention to the study of long distance physics in radiative decays within the framework of chiral perturbation theory (χPT). We discuss the experiments that will run in the near future and the modes that they will be able to study.

---

*To appear in Annual Review of Nuclear and Particle Science, Volume 43.

Contents

1 Introduction

Rare kaon decays offer the possibility of probing high energy scales by doing precise low energy measurements. In this case, the precision is obtained by looking at very rare decays. The advantage of the kaon system is, of course, the long lifetime of both the K_L and the $K^{\pm}$. In this paper we review the status of theory and experiment of rare, forbidden and radiative kaon decays. Other recent reviews include Refs. [1, 2, 3, 4, 5, 6, 7, 8, 9].

We concentrate in three distinct classes of decays. We first discuss a set of modes that does not occur in the standard model. Studies of these modes constitute searches for new physics, and in some cases these rare kaon decays are the most sensitive probes for certain kinds of new interactions.

We then study those modes that occur in the standard model mostly through short distance physics, and that are thus amenable to a conventional perturbative treatment. These modes occur at the one-loop level, via penguin and box diagrams as discussed in section 4. The calculation of these transitions is by now standard[10, 11], and they are dominated by the top-quark intermediate state. The contribution of the charm-quark, as well as perturbative QCD corrections, are also known. The theoretical aspects of these calculations have been recently reviewed in the literature by Buras and Harlander, Ref. [9].

The interest of these modes lies in the possibility of measuring some of the parameters in the standard model. The rates are sensitive to the values of the top quark mass and of the CKM mixing angles. For our discussion, we will assume a unitary 3×3 CKM matrix as parameterized by Wolfenstein [12]. The advantage of this approximate parameterization is that it exhibits the hierarchical structure of the

CKM matrix. It yields expressions that show what is the mixing angle suppression of a transition. This form of the CKM matrix is:

$$V = \begin{pmatrix} 1-\lambda^2/2 & \lambda & A\lambda^3(\rho - i\eta) \\ -\lambda & 1-\lambda^2/2 & A\lambda^2 \\ A\lambda^3(1-\rho-i\eta) & -A\lambda^2 & 1 \end{pmatrix} \tag{1.1}$$

The present knowledge of the mixing angles in the CKM matrix. Eq. 1.1, is summarized in Ref. [8, 9]:

$$\lambda = 0.22 \tag{1.2}$$

$$A = 0.9 \pm 0.1 \tag{1.3}$$

$$\sqrt{\rho^2+\eta^2} = \begin{cases} 0.4 \pm 0.2 & [8] \\ 0.59 \pm 0.18 & [9] \end{cases} \tag{1.4}$$

Eq. 1.2 is known from K_{l3} and hyperon decays [13], while Eq. 1.3 is now usually extracted from analyses of $B \to D(D^*)e\nu$ decays [14]. Eq. 1.4 is obtained by fitting the observed lepton energy spectrum from B semileptonic decay as a sum of $b \to c$ and $b \to u$ contributions [15]. The two different numbers result from the new CLEO value for V_{ub} and the from the old CLEO and ARGUS result. To obtain separate determinations of ρ and η, additional input is necessary. However, the other currently available sources of information, such as $\overline{B} - B$ mixing, ϵ and ϵ'/ϵ are afflicted both by dependence on the top-quark mass and calculational difficulties. Since we expect a direct measurement of the top-quark mass from collider experiments before too long, the latter problem is perhaps more severe. Here rare kaon decays have the potential to contribute substantially. The measurement of the decay rates of processes such as $K^+ \to \pi^+\nu\overline{\nu}$ and $K_L \to \pi^0\nu\overline{\nu}$ can provide constraints on ρ and η with very little theoretical uncertainty, once the top quark mass is measured. Other measurements such as that of the parity-violating μ^+ decay asymmetry in $K^+ \to \pi^+\mu^+\mu^-$ can

provide complementary information, given only modest theoretical input. The first measurements of ρ and η will complete our knowledge of the CKM matrix. Subsequent determinations of any of the parameters will permit us to test the three generation structure of the standard model.

Finally we discuss radiative decays that are expected to be dominated by long distance physics. In this case we do not have predictions directly from the standard model because we do not know how to handle the non-perturbative aspects of the strong interactions. Although we expect that this problem will be solved at some point by lattice calculations, at present, the only systematic framework we have to study these modes is chiral perturbation theory. Within χPT, we parameterize our ignorance of strong interaction dynamics in terms of a few unknown coupling constants. These constants are then measured in some processes, and after that, they can be used to predict additional decay modes. We review the basics of this approach in the following section.

2 Chiral perturbation theory

A conventional calculation of non-leptonic kaon decays in the standard model leads to the evaluation of matrix elements of four-quark operators between meson states. This is a non-perturbative problem that remains unsolved. In χPT one replaces the standard model with an effective low energy field theory written directly in terms of meson fields. Effective field theories contain an infinite number of operators and are, therefore, not very useful unless one has a way to organize the operators and to identify the most important ones. χPT organizes the operators in the low energy effective Lagrangian in terms of the number of derivatives (and external fields) that occur. This corresponds to an expansion of amplitudes in powers of the momentum (or energy) of the external particles. The energy scale for this expansion is set by the scale of chiral symmetry breaking, Λ_{CSB}, empirically about 1 GeV [16, 17, 18, 19].

The effective Lagrangian is constructed on the basis of chiral symmetry, an approximate symmetry of the QCD Lagrangian. In the limit of massless u, d and s quarks QCD has a global $SU(3)_L \times SU(3)_R$ chiral symmetry that is broken spontaneously to $SU(3)_V$. The chiral Lagrangian is a compact way to keep track of the $SU(3)_V$ relations between amplitudes, as well as of the relations between amplitudes with different numbers of pions that follow from the spontaneously broken global symmetry (the soft pion theorems).

Apart from including all possible operators that are chirally invariant (organized in terms of number of derivatives), χPT incorporates deviations from chiral symmetry due to the small quark masses. This leads to other operators that are organized as an expansion in powers of meson masses (and number of derivatives).

Since the typical momentum of particles in a kaon decay is roughly the kaon mass,

we can give a very rough estimate for the size of the corrections that one can expect in a χPT calculation: they will be of order $m_K^2/1\ \mathrm{GeV}^2 \sim 25\%$ of the highest order kept in the calculation.

The framework of χPT has proved extremely useful for analyzing low energy processes involving the pseudoscalar meson octet and photons. At low energies, the strong and electromagnetic interactions of these particles can be adequately described with a chiral Lagrangian with up to four derivatives. The most general chiral Lagrangian to this order has been written down by Gasser and Leutwyler [17]. It consists of two terms at leading order, $\mathcal{O}(p^2)$:

$$\mathcal{L}_S^{(2)} = \frac{f_\pi^2}{4}\mathrm{Tr}\Big(D_\mu U D^\mu U^\dagger\Big) + B_0\frac{f_\pi^2}{2}\mathrm{Tr}\Big(MU + U^\dagger M\Big). \tag{2.1}$$

M is the diagonal matrix (m_u, m_d, m_s), and the meson fields are contained in the matrix $U = \exp(2i\phi/f_\pi)$ with:

$$\phi \;=\; \frac{1}{\sqrt{2}}\begin{pmatrix} \pi^0/\sqrt{2}+\eta/\sqrt{6} & \pi^+ & K^+ \\ \pi^- & -\pi^0/\sqrt{2}+\eta/\sqrt{6} & K^0 \\ K^- & \overline{K^0} & 2\eta/\sqrt{6} \end{pmatrix} \tag{2.2}$$

U transforms under the chiral group as $U \to RUL^\dagger$. We will restrict ourselves to the case where photons are the only external fields. In this case the covariant derivative is given by (we will not discuss radiative semileptonic decays [20]):

$$D_\mu U = \partial_\mu U - ieA_\mu[Q, U]. \tag{2.3}$$

and Q is the diagonal matrix $(-2/3, 1/3, 1/3)$. The two constants that appear at this order are the pion decay constant [21],

$$f_\pi = (92.4 \pm 0.2)\ \mathrm{MeV} \tag{2.4}$$

and the ratio between meson masses and current quark masses B_0. Ignoring isospin breaking, $m_u = m_d = m$, B_0 is given by:

$$B_0 = \frac{m_\pi^2}{2m} = \frac{m_K^2}{m + m_s} = \frac{3m_\eta^2}{2m + 4m_s} \tag{2.5}$$

At this order, the Gell-Mann-Okubo relation follows:

$$3m_\eta^2 + m_\pi^2 = 4m_K^2 \tag{2.6}$$

At next to leading order, $\mathcal{O}(p^4)$, there are ten more operators [17] without epsilon tensors. For the processes of interest we will only need two out of these ten terms. When photons are the only external fields they read:

$$\mathcal{L}_S^{(4)} = -ieL_9 F_{\mu\nu}\mathrm{Tr}Q\Big(D^\mu U^\dagger D^\nu U + D^\mu U D^\nu U^\dagger\Big) + eL_{10}F^{\mu\nu}F_{\mu\nu}\mathrm{Tr}\Big(UQU^\dagger Q\Big) \tag{2.7}$$

and $F_{\mu\nu}$ is the usual electromagnetic field strength tensor. At this same order there are also terms that contain epsilon tensors. These have the same origin as the triangle anomaly responsible for $\pi^0 \to \gamma\gamma$, and do not involve any unknown coefficients. They are contained in the Wess-Zumino-Witten anomalous action [22], and the terms of interest to us are:

$$\begin{aligned}\mathcal{L}_{WZW}^{(4)} &= \frac{\alpha}{8\pi f_\pi}\epsilon_{\mu\nu\rho\sigma}F^{\mu\nu}F^{\rho\sigma}\left(\pi^0 + \frac{\eta}{\sqrt{3}}\right) \\ &- \frac{ie}{4\pi^2 f_\pi^3}\epsilon_{\mu\nu\rho\sigma}A^\mu\partial^\nu\pi^+\partial^\rho\pi^-\partial^\sigma\left(\pi^0 + \frac{\eta}{\sqrt{3}}\right)\end{aligned} \tag{2.8}$$

A complete calculation to $\mathcal{O}(p^4)$ consists of tree-level diagrams with vertices from Eqs. 2.1, 2.7, and 2.8, and of one-loop diagrams using only Eq. 2.1. The divergences that appear in the loop calculation are absorbed by renormalization of the couplings in Eq. 2.7. The renormalized couplings that we will use are defined by regularizing in $n = 4 - \epsilon$ dimensions. In terms of $\lambda_0 \equiv (2/\epsilon + \ln 4\pi + 1 - \gamma - \ln\mu^2)/32\pi^2$, they are

[17]: $L^r_{9,10}(\mu) = L_{9,10} \pm \lambda_0/4$. These, and the other eight coupling constants have been fixed from experiment [17]. This completes the framework needed to discuss strong and electromagnetic processes involving the pseudoscalar meson octet and photons.

To study kaon decays we need, in addition, an effective Lagrangian for the weak interactions. In the standard model, the dominant $|\Delta S| = 1$ operators in the effective weak Hamiltonian transform as $(8_L, 1_R)$ or $(27_L, 1_R)$ under chiral rotations. We can write a chiral representation for operators with these transformation properties, and once again organize them in terms of the number of derivatives. The lowest order Lagrangian constructed in this way contains two derivatives [23]:

$$\begin{aligned} \mathcal{L}_W^{(2)} &= \frac{G_F}{\sqrt{2}} |V_{ud} V_{us}^*| \Big[g_8 \mathrm{Tr}\Big(\lambda_6 L_\mu L^\mu\Big) + g_{27}^{|\Delta I|=\frac{1}{2}} \Big(L_{\mu 13} L_{21}^\mu + L_{\mu 23}(4 L_{11}^\mu + 5 L_{22}^\mu)\Big) \\ &+ g_{27}^{|\Delta I|=\frac{3}{2}} \Big(L_{\mu 13} L_{21}^\mu + L_{\mu 23}(L_{11}^\mu - L_{22}^\mu)\Big)\Big] \end{aligned} \tag{2.9}$$

where $L_\mu = i f_\pi^2 U D_\mu U^\dagger$. We can use this Lagrangian to compute $K \to \pi\pi$ decays, and fit the unknown constants from experiment [23, 24, 25]. The result is well known, the amplitudes with $|\Delta I| = 3/2$ are much smaller than those with $|\Delta I| = 1/2$. In terms of the couplings of Eq. 2.9 the result is:

$$\frac{|g_8 + g_{27}^{|\Delta I|=\frac{1}{2}}|}{|g_{27}^{|\Delta I|=\frac{3}{2}}|} \approx \frac{5.1}{0.16} \approx 32. \tag{2.10}$$

From now on, we will use $|g_8| \approx 5.1$ and drop the terms that transform as $(27_L, 1_R)$. We will also use the notation:

$$G_8 \equiv \frac{G_F}{\sqrt{2}} |V_{ud} V_{us}^*| g_8 \approx 9.1 \times 10^{-6}\ \mathrm{GeV}^{-2}. \tag{2.11}$$

The situation at next to leading order is much more complicated: a very large number of operators, and therefore of unknown coupling constants, has been identified

[26]. However, for the radiative decays that we will consider, only a few of those operators play a role under the following assumptions [27]:

1. Octet dominance. We will not include $|\Delta I| = 3/2$ operators.

2. CPS symmetry. The effective weak Hamiltonian in the standard model is invariant under a CP transformation followed by the interchange of $d \leftrightarrow s$. This same symmetry is imposed on the effective Lagrangian.

3. Photons are the only external fields, so that $F^L_{\mu\nu} = F^R_{\mu\nu} = eQF_{\mu\nu}$.

4. For the normal (odd) intrinsic parity terms (those without (with) an epsilon tensor), we will be interested only in terms with at most two (three) meson fields.

The next to leading order weak Lagrangian then reads [27, 28]:

$$\begin{aligned}\mathcal{L}_W^{(4)} &= -ie\frac{G_8}{f_\pi^2}F^{\mu\nu}\Big[w_1\mathrm{Tr}\Big(Q\lambda_6 L_\mu L_\nu\Big) \\ &+ w_2\mathrm{Tr}\Big(QL_\mu\lambda_6 L_\nu\Big) + ief_\pi^4 w_4 F_{\mu\nu}\mathrm{Tr}\Big(\lambda_6 QUQU^\dagger\Big)\Big] \qquad (2.12)\end{aligned}$$

for the normal intrinsic parity sector, and [29, 30]:

$$\begin{aligned}\mathcal{L}_W^{(4)} &= ie\frac{G_8}{f_\pi^2}\epsilon^{\rho\sigma\mu\nu}F_{\rho\sigma}\Big[a_1\mathrm{Tr}\Big(QL_\mu\Big)\mathrm{Tr}\Big(\lambda_6 L_\nu\Big) \\ &+ a_2\mathrm{Tr}\Big(UQU^\dagger L_\mu\Big)\mathrm{Tr}\Big(\lambda_6 L_\nu\Big) + a_3\mathrm{Tr}\Big(\lambda_6[UQU^\dagger, L_\mu L_\nu]\Big)\Big] \qquad (2.13)\end{aligned}$$

for the odd intrinsic parity sector.

As in the case of the strong interaction Lagrangian, a calculation to $\mathcal{O}(p^4)$ involves tree and one-loop graphs with Eq. 2.9, and tree graphs with Eqs. 2.12, 2.13. The loop graphs are again divergent, and the divergences are absorbed by renormalization of the couplings in Eq. 2.12 [27]: $w^r_{1,2}(\mu) = w_{1,2} \mp \lambda_0$, $w^r_4(\mu) = w_4 - \frac{1}{2}\lambda_0$. After using a few

experimental results as input to fit the unknown coefficients, we can proceed to make predictions for other processes. A detailed fit of these constants from experiment is in itself interesting, as it provides a compact parameterization of low energy data that can be used to compare with first principles calculations when these become available. In the meantime, they also provide a framework for systematic tests of different models.

There have been some attempts to derive the effective Lagrangian. The case of Eq. 2.9 has been studied in detail using a $1/N_c$ analysis of the strong interactions [31], and a quark model [32]. There has also been considerable activity using resonance saturation models [33] and quark models [34] to estimate the $\mathcal{O}(p^4)$ coupling constants. We summarize our knowledge of the couplings in the strong interaction sector in Table 1 [35].

Table 1: Values of $L_{9,10}$.

	$L_9^r(\mu = m_\rho)$	$L_{10}^r(\mu = m_\rho)$
Experiment	$(6.9 \pm 0.2) \times 10^{-3}$	$(-5.2 \pm 0.3) \times 10^{-3}$
Vector Dominance	7.3×10^{-3}	-5.8×10^{-3}
Quark Models	6.3×10^{-3}	-3.2×10^{-3}

The vector dominance model is a tree-level resonance saturation model. It produces scale independent couplings, and the resonance saturation assumption is implemented by identifying them with the running couplings at a scale equal to the resonance mass. There are many variations of the quark model results, but they all start from considering a free quark loop. These models are inspired by the $1/N_c$ expansion, but they are not complete calculations to leading order in $1/N_c$. They also result in couplings that are scale independent. We will identify them with the running couplings at a scale equal to twice the constituent quark mass, roughly the

rho mass (the scale dependence is non-leading in $1/N_c$ so we are free to choose any scale). Attempts to incorporate gluonic corrections seem to improve the agreement with experiment, although precise quantitative predictions are not available [34].

For the weak interaction parameters there are also several models. Among them the weak deformation model [36], and quark models [37, 38]. We summarize these results in Table 2.

Table 2: Model calculations of w_i

	w_1	w_2	w_4
weak deformation model [36]	0.007	0.028	−0.021
factorization [37]	0.025	0.025	0.0
quark model [38]	−0.003	0.013	−0.005

Similarly, the large-N_c factorizable contributions to the constants in Eq. 2.13 are [29, 30]:

$$a_1 = \frac{1}{4\pi^2},\ a_2 = \frac{1}{8\pi^2},\ a_3 = \frac{1}{16\pi^2}. \tag{2.14}$$

For some of the modes that we will discuss, we will need the matrix elements of currents; in analogy with the semileptonic decays. For these we will use the following form of the currents in terms of mesons:

$$\begin{aligned} \bar{s}\gamma_\mu u &\rightarrow -i\left[\left(\pi^+\partial_\mu K^0 - K^0\partial_\mu\pi^+\right) + \frac{1}{\sqrt{2}}\left(\pi^0\partial_\mu K^+ - K^+\partial_\mu\pi^0\right)\right] \\ \bar{s}\gamma_\mu\gamma_5 u &\rightarrow -\sqrt{2}f_\pi\partial_\mu K^+ \end{aligned} \tag{2.15}$$

for the charged current, and

$$\begin{aligned} \bar{s}\gamma_\mu d &\rightarrow -i\left[\left(\pi^-\partial_\mu K^+ - K^+\partial_\mu\pi^-\right) + \frac{1}{\sqrt{2}}\left(K^0\partial_\mu\pi^0 - \pi^0\partial_\mu K^0\right)\right] \\ \bar{s}\gamma_\mu\gamma_5 d &\rightarrow -\sqrt{2}f_\pi\partial_\mu K^0 \end{aligned} \tag{2.16}$$

for the neutral current. These results follow from Eq. 2.1 [18], and are valid to lowest order in χPT. We have only kept terms with up to two mesons. From Eq. 2.16 we can also find expressions for the scalar and pseudoscalar densities:

$$\begin{aligned} \bar{s}d &\rightarrow iB_0\left(\pi^- K^+ + \frac{1}{\sqrt{2}} K^0 \pi^0\right) \\ \bar{s}\gamma_5 d &\rightarrow \sqrt{2} f_\pi B_0 K^0 \end{aligned} \tag{2.17}$$

B_0 is the same as that in Eq. 2.5. Although B_0 is not a physical quantity, we will simply use $B_0/m_\mu \approx 15$. We have divided by the muon mass for convenience. This number reflects that matrix elements of scalar operators are somewhat enhanced.

3 Lepton family number violating decays

In the minimal standard model with massless neutrinos, the lepton family number is absolutely conserved so these decays do not occur. The observation of $K_L \to \mu^{\pm} e^{\mp}$ or $K \to \pi\mu e$ decays would therefore be a clear indication of new physics.

A model independent study of this type of processes can be done following the approach of Buchmüller and Wyler, Ref. [39]. The physics beyond the standard model is parameterized by an effective Lagrangian that is gauge invariant under $SU(3)_c \times SU(2)_L \times U(1)_Y$. The leading effective Lagrangian, relevant for our discussion, is given by the sum of four fermion operators of the form:

$$\begin{aligned} \mathcal{O}_{V-A} &= C_{V-A}\frac{g_n^2}{\Lambda^2}\overline{\mu}\gamma_\mu\frac{(1+\gamma_5)}{2}e\overline{s}\gamma^\mu\frac{(1+\gamma_5)}{2}d \\ \mathcal{O}_{S\pm P} &= C_{S\pm P}\frac{g_n^2}{\Lambda^2}\overline{\mu}\frac{(1-\gamma_5)}{2}e\overline{s}\frac{(1+\gamma_5)}{2}d \end{aligned} \tag{3.1}$$

We have included a (weak) gauge coupling g_n^2 to reflect the fact that we think of these operators as originating in the exchange of a heavy gauge boson (or perhaps a scalar) in the new physics sector. We will take $g_n = g_2$ for simplicity and absorb any difference, as well as any mixing angles or other factors into the coefficient C_i. The factors of 2 have been included for later convenience. In the absence of any dynamical information to the contrary, it is natural to assume that C_i is of order $\mathcal{O}(1)$. Λ is the scale that characterizes the heavy degrees of freedom, typically the mass of the exchanged boson. It is then conventional to take $C_i = 1$ and interpret the bounds on the decays induced by these operators as bounds on the "scale of new physics" Λ. We have not listed all possible Dirac structures in Eq. 3.1, but just two illustrative ones. The operators could be purely vector or axial-vector operators, for example. Tensor operators, however, can be reduced to the others by Fierz rearrangements [39].

We compare the rates induced by these operators with Standard Model rates using the S.M. effective four-fermion operator for semileptonic decays:

$$\mathcal{L} = \frac{g_2^2}{2m_W^2} V_{us} \bar{\nu} \gamma_\mu \frac{(1+\gamma_5)}{2} \mu \bar{s} \gamma_\mu \frac{(1+\gamma_5)}{2} u \tag{3.2}$$

and using Eqs. 2.15, 2.16, 2.17.

Models that violate lepton flavor number will also induce processes like $\mu \to e\gamma$, $\mu^\pm \to e^\pm e^+ e^-$, $\mu \to e$ conversion in the field of a heavy nucleus, and $\Delta M(K_L - K_S)$ among others. For the latter one finds, $\Delta M = f_K^2 m_K / 3\Lambda^2$ [39]. The experimental value $\Delta M(K_L - K_S) = (3.522 \pm 0.016) \times 10^{-12}$ MeV [40], places a bound $\Lambda > 830$ TeV for $(V-A) \otimes (V-A)$ operators. This bound will be better than the one obtained from $K_L \to \mu^\pm e^\mp$ until this process reaches a sensitivity around 10^{-15}. However, this comparison of different processes assumes that all the coefficients C_i in the effective Lagrangian are of the same order. Although this is a natural assumption, it may not be true for given coefficients in specific models. Therefore, it is important to study all the different processes, since at some level they provide complementary information.

3.1 $K_L \to \mu^\pm e^\mp$

It is standard to compare this mode to the rate for $K^+ \to \mu^+ \nu$, since in the limit of vanishing electron mass it has the same kinematics. Given the pseudoscalar nature of the kaon, only the axial vector quark current or pseudoscalar density can contribute, as can be seen from Eqs. 2.16, 2.17. One finds:

$$\frac{\Gamma(K_L \to \mu^+ e^-)}{\Gamma(K^+ \to \mu^+ \nu)} = 2 \frac{C_{V-A}^2}{|V_{us}|^2} \left(\frac{g_n}{g_2}\right)^4 \left(\frac{m_W}{\Lambda}\right)^4 \tag{3.3}$$

for $V-A$ operators, and

$$\frac{\Gamma(K_L \to \mu^+ e^-)}{\Gamma(K^+ \to \mu^+ \nu)} = 2\frac{C_{S\pm P}^2}{|V_{us}|^2}\left(\frac{g_n}{g_2}\right)^4\left(\frac{m_W}{\Lambda}\right)^4\left(\frac{B_0}{m_\mu}\right)^2 \tag{3.4}$$

for scalar, pseudoscalar operators.

Fig. 1 a and b show the recent results in the search for $K_L \to \mu e$. The lack of a signal in the region corresponding to $M(\mu e) \sim M_K$ with aligned initial and final states allows 90% *c.l.* upper limits to be set. These are $B(K_L \to \mu^\pm e^\mp) < 9.4 \times 10^{-11}$ for KEK-137 [41] and $B(K_L \to \mu^\pm e^\mp) < 3.3 \times 10^{-11}$ for AGS-791 [42]. For purely left handed operators, the latter experimental limit places the bound $\Lambda > 108$ TeV. For scalar operators as in Eq. 3.1, we find from Eq. 3.4 $\Lambda > 420$ TeV. These results can be interpreted as bounds on the mass of new particles in different models. For example, we identify $\Lambda \to \sqrt{2}m_H$; the mass of a $\Delta G = 0$ horizontal gauge boson as discussed in Ref. [43], to obtain $m_H > 77$ TeV. The bound on the family replication model of Ref. [44] is placed by the scalar operators. Using Eq. 3.4 and $g_n^2/\Lambda^2 \to 4\sqrt{2}g_{hc}^2 \sin^4\alpha/\Lambda_0^2$ we find $\Lambda_0 > 10^5$ TeV when we use the parameters $\sin\alpha = 0.04$ and $g_{hc} = 1$. Similarly, we can use Eq. 3.4 to compare with the scalar leptoquark operators of Ref. [45] to obtain $m_H > 15$ TeV, and $m_P > 2.8$ TeV for pseudoscalar leptoquarks. In this case the bounds on the particle mass are not as strong as implied by Eq. 3.4 because the couplings $C_{S\pm P}$ in these models are suppressed by small mass ratios m_f/m_W.

One can also use the form of the new operators Eq. 3.1 to compare the reach of the rare kaon decay experiments with that of rare B decays. For example, taking a purely $(V-A)\otimes(V-A)$ operator one finds [7]:

$$\frac{B(B^0 \to \mu^\pm e^\mp)}{B(K_L \to \mu^\pm e^\mp)} = \left(\frac{C_{V-A}^B}{C_{V-A}^K}\right)^2 \frac{m_B}{m_K}\frac{\tau_B}{\tau_{K_L}} \approx 3 \times 10^{-4} \tag{3.5}$$

In the last step we have assumed that the B and K coupling constants are of the same order. This indicates that rare kaon decays are more likely to be sensitive to this kind of new physics than rare B decays. Of course, the situation may be different for other operators.

These decays are also allowed in minimal extensions of the Standard Model in which the neutrinos are given a mass. The decays then proceed via box diagrams as in Fig. 2. The decay rate for $K_L \to \mu^\pm e^\mp$ is proportional to the product of mixing angles between the μ, e and the heavy neutral lepton N: $|U_{Ne}U^*_{N\mu}|^2$. Using the result $B(\mu \to e\gamma) < 4.9 \times 10^{-11}$ [46], the authors of Ref. [47] find $|U_{Ne}U^*_{N\mu}|^2 < 7 \times 10^{-6}$ for $m_N > 45$ GeV. From this they conclude that $B(K_L \to \mu^\pm e^\mp)$ is at most 10^{-15} in this type of models. Marciano [48] has pointed out that there is a better bound $|U_{Ne}U^*_{N\mu}|^2 < 10^{-8}$ coming from $\mu \to e$ conversion in the field of a heavy nucleus. With this bound one finds $B(K_L \to \mu^\pm e^\mp)$ to be at most a few times 10^{-18}. By using the additional theoretical prejudice that the mixing angles should be proportional to mass ratios of the form m_e/m_N, the authors of Ref. [49, 50] find the much stronger limit $B(K_L \to \mu^\pm e^\mp) < 10^{-25}$. At this level the decay is completely unobservable. If, in addition, one considers left-right symmetric models, the authors of Ref. [49, 50] find that the rate $B(K_L \to \mu^\pm e^\mp)$ can be as large as 10^{-13}, although this happens only in a small corner of parameter space.

There is an ultimate background to the decays $K_L \to \mu^\pm e^\mp$. It is given by the standard model process $K_L \to \mu^\pm e^\mp \nu_\mu \nu_e$. To leading order in χPT this process is dominated by $K_L \to \pi^\pm e^\mp \nu_e$ followed by $\pi^\pm \to \mu^\pm \nu_\mu$. The branching ratio for this chain can be estimated using the narrow width approximation to be a huge 38%. However, it is easy to see that the maximum invariant mass of the lepton pair is $m_{\mu e} < 489$ MeV. It is therefore possible to remove this background with a cut on

the lepton pair invariant mass. Going beyond the narrow width approximation, and including next to leading order terms in χPT can yield a lepton pair invariant mass larger than 489 MeV. However, after the 489 MeV cut is imposed, the rate is reduced to the 10^{-23} level [51].

3.2 $K^+ \to \pi^+\mu^\pm e^\mp$

In this case we compare the rate to that of $K^+ \to \pi^0\mu^+\nu$. From Eqs. 2.16, 2.17 we can see that this mode is only sensitive to the vector quark current or scalar density. In general, this mode is thus probing different operators than the previous one. For $V-A$ operators we find:

$$\frac{\Gamma(K^+ \to \pi^+\mu^+e^-)}{\Gamma(K^+ \to \pi^0\mu^+\nu)} = 8\frac{C_{V-A}^2}{|V_{us}|^2}\left(\frac{g_n}{g_2}\right)^4\left(\frac{m_W}{\Lambda}\right)^4 \tag{3.6}$$

Fig. 1 c shows the data from the most recent search for $K^+ \to \pi^+\mu^+e^-$ [52]. The lack of candidates within the search region allows the 90% *c.l.* upper bound $B(K^+ \to \pi^+\mu^+e^-) < 2.1\times10^{-10}$ to be set. The corresponding bound on the state with opposite lepton charges, $B(K^+ \to \pi^+\mu^-e^+) < 6.9\times10^{-9}$ [53], was set in an earlier experiment. Using these experimental bounds we find $\Lambda > 76$ TeV. Once again, we can use this result to place bounds on masses of new particles within specific models.

Given the large number of parameters in extensions of the standard model, it is very difficult to make definite predictions for any of the rare decays. Most of these models, however. will give rise to both $K \to \mu e$ and $K \to \pi\mu e$, as well as additional contributions to processes that do occur in the minimal standard model such as $K \to \pi\nu\overline{\nu}$, $K_L \to \ell^+\ell^-$ and $\Delta M(K_L - K_S)$. Discussions of how to use the experimental limits on all these processes to constrain the parameters in the models can be found in Ref. [54].

4 Short distance dominated processes

These are modes that can be computed reliably from the standard model, because they are not affected significantly by the non-perturbative aspects of the strong interactions. Within the standard model they are sensitive to the CKM parameters ρ and η, and to the top quark mass. Physics beyond the standard model, as in the models that gave rise to the modes studied in the previous section, can also affect these decay modes. We will concentrate on the standard model, but, as we will see, current experiments have not yet reached the sensitivity required to observe the standard model rates. This means that for the time being, these modes constitute a window to possible new physics.

4.1 $K^+ \to \pi^+ \nu\overline{\nu}$

In the standard model this process is mediated by the electroweak penguin and box diagrams depicted schematically in Fig. 3. The top-quark contribution is calculated to be [10]:

$$M = A^2\lambda^5(1-\rho-i\eta)\frac{G_F}{\sqrt{2}}\frac{\alpha}{2\pi\sin^2\theta_W}X(x_t) < \pi^+|\overline{s}\gamma_\mu d|K^+ > \overline{\nu}\gamma^\mu(1+\gamma_5)\nu \qquad (4.1)$$

where $x_t = m_t^2/m_W^2$ and:

$$X(x_t) = \frac{x_t}{8}\left(\frac{x_t+2}{x_t-1} + \frac{3x_t-6}{(x_t-1)^2}\ln x_t\right) \qquad (4.2)$$

Ref. [11] gives the approximate result $X(x_t) \approx 0.650 x_t^{0.59}$. The hadronic matrix element can be related by isospin to that occurring in $K^+ \to \pi^0 e^+\nu$ (equivalently using Eq. 2.16), and this allows one to write:

$$\frac{B(K^+ \to \pi^+\nu\overline{\nu})}{B(K^+ \to \pi^0 e^+\nu)} = \left(\frac{\alpha}{\pi\sin^2\theta_W}\right)^2 A^4\lambda^8\Big[(1-\rho)^2+\eta^2\Big]\Big[X(x_t)\Big]^2 \qquad (4.3)$$

for each neutrino flavor. The contribution of the charm quark intermediate state has also been computed. In this case, however, additional kinematical factors for the lepton masses, as well as QCD corrections do not allow us to write a simple expression. The authors of Ref. [11] provide us with an approximate expression for the total rate with three generations of neutrinos:

$$B(K^+ \to \pi^+ \nu\overline{\nu}) \approx 1.97 \times 10^{-11} A^4 x_t^{1.18} [\eta^2 + (\overline{\rho_0} - \rho)^2] \qquad (4.4)$$

The parameter $\overline{\rho_0}$ measures the charm quark contribution and is given in Ref. [11], a typical value for it being 1.5. This same reference finds $B(K^+ \to \pi^+ \nu\overline{\nu})$ to be in the range $(0.5 - 8.0) \times 10^{-10}$ when all uncertainties are included.

One can think of long distance contributions to this process that occur via μ pole diagrams as in Fig. 4, but these have been estimated to be at the level of 10^{-15}, much smaller than the short distance contributions [2].

It has been argued that minimal extensions of the standard model are unlikely to affect this process significantly, so that its main interest remains the constraining the CKM parameters [55]. However, even in Ref.[55], several less minimal extensions were discussed in which the current experimental upper bound could easily be saturated. In addition experiments sensitive to $K^+ \to \pi^+ \nu\overline{\nu}$ can also see $K^+ \to \pi^+ X^0$ where X^0 is a new light weakly-interacting particle. Candidates for such an X^0 include axions [56], familons [57], and hyperphotons [58]. Thus the possibility of novelty in the topology $K^+ \to \pi^+ +$ "nothing" should not be forgotten.

Fig. 5, shows recent data from AGS-787. There were separate analyses for the kinematic regions with π^+ momenta above and below that corresponding to the background $K^+ \to \pi^+ \pi^0$ process. No candidates were found within the search regions. The 90% c.l. upper limits extracted were $B(K^+ \to \pi^+ \nu\overline{\nu}) < 7.5 \times 10^{-9}$ and 1.7×10^{-8}

respectively[59, 60]. Assuming a vector momentum spectrum for the π^+, these can be combined into an overall upper limit $B(K^+ \to \pi^+\nu\overline{\nu}) < 5.2 \times 10^{-9}$. The corresponding limit on $K^+ \to \pi^+ X^0$ for a massless, long-lived X^0 is 1.7×10^{-9}. An upgrade of this experiment expects to reach a sensitivity of 10^{-10}, at which point one can begin to extract useful constraints on ρ and η.

4.2 $K_L \to \pi^0\nu\overline{\nu}$

The neutral version of the previous mode is completely dominated by the top-quark intermediate state. The result for three neutrino species can be written as [11]:

$$\frac{B(K_L \to \pi^0\nu\overline{\nu})}{B(K^+ \to \pi^0 e^+\nu)} = \frac{3}{2}\frac{\tau_{K_L}}{\tau_{K^+}}\left(\frac{\alpha}{\pi \sin^2\theta_W}\right)^2 A^4\lambda^8\eta^2\Big[X(x_t)\Big]^2 \tag{4.5}$$

The expected rate in the standard model is of order 10^{-10}, and this decay would directly measure η [61]. The potential long distance contributions to this decay are expected to be very small. Recently, the QCD corrections to the top-quark contribution to this decay (and to the charged mode as well) have been computed in Ref. [62]. This calculation reduces the uncertainty in the rates due to the dependence of the top mass on the renormalization scale from $\mathcal{O}(25\%)$ to $\mathcal{O}(3\%)$. This makes this mode a particularly clean one to measure η within the standard model. In principle this measurement can also be combined with that of the charged mode to reduce uncertainties due to m_t and to A.

At present the best limit comes from FNAL-731 [63], it is $B(K_L \to \pi^0\nu\overline{\nu}) < 2.2 \times 10^{-4}$. In this experiment the decay was sought in the Dalitz mode where the π^0 decays to $e^+e^-\gamma$. Using this technique, FNAL-799 expects to reach sensitivity in the 10^{-8} region. The KAMI conceptual design report [64] claims an eventual sensitivity of a few $\times 10^{-12}$ for this decay at the FNAL Main Injector. There is also a letter of

intent for an experiment [65] at KEK with an eventual sensitivity of $< 10^{-11}$/event. Other versions of this experiment are under consideration at a number of institutions.

5 Long distance dominated radiative decays

In this section we consider radiative decays and some of the Dalitz pair modes associated with them. These decays are sensitive to the non-perturbative aspects of the strong interactions, and thus they cannot be predicted reliably from the standard model at present. We resort to the framework of χPT to study these modes. As we will see, the current state of the art, $\mathcal{O}(p^4)$ calculations, is not always sufficient for an adequate description of these modes. These modes are interesting in their own right because they yield information on the long distance strong interactions. In some cases, a detailed understanding of these modes is also necessary in the analyses of other modes that look for CP violation, CKM angles, or new physics.

5.1 $K_S \to \gamma\gamma$

The processes $K_S \to \gamma\gamma$ and $K_L \to \pi^0\gamma\gamma$ share the remarkable feature of being independent of the couplings in Eqs. 2.12, 2.13 at $\mathcal{O}(p^4)$. They are therefore among the cleanest predictions of χPT. They can be studied by considering the diagrams shown in Fig. 6. A considerable simplification in the calculation is obtained when one uses the "diagonal" basis of Ecker *et. al.*, Ref. [66]. Defining $z = q_2^2/m_K^2$, $r_\pi^2 = m_\pi^2/m_K^2$, we write the amplitude for $K_1^0 \to \gamma(q_1)\gamma^*(q_2)$ as restricted by gauge invariance:

$$M_\nu = \epsilon^\mu(q_1)\Big(\frac{m_K^2}{2}(z-1)g_{\mu\nu} + q_{2\mu}q_{1\nu}\Big)b(0,z). \tag{5.1}$$

The $\mathcal{O}(p^4)$ result is given by [28]:

$$b(0,z) = \frac{\alpha}{\pi}G_8 2\sqrt{2}f_\pi(1-r_\pi^2)H(z). \tag{5.2}$$

The function $H(z)$ can be written as:

$$H(z) = \frac{1}{2(1-z)^2}\left\{zF\left(\frac{z}{r_\pi^2}\right) - F\left(\frac{1}{r_\pi^2}\right) - 2z\left[G\left(\frac{z}{r_\pi^2}\right) - G\left(\frac{1}{r_\pi^2}\right)\right]\right\}; \qquad (5.3)$$

the function $F(x)$ is given by:

$$F(x) = \begin{cases} 1 - \frac{4}{x}\left(\arcsin\frac{\sqrt{x}}{2}\right)^2 & x \leq 4 \\ 1 + \frac{1}{x}\left(\log\frac{1-\sqrt{1-4/x}}{1+\sqrt{1-4/x}} + i\pi\right)^2 & x > 4\ ; \end{cases} \qquad (5.4)$$

and $G(x)$ is given by:

$$G(x) = \begin{cases} \sqrt{\frac{4}{x} - 1}\left(\arcsin\frac{\sqrt{x}}{2}\right)^2 & x \leq 4 \\ \frac{1}{2}\sqrt{1 - \frac{4}{x}}\left(\log\frac{1+\sqrt{1-4/x}}{1-\sqrt{1-4/x}} - i\pi\right)^2 & x > 4\ . \end{cases} \qquad (5.5)$$

The situation in $K_S \to \gamma\gamma$ looks very good, with $z = 0$ in Eq. 5.2, one finds a branching ratio of 2.0×10^{-6} [67] and the NA31 measurement is $(2.4 \pm 1.2) \times 10^{-6}$ [68]. However, we note the very large error in the data. Given the fact that the theoretical prediction is rather clean, it is very important to reduce the experimental error. It is also possible to study this prediction in the related Dalitz pair decays $K_1^0 \to \ell^+\ell^-\gamma$, for which one finds [28]:

$$\frac{d\Gamma}{dz} = \frac{\alpha}{3\pi}\Gamma(K_1^0 \to \gamma\gamma)\frac{2}{z}(1-z)^3\left|\frac{H(z)}{H(0)}\right|^2(1 + 2r_\ell^2/z)\sqrt{1 - 4r_\ell^2/z} \qquad (5.6)$$

Ignoring CP violation the predicted branching ratios are then:

$$\frac{\Gamma(K_S \to \ell^+\ell^-\gamma)}{\Gamma(K_S \to \gamma\gamma)} = \begin{cases} 0.016 & \ell = e \\ 3.75 \times 10^{-4} & \ell = \mu \end{cases} \qquad (5.7)$$

5.2 $K_L \to \pi^0\gamma\gamma$

The amplitude for $K_L(p) \to \pi^0(p')\gamma(q_1,\epsilon_1)\gamma(q_2,\epsilon_2)$; $M = \epsilon_1^\mu(q_1)\epsilon_2^\nu(q_2)M_{\mu\nu}$, is restricted by gauge invariance and CP conservation to be of the form:

$$\begin{aligned} M_{\mu\nu} &= A(z,\nu)\Big(-m_K^2\frac{z}{2}g_{\mu\nu} + q_{2\mu}q_{1\nu}\Big) + \\ &\quad B(z,\nu)\Big(-m_K^2 x_1 x_2 g_{\mu\nu} - \frac{z}{2}p_\mu p_\nu + x_1 q_{2\mu}p_\nu + x_2 p_\mu q_{1\nu}\Big) \end{aligned} \tag{5.8}$$

where $x_i = p\cdot q_i/m_K^2$, $z = 2q_1\cdot q_2/m_K^2$, and $\nu = x_1 - x_2$. The lowest order amplitude $K_L \to \pi^0\gamma\gamma$, $\mathcal{O}(p^4)$, obtained from chiral loops gives rise only to the form factor $A(z,\nu)$[66]. To this lowest order result we can add the next order terms, $\mathcal{O}(E^6)$, as they appear in some models. They can be parameterized in terms of a single constant a_V, and the combined result is:

$$\begin{aligned} A(z,\nu) &= \frac{\alpha}{\pi}G_8\Big[F\Big(\frac{z}{r_\pi^2}\Big)\Big(1-\frac{r_\pi^2}{z}\Big) + F(z)\Big(\frac{1+r_\pi^2}{z}-1\Big) + a_V\Big(3+r_\pi^2-z\Big)\Big] \\ B(z,\nu) &= -4a_V\frac{\alpha}{\pi}G_8 \quad . \end{aligned} \tag{5.9}$$

The function $F(x)$ is given in Eq. 5.4.

The constant a_V has been calculated in several models. The simplest ones are those that consider only pole diagrams for the E^6 terms, such as those of Fig. 7. One should also consider direct weak counterterms as depicted schematically in Fig. 7. A model to compute these direct counterterms is the "weak deformation model" of [36]. For this mode, the model predicts the direct weak counterterm contribution to a_V to be twice as large as that from the pole terms and to have the opposite sign. The net effect is thus to change the sign of the constant a_V calculated from pole diagrams alone.

$$a_V = \begin{cases} 0.32 & \text{VMD (poles); } -0.32 \text{ (poles + WDM) [36]} \\ 0.22 & \text{Q.M. (poles); } -0.22 \text{ (poles + WDM) [69]} \end{cases} \tag{5.10}$$

We compare these results with experiment [70, 71] in Fig. 8. In Fig. 8 a, the various predictions have been mutually normalized. It is apparent in Fig. 8 b, that the shape of the data of Ref. [70] is well fit by the $\mathcal{O}(p^4)$ prediction (this is also true of the data of Ref. [71]). The shape of the distribution is affected very little by the small p^6 corrections. The corrections (both in the quark model and in the vector dominance model) tend to increase the number of events to be expected for the lower values of the photon pair invariant mass. However, this is a very small effect, and it is difficult to check given the currently available statistics.

The branching fraction with a cut on the invariant mass of the photon pair, $M_{\gamma\gamma} > 280$ MeV, is [70, 71]:

$$B(K_L \to \pi^0\gamma\gamma) = \begin{cases} (0.57^{+0.11}_{-0.06}) \times 10^{-6} & \chi\text{PT}, \\ (1.7 \pm 0.3) \times 10^{-6} & \text{NA31}, \\ (1.86 \pm 0.6) \times 10^{-6} & \text{FNAL-731}. \end{cases} \tag{5.11}$$

The central value for the theory number corresponds to the $\mathcal{O}(p^4)$ result. The error represents the variation obtained by including the $\mathcal{O}(p^6)$ terms with a_V from Eq. 5.10. The predictions are significantly smaller than the data. Other models (outside the realm of χPT), have predicted larger branching ratios [72]; however, they predict a $\gamma\gamma$ spectrum that strongly disagrees with experiment, whereas χPT appears to reproduce the data very well (see Fig. 8). These other models include vector meson exchange diagrams such as those of Fig. 7. This has created the incorrect impression in the literature that it is the inclusion of vector mesons that is responsible for the large rate. That this is not so can be seen, for example, in the model of Ref. [36], Eq. 5.10, that includes the vector mesons as well. As noted in Ref. [69], what leads to large rates in the models of Ref. [72] is the very specific form in which they include the η' pole. This pole, unlike the π^0 and η poles of Fig. 7, cannot be treated unambiguously

at present. It enters at the same order as $\eta-\eta'$ mixing and other higher order $SU(3)_V$ breaking effects. The authors of Ref. [72] include only some of these effects, and the rate is very sensitive to the precise way in which this is done. The very large model dependence introduced by these terms can be appreciated in the mode $K_L \to \gamma\gamma$ where a similar situation occurs [73].

From the shape of the spectrum, NA31 has derived the bound [70]:

$$-0.32 < a_V < 0.19 \tag{5.12}$$

at 90% confidence level. One must notice, however, that with this range for a_V, the branching ratio (with $M_{\gamma\gamma} > 280$ MeV) is not reproduced:

$$0.53 \times 10^{-6} \leq B(K_L \to \pi^0\gamma\gamma) \leq 0.68 \times 10^{-6}. \tag{5.13}$$

Conversely, a fit to the branching ratio yields $a_V \approx -2.0$, which does not reproduce the shape of the spectrum. The shape of the spectrum appears to indicate that the χPT arguments are correct, and that models with very large D-wave amplitudes are ruled out. The discrepancy in the branching ratio tells us that this mode will require more theoretical and experimental efforts in the years to come.

The contribution of the $\Delta I = 3/2$ amplitudes has been recently estimated in Ref. [74]. These authors found that it introduced a small $\mathcal{O}(10\%)$ correction that tends to make the branching ratio smaller. The amplitude computed in Ref. [74] contributes only to the $A(z,\nu)$ form factor, so the spectrum still has the shape given by lowest order χPT. These same authors have studied possible effects of higher order terms by using the experimental amplitude for the $K \to 3\pi$ vertex. They find an enhancement of about 26% in the branching ratio, that comes mostly from contributions to $A(z,\nu)$. Although this does go in the right direction, it is too small

to account for the discrepancy with experiment. We should also remember that the naive estimate for the size of p^6 corrections to a p^4 amplitude is about 25% as well.

5.3 $K^+ \to \pi^+\gamma\gamma$

This process is similar to the neutral mode in that the one-loop amplitude in χPT is finite. Unlike the neutral mode, however, this mode does receive contributions at order $\mathcal{O}(E^4)$ from local counterterms. An additional feature is the possibility of looking for CP violation by comparing the two charged modes. The amplitude for this process is restricted by gauge invariance to be of the form:

$$M = \epsilon_1^\mu \epsilon_2^\nu \Big[A(z,\nu)\Big(-m_K^2 \frac{z}{2} g_{\mu\nu} + q_{2\mu} q_{1\nu}\Big) + C(z,\nu)\epsilon_{\mu\nu\rho\sigma} q_1^\rho q_2^\sigma \Big] \tag{5.14}$$

The form factor $A(z,\nu)$ to $\mathcal{O}(p^4)$ is given by [28],

$$\begin{aligned} A(z,\nu) &= \frac{\alpha}{\pi} G_8 \frac{1}{2z}\Big[\Big(r_\pi^2 - 1 - z\Big)F\Big(\frac{z}{r_\pi^2}\Big) + \Big(1 - z - r_\pi^2\Big)F(z) + \hat{c}z\Big] \\ \hat{c} &= 32\pi^2\Big(4(L_9 + L_{10}) - \frac{1}{3}(w_1 + 2w_2 + 2w_4)\Big) \end{aligned} \tag{5.15}$$

The constant $\hat{c}$ is a scale independent combination of couplings in the effective Lagrangian, reflecting the fact that the loop contributions to this process are finite. Its real part, Re$\hat{c}$, has been estimated in several models to be: 0.0 [36]; $0.35^{+0.50}_{-0.30}$ [38]; and -4.0 [37].

The form factor $C(z,\nu)$ occurs via the pole diagrams of Fig. 9. The transition $K^+ \to \pi^+\pi^0$ occurs on-shell via the $(27_L, 1_R)$ operators only. The $K^+ \to \pi^+\pi^0$ decay, followed by $\pi^0 \to \gamma\gamma$ gives a very large contribution to $K^+ \to \pi^+\gamma\gamma$, however, it can be subtracted by implementing a cut in the invariant mass of the photon pair to exclude the region near m_{π^0}. The off-shell transition is mediated by the octet

operator in Eq. 2.9 and results in [28]:

$$C(z,\nu) = \frac{\alpha}{\pi} G_8 \left[\frac{z - r_\pi^2}{z - r_\pi^2 + i r_\pi \Gamma_{\pi^0}/m_K} - \frac{z - \frac{1}{3}(2 + r_\pi^2)}{z - r_\eta^2} \right] \tag{5.16}$$

The two form factors do not interfere, and one obtains:

$$\frac{d\Gamma}{dz} = \frac{m_K^5}{1024\pi^3} z^2 \lambda^{\frac{1}{2}}(1, z, r_\pi^2) \Big(|A(z)|^2 + |C(z)|^2 \Big) \tag{5.17}$$

In this case, χPT predicts a correlation between the rate and the spectrum. The rate is given by the expression:

$$B(K^+ \to \pi^+ \gamma\gamma) = (5.26 + 1.64\hat{c} + 0.32\hat{c}^2 + 0.49) \times 10^{-7}. \tag{5.18}$$

and the current experimental limit [75] is:

$$B(K^+ \to \pi^+ \gamma\gamma) < \begin{cases} 1.0 \times 10^{-6} & \text{Phase space spectrum} \\ 1.5 \times 10^{-4} & \chi\text{PT spectrum} \end{cases} \tag{5.19}$$

The rate for $K^- \to \pi^- \gamma\gamma$ can be obtained from Eq. 5.15 by replacing G_8 and $\hat{c}$ with their complex conjugates. An imaginary part of $\hat{c}$ would interfere with the absorptive part of the amplitude (due to a real $\pi^+\pi^-$ intermediate state) generating a CP odd rate asymmetry [28]:

$$\Gamma(K^+ \to \pi^+ \gamma\gamma) - \Gamma(K^- \to \pi^- \gamma\gamma) = 1.5 \times 10^{-23} \mathrm{Im}\hat{c} \text{ GeV} \tag{5.20}$$

To estimate Im$\hat{c}$, the authors of Ref. [28] point out that at the quark level, the CP phase appears via the electromagnetic penguin operator [76]:

$$\mathcal{L} = -\frac{G_F}{\sqrt{2}} |V_{ud} V_{us}| C_7(\mu^2) \alpha \bar{s} \gamma_\mu (1 + \gamma_5) d \bar{\ell} \gamma^\mu \ell \tag{5.21}$$

This operator transforms as an octet under $SU(3)_V$. By requiring its chiral realization to transform in the same way, the authors of Ref. [28] conclude that:

$$\mathrm{Im}(g_8 w_1) \approx \frac{1}{3\pi^2} \ln\left(\frac{m_t}{m_c}\right) A^2 \lambda^4 \eta \tag{5.22}$$

Arguing that this is the only contribution to the phase of $\hat{c}$ they find:

$$|\mathrm{Im}\hat{c}| = \frac{32}{3}\pi^2|\mathrm{Im}w_1| \approx 0.005\eta \tag{5.23}$$

Noticing that the rate for $K^+ \to \pi^+\gamma\gamma$ given by Eq. 5.18 has a minimum for $\hat{c} = -2.56$, they conclude that:

$$\left|\frac{\Gamma(K^+ \to \pi^+\gamma\gamma) - \Gamma(K^- \to \pi^-\gamma\gamma)}{\Gamma(K^+ \to \pi^+\gamma\gamma) + \Gamma(K^- \to \pi^-\gamma\gamma)}\right| \leq 0.002\eta \tag{5.24}$$

However, the authors of Ref. [38] have pointed out that the electromagnetic penguin operator also contributes a phase to w_4. They find that this contribution essentially cancels the one from w_1 so that $\mathrm{Im}\hat{c} = 0$ and there is no charge asymmetry in the standard model. Given the potentially large asymmetry, Eq. 5.24, it is important to resolve this issue.

5.4 $K_L \to \gamma\gamma$

This process is not a very rare decay, but its calculation in χPT illustrates some of the problems that one encounters in other weak decays. To order $\mathcal{O}(p^4)$ this process occurs via the π^0, η poles of Fig. 10. Using Eqs. 2.8 and 2.9 one finds in the limit of CP conservation that $M(K_L \to \gamma(q_1)\gamma(q_2))$ is:

$$M = \frac{2m_K^2 f_\pi^2}{m_K^2 - m_\pi^2}\frac{\alpha G_8}{\pi f_\pi}\left(1 + \frac{1}{3}\frac{m_K^2 - m_\pi^2}{m_K^2 - m_\eta^2}\right)\epsilon_{\mu\nu\rho\sigma}q_1^\mu q_2^\nu \epsilon_1^\rho \epsilon_2^\sigma \tag{5.25}$$

At this order in χPT, however, we are instructed to use the Gell-Mann-Okubo mass relation Eq. 2.6, so the amplitude vanishes. The first non-zero contributions result from higher order $SU(3)$ breaking. We can parameterize these higher order effects with a constant F_1, such that:

$$M = \frac{\alpha}{\pi}2G_8 f_\pi F_1 \epsilon_{\mu\nu\rho\sigma}q_1^\mu q_2^\nu \epsilon_1^\rho \epsilon_2^\sigma \tag{5.26}$$

to find:

$$B(K_L \to \gamma\gamma) = \begin{cases} (7.3 \times 10^{-4})|F_1|^2 & \\ (5.70 \pm 0.27) \times 10^{-4} & \text{PDB average [40]} \end{cases} \tag{5.27}$$

A fit to the experimental result yields a value $|F_1| \approx 0.88$. A detailed analysis that tried to predict the value of F_1 was carried out in Ref. [73]. It included $SU(3)$ breaking effects in the vertices as well as the decay constants; and also the effects of the $SU(3)$ singlet and of $\eta - \eta'$ mixing. Ref. [73] found that it was possible to accommodate the experimental result, but that it was not possible to predict it with any certainty. Recently, the authors of Ref. [77] have criticized the treatment of the $SU(3)$ singlet in Ref. [73], however, this does not change the conclusion.

It is also of interest to study this amplitude for off-shell photons, since this will give the dominant contribution to the decays $K_L \to \ell^+\ell^-\gamma$ and $K_L \to \ell^+\ell^-\ell^+\ell^-$. In the limit of CP conservation, gauge invariance requires the amplitude for $K_L \to \gamma^*\gamma^*$ to be of the form:

$$M = M(K_L \to \gamma(q_1)\gamma(q_2))C(q_1^2, q_2^2) \tag{5.28}$$

where we have normalized it so that $C(0,0) = 1$. Bose symmetry requires $C(q_1^2, q_2^2)$ to be symmetric under $q_1 \leftrightarrow q_2$, so we write:

$$C(q_1^2, q_2^2) = 1 + \sigma\left(\frac{q_1^2 + q_2^2}{m_K^2}\right) + \cdots \tag{5.29}$$

5.5 $K_L \to \gamma\gamma$ Dalitz decays

Using the previous result, and defining $r_\ell = m_\ell/m_K$, $z = m_{\ell\ell}^2/m_K^2$, we can now study the process $K_L \to \ell^+\ell^-\gamma$. The differential decay rate is:

$$\frac{d\Gamma}{dz} = \Gamma(K_L \to \gamma\gamma)\frac{2\alpha}{3\pi}\left|C(0,z)\right|^2 \frac{(1-z)^3}{z}\sqrt{1 - \frac{4r_\ell^2}{z}}\left(1 + 2\frac{r_\ell^2}{z}\right), \tag{5.30}$$

and the total rates are:

$$\frac{\Gamma(K_L \to \ell^+\ell^-\gamma)}{\Gamma(K_L \to \gamma\gamma)} = \begin{cases} 0.016(1+0.05\sigma) & \ell = e \\ 0.016 \pm 0.001 & \text{AGS-845, NA31 [78, 79]} \\ 4.09 \times 10^{-4}(1+0.64\sigma) & \ell = \mu \\ (6.81 \pm 0.64) \times 10^{-4} & \text{FNAL-799 [80]} \end{cases} \tag{5.31}$$

It has become usual in the literature to parameterize the form factor following a model of Bergstrom *et. al.* [81], in terms of a constant α_K. This model, with $\alpha_K = 0$ corresponds to the vector dominance model of Quigg and Jackson [82]. Expanding the pole model parameterization, we identify $\sigma = 0.418 - 1.29\alpha_K$. In terms of this pole model, AGS-845 [78, 79] found $\alpha_K = -0.28 \pm 0.083$ by fitting the $m_{\ell\ell}$ spectrum with QED radiative corrections, and $\alpha_K = -0.18 \pm 0.077$ without QED radiative corrections. This is consistent with the NA31 result, $\alpha_K = -0.28 \pm 0.13$.

The branching ratio $\Gamma(K_L \to e^+e^-\gamma)/\Gamma(K_L \to \gamma\gamma)$ is not very sensitive to the form factor. With the form Eq. 5.29, we find a variation from 0.0162 to 0.0165 when we take α_K from 0 to -0.28. With the pole model of Ref. [81], the branching ratio varies from 0.0163 to 0.0167 for this same range of α_K.

The branching ratio $\Gamma(K_L \to \mu^+\mu^-\gamma)/\Gamma(K_L \to \gamma\gamma)$, is more sensitive to the form factor. With the same range for α_K as before, it varies from (5.18 to 6.13)$\times 10^{-4}$ using Eq. 5.29; and from (5.58 to 7.28) $\times 10^{-4}$ with the model of Ref. [81]. The preliminary result from FNAL-799 cited in Eq. 5.31, can be used to extract from Ref. [81]:

$$\alpha_K = -0.21 \pm 0.11 \tag{5.32}$$

Which is consistent with the value of α_K found by the $K_L \to e^+e^-\gamma$ experiments, and inconsistent with $\alpha_K = 0$ at the two σ level. Preliminary reports from FNAL-799 indicate that the $m_{\ell\ell}$ spectrum for this decay is adequately fit by an unmodified Kroll-Wada form [83].

Finally, there have been several recent results on the double Dalitz decay, $K_L \to e^+e^-e^+e^-$[84, 85, 86, 87], which are summarized in Table 3.

Table 3: Experimental Results on $K_L \to e^+e^-e^+e^-$

Experiment	Result	Comments
NA31	$(4 \pm 3) \times 10^{-8}$ [84]	the first 2 events
AGS-845	$(3.04 \pm 1.24 \pm 0.26) \times 10^{-8}$ [85]	6 events
KEK-137	$(6 \pm 2 \pm 1) \times 10^{-8}$ [86]	partial reconstruction
FNAL-799	$(4.17 \pm 0.83) \times 10^{-8}$ [87]	28 events, preliminary result

These results should be compared with the theoretical expectation of 3.6×10^{-8} [82]. Larger samples will allow form factor effects to be studied. FNAL-799 also expects to observe the closely related process $K_L \to \mu^+\mu^-e^+e^-$ which is predicted at 0.8×10^{-9} [88]. Reference [88] also predicts $B(K_L \to \mu^+\mu^-\mu^+\mu^-) = 5.4 \times 10^{-13}$, putting it beyond reach for the moment. The predictions for these modes that one finds in the literature do not always agree [82, 88].

5.6 Direct emission $K_L \to \pi^+\pi^-\gamma$

In the limit of CP conservation, this process does not occur at order $\mathcal{O}(p^2)$ [89, 90]. The lowest order weak Lagrangian Eq. 2.9 contributes to the process $K_1^0 \to \pi^+\pi^-\gamma$, and thus it contributes to $K_L \to \pi^+\pi^-\gamma$ an indirect CP violating term. This term has a characteristic bremsstrahlung spectrum and has been observed [91, 92]. Of greater interest to us is the so called direct emission term. From a theoretical point of view, we will define it as the amplitude that starts at $\mathcal{O}(p^4)$. Experimentally, it is observed by subtracting the bremsstrahlung portion from the full amplitude. Gauge invariance

requires the amplitude for $K_L(k) \to \pi^+(p^+)\pi^-(p^-)\gamma(q)$ to be of the form:

$$M = \frac{eG_8 f_\pi^2}{m_K}\epsilon^\mu\left[\xi_E(z,\nu)\Big(\nu(p^+ + p^-)_\mu - z(p^+ - p^-)_\mu\Big) + \frac{4i}{m_K^2}\xi_M(z,\nu)\epsilon_{\mu\nu\alpha\beta}k^\nu p^{+\alpha}p^{-\beta}\right] \tag{5.33}$$

where $z = 2k\cdot q/m_K^2$, $x^\pm = 2k\cdot p^\pm/m_K^2$, and $\nu = x^+ - x^-$. The "magnetic" form factor ξ_M receives contributions from π^0, η poles as in Fig. 11, and vertices from Eq. 2.8. At order $\mathcal{O}(p^4)$ we find:

$$\xi_M = \frac{m_K^2}{m_K^2 - m_\pi^2}\frac{m_K^3}{8\pi^2 f_\pi^3}\left(1 + \frac{1}{3}\frac{m_K^2 - m_\pi^2}{m_K^2 - m_\eta^2}\right) \tag{5.34}$$

However, when the Gell-Mann-Okubo relation (Eq. 2.6) is applied, one gets the same cancellation that occurred in $K_L \to \gamma\gamma$. We can parameterize the $SU(3)_V$ violating terms that make the amplitude non-zero, as well as terms of order $\mathcal{O}(p^6)$ with a naive expansion of the form factors. We follow Ref. [90] and include the strong rescattering phases δ_J^I for the spin J, isospin I $\pi-\pi$ scattering at a center of mass energy squared $(p_+ + p_-)^2 = m_K^2(1-z)$. With all this we write:

$$\begin{aligned}
\xi_E(z,\nu) &= i\frac{8(m_K^2 - m_\pi^2)}{m_K f_\pi}\frac{\eta_{+-}}{z^2 - \nu^2} + \left[F_E\Big(1 + \sigma_E z\Big)e^{i(\delta_1^1 - \delta_0^0)} + ig_E\nu e^{i(\delta_2^0 - \delta_0^0)}\right] \\
\xi_M(z,\nu) &= \frac{m_K^3}{8\pi^2 f_\pi^3}\left[F_M\Big(1 + \sigma_M z\Big)e^{i(\delta_1^1 - \delta_0^0)} + ig_M\nu e^{i(\delta_2^0 - \delta_0^0)}\right].
\end{aligned} \tag{5.35}$$

We have included in ξ_E the inner bremsstrahlung contribution which can interfere with F_E in the rate. We have not included possible $\mathcal{O}(p^6)$ $\Delta I = 3/2$ terms. The terms F_E, and g_M are CP violating. The differential decay rate is given by:

$$\frac{d\Gamma}{dz\,d\nu} = \frac{\alpha m_K}{128\pi^2}G_8^2 f_\pi^4\Big(|\xi_E|^2 + |\xi_M|^2\Big)\left[(1-z)(z^2 - \nu^2) - 4r_\pi^2 z^2\right] \tag{5.36}$$

A detailed analysis of the Dalitz plot for this decay should allow a determination of the parameters in Eq. 5.35. The simplest thing we can do is to set all the new

constants in Eq. 5.35 to zero except F_M. In that case we find for the direct emission (with $E_\gamma > 20$ MeV):

$$B(K_L \to \pi^+\pi^-\gamma)_{DE} = \begin{cases} (3.35 \times 10^{-5})|F_M|^2 & \\ (2.89 \pm 0.28) \times 10^{-5} & \text{BNL [91]} \\ (3.19 \pm 0.16) \times 10^{-5} & \text{FNAL-731 [92]} \end{cases} \tag{5.37}$$

which results in $F_M \approx 0.95$. One can try to predict F_M in a model that includes $SU(3)$ breaking effects, similar to the one used by Ref. [73] for $K_L \to \gamma\gamma$. One finds that it is possible to accommodate the result [93], but not to predict it with certainty. If we set F_M to zero and keep F_E in Eq.5.35, we find that this direct emission rate is also consistent with an interference of the bremsstrahlung amplitude and a CP violating term $F_E \sim 1.4$. Keeping only F_M and F_E, Ref. [91] found a best fit to the spectrum with an admixture of CP violating direct decay $F_E \approx 0.26 F_M$, lying $< 2\sigma$ from the no-interference fit. However, naive dimensional analysis suggests that CP violation in the standard model is much smaller than this [93]. The fits of Ref. [91] found no evidence for the quadrupole term g_E at the 25% level.

Assuming CP conservation in the direct emission, a fit to the distribution $d\Gamma/dz$ provides information on the slope σ_M:

$$\sigma_M = \begin{cases} -0.91 & \text{FNAL-731} \\ -0.89 & \text{BNL} \end{cases} \tag{5.38}$$

One can resort to models to predict the $\mathcal{O}(p^6)$ form factors like σ_M [93, 94, 95]. It appears that a vector meson dominance model does not reproduce the spectrum shape unless one includes $SU(3)_V$ breaking effects. A more careful study is needed.

By observing the interference between K_S and K_L decays into $\pi^+\pi^-\gamma$, FNAL-731 [92] has measured:

$$|\eta_{+-\gamma}| = \frac{M(K_L \to \pi^+\pi^-\gamma)_{E1}}{M(K_S \to \pi^+\pi^-\gamma)_{E1}} = (2.15 \pm 0.26 \pm 0.20) \times 10^{-3} \tag{5.39}$$

with a phase $\phi_{+-\gamma} = (72 \pm 23 \pm 17)°$. Since $|\eta_{+-}| = (2.268 \pm 0.023) \times 10^{-3}$ [40], the FNAL-731 result is consistent with no CP violation beyond that present in $K \to \pi\pi$ decays.

Additional information can be obtained by studying the Dalitz decay $K_L \to \pi^+\pi^-e^+e^-$. Separating the I.B and D.E. contributions, and using for the D.E. a constant coupling F_M that fits the $(K_L \to \pi^+\pi^-\gamma)_{DE}$ rate, Ref. [96] calculates $B(K_L \to \pi^+\pi^-e^+e^-) = (1.3 + 1.8) \times 10^{-7}$. This decay has been recently observed by FNAL-799, but a branching ratio has not yet been reported. The authors of Ref. [96] have also studied a CP odd correlation between the $\pi^+\pi^-$ and e^+e^- planes and predict a 14% asymmetry. Unfortunately this asymmetry is mostly due to indirect CP violation through the parameter ϵ, making an extraction of direct CP violation very difficult.

6 Decays into charged lepton pairs

These modes generally receive both long and short distance contributions that are of comparable size. Some of them are dominated by the long distance component, but exhibit interesting interference effects with the smaller short distance contribution. Their primary interest is the study of the short distance parameters ρ and η, but to do so one needs some understanding of the long distance contributions. In this respect they also allow one to test the ideas of χPT. The observables that probe the short distance physics are also sensitive to new interactions, however, we will restrict ourselves to a discussion of the standard model.

6.1 Short Distance $K_L \to \ell^+\ell^-$

The short distance contribution to these processes comes from the box and electroweak penguin diagrams of Fig. 12. To compute the amplitude for this process, one relates the matrix element $< 0|\bar{s}\gamma_\mu(1+\gamma_5)d|K_L >$ to that occurring in $K^+ \to \ell^+\nu$ (see Eq. 2.16). The top-quark contribution is easily computed to be [10]:

$$\frac{B(K_L \to \ell^+\ell^-)_{SD}}{B(K^+ \to \ell^+\nu)} = \frac{\tau_{K_L}}{\tau_{K^+}}\left(\frac{\alpha}{\pi \sin^2\theta_W}\right)^2 A^4\lambda^8(1-\rho)^2\Big[Y(x_t)\Big]^2 \tag{6.1}$$

where the function $Y(x_t)$ is given by:

$$Y(x_t) = \frac{x_t}{8}\left(\frac{x_t-4}{x_t-1} + \frac{3x_t}{(x_t-1)^2}\ln x_t\right) \tag{6.2}$$

An approximate expression is provided by Ref. [9] $Y(x_t) \approx 0.315 x_t^{0.78}$. The contribution of the charm-quark, with perturbative QCD corrections can be found in Ref. [11]. These authors provide us with the approximate expression for the complete result:

$$B(K_L \to \mu^+\mu^-)_{SD} = 1.7 \times 10^{-10} x_t^{1.56} A^4(\rho_0 - \rho)^2 \tag{6.3}$$

where deviations of ρ_0 from 1 measure the charm-quark contribution with QCD corrections. For typical values of all the parameters involved, $\rho_0 \sim 1.27$.

An interesting feature of this decay is the longitudinal polarization of the final lepton, a CP violating observable [97]:

$$P_L \equiv \frac{N_L - N_R}{N_L + N_R} \tag{6.4}$$

The latest estimate of this quantity within the standard model is about 2×10^{-3} [98]. This number, however, is directly proportional to ϵ [99]. Since this is probably too small to be measured, P_L is a very good place to look for direct CP violation outside the standard model.

6.2 Long distance $K_L \to \ell^+\ell^-$

The long distance contribution to these decays is expected to be dominated by the two photon intermediate state as in Fig. 13. It is straightforward to compute the absorptive part of the amplitude by using the experimental rate for $K_L \to \gamma\gamma$. The result is ($r_\ell^2 = m_\ell^2/m_K^2$):

$$\begin{aligned} B(K_L \to \ell^+\ell^-)_{abs} &= \frac{1}{2}\alpha^2 r_\ell^2 \frac{1}{\beta}\left|\ln\frac{1+\beta}{1-\beta}\right|^2 B(K_L \to \gamma\gamma) \\ \beta &= \sqrt{1-4r_\ell^2} \end{aligned} \tag{6.5}$$

This can be compared to the latest measurements:

$$\begin{aligned} B(K_L \to \mu^+\mu^-) &= \begin{cases} (6.8 \pm 0.3) \times 10^{-9} & \text{absorptive} \\ (7.9 \pm 0.7) \times 10^{-9} & \text{KEK 137 [100]} \\ (6.86 \pm 0.37) \times 10^{-9} & \text{AGS-791 [101]} \end{cases} \\ B(K_L \to e^+e^-) &= \begin{cases} (3.0 \pm 0.1) \times 10^{-12} & \text{absorptive} \\ < 4.7 \times 10^{-11} & \text{AGS-791 [42]} \end{cases} \end{aligned} \tag{6.6}$$

A calculation of the dispersive part of the long distance effects is not possible at present within χPT. There are two problems: the on-shell $K_L \to \gamma\gamma$ vertex cannot be computed reliably as already explained; and the divergence of the loop diagram implies that there are counterterms for this process. These counterterms are similar to those occurring in the decay $\pi^0 \to e^+e^-$ [102], but they are not the same and have not been determined. However, we can resort to models to estimate the dispersive contribution. A vector dominance model gives results that can be written compactly in the limit $m_\ell/m_P \to 0$ [103]:

$$\begin{aligned} \frac{\Gamma(P^0 \to \ell^+\ell^-)}{\Gamma(P^0 \to \gamma\gamma)} &= \frac{2\alpha^2 m_\ell^2}{m_P^2}\left[X^2 + \left(\ln\frac{m_P}{m_\ell}\right)^2\right] \\ X &= \frac{\pi}{12} + \frac{1}{4\pi} + \frac{1}{\pi}\left(\ln\frac{m_P}{m_\ell}\right)^2 - \frac{3}{\pi}\ln\frac{m_V}{m_\ell} \end{aligned} \tag{6.7}$$

where m_V is the rho mass. Although this is a convenient expression for decays into electrons, it is not accurate by about a factor of two for muons. One also finds in the literature the model of Ref. [81], in which one allows an additional form-factor for the $K_L \to \gamma\gamma$ vertex itself. This is modelled by a $K^* \to \rho$ transition in terms of the parameter α_K of section 5.5. The result can be written as [81]:

$$B(K_L \to \mu^+\mu^-)^{\gamma\gamma}_{disp} = 4.7 \times 10^{-10}\left(1.3 + 4.9\alpha_K\right)^2, \tag{6.8}$$

and the $\alpha_K = 0$ case corresponds to the vector dominance model of Quigg and Jackson. The contributions from a negative α_K tend to cancel the first term in the above result, and this cancellation is almost complete for $\alpha_K = -0.28$. We regard this cancellation as accidental, and prefer the result with $\alpha_K = 0$ as a more conservative estimate for the long distance dispersive rate.

In view of the large model dependence in estimating the long distance contribution to the dispersive part of $K_L \to \mu^+\mu^-$, it would seem very difficult to extract mean-

ingful constraints on the short distance contribution. Nevertheless, recent attempts to do so can be found in Ref. [104].

From Eq. 6.7 we can also compute the two-photon contribution to $B(K_L \to e^+e^-)_{disp}$, we find 4.6×10^{-12}. The long distance contributions to $K_L \to e^+e^-$ are about 15 times as large as one would expect by a naive scaling of $K_L \to \mu^+\mu^-$ with m_e^2/m_μ^2. This factor can be traced back to the logarithms in Eqs. 6.5, 6.7. There is no analogous factor in the short distance contribution, which then has the naive scaling. This means that it is even harder to observe the short distance contribution in $K_L \to e^+e^-$ than it is in $K_L \to \mu^+\mu^-$ [4].

6.3 $K \to \pi\gamma^*$

This is the most important long distance contribution to the CP conserving decays of the form $K \to \pi\ell^+\ell^-$. It can be computed to $\mathcal{O}(p^4)$ in χPT in terms of a few unknown constants. The most general form allowed by electromagnetic gauge invariance for the amplitude $A(K^{\pm,0}(k) \to \pi^{\pm,0}(p)\gamma^*(\epsilon,q))$ is [27]:

$$A^{\pm,0} = \frac{eG_8}{16\pi^2}\epsilon^\mu\Big(q^2(k+p)_\mu - (m_K^2 - m_\pi^2)q_\mu\Big)C^{\pm,0}(z) \tag{6.9}$$

where $z = q^2/m_K^2$.

It can be seen immediately that gauge invariance requires the amplitude to have at least three external momenta (and there is one external photon), so that it can only start at $\mathcal{O}(p^4)$. Eq. 6.9 also shows that the process $K \to \pi\gamma$ with an on-shell photon is forbidden by gauge invariance. Computing the diagrams in Fig.14, one finds the form factor $C(z)$ to $\mathcal{O}(p^4)$ in χPT in terms of the couplings of section 2 and

the function:

$$\phi_K(z) = \begin{cases} \frac{1}{3}\left[\left(\frac{4}{z}-1\right)^{\frac{3}{2}}\text{atan}\sqrt{\frac{z}{4-z}} - \frac{4}{z} + \frac{5}{6}\right] & z \leq 4 \\ \frac{1}{3}\left[\frac{1}{4}\left(1-\frac{4}{z}\right)^{\frac{3}{2}}\left(\ln\left(\frac{z-2-\sqrt{z(z-4)}}{z-2+\sqrt{z(z-4)}}\right)+i2\pi\right) - \frac{4}{z} + \frac{5}{6}\right] & z > 4 \end{cases} \tag{6.10}$$

The function $\phi_\pi(z)$ is obtained by replacing $z \to zm_K^2/m_\pi^2$ in Eq. 6.10. One finds for the charged mode [27]:

$$\begin{aligned} C^{\pm}(z) &= \frac{1}{3}\Big[(4\pi)^2\Big(w_1^r(\mu) - w_2^r(\mu)\Big) + 3(4\pi)^2\Big(w_2^r(\mu) - 4L_9^r(\mu)\Big) \\ &+ \ln\Big(\frac{m_K m_\pi}{\mu^2}\Big)\Big] - \Big(\phi_\pi(z) + \phi_K(z)\Big) \\ &\equiv -\Big(w_+ + \phi_\pi(z) + \phi_K(z)\Big), \end{aligned} \tag{6.11}$$

and for the neutral mode:

$$\begin{aligned} C^0(z) &= -\frac{\sqrt{2}}{6}\Big[(4\pi)^2\Big(w_1^r(\mu) - w_2^r(\mu)\Big) + \ln\Big(\frac{m_K^2}{\mu^2}\Big)\Big] + \sqrt{2}\phi_K \\ &\equiv \sqrt{2}\Big(\frac{w_S}{2} + \phi_K(z)\Big) \end{aligned} \tag{6.12}$$

6.4 $K^+ \to \pi^+\ell^+\ell^-$

We can now study the processes $K^+(k) \to \pi^+(p)\ell^+(k^+)\ell^-(k^-)$ that are dominated by the one photon intermediate state. The matrix element is given by ($z = (k-p)^2/m_K^2$):

$$M^{(1)} = -\frac{\alpha G_8}{4\pi} C^+(z)\overline{u}(k^-)(\not{k} + \not{p})v(k^+) \tag{6.13}$$

From this, it is straightforward to compute the decay distribution [27]:

$$\frac{d\Gamma}{dz} = \frac{G_8^2\alpha^2 m_K^5}{12\pi(4\pi)^4}\lambda^{\frac{3}{2}}(1,z,r_\pi^2)\Big(1-4\frac{r_\ell^2}{z}\Big)^{\frac{1}{2}}\Big(1+2\frac{r_\ell^2}{z}\Big)\Big|C^+(z)\Big|^2 \tag{6.14}$$

This is shown in Fig. 15. Integrating Eq. 6.14 from $4r_\ell^2$ to $(1-r_\pi)^2$ and using Eqs. 6.10, 6.11 we can get a prediction for the rates $K^+ \to \pi^+\ell^+\ell^-$ in terms of the

unknown constant w_+:

$$\begin{aligned} B(K^+ \to \pi^+ e^+ e^-) &= (3.15 - 21.1 w_+ + 36.1 w_+^2) \times 10^{-8} \\ B(K^+ \to \pi^+ \mu^+ \mu^-) &= (3.93 - 32.7 w_+ + 70.5 w_+^2) \times 10^{-9} \end{aligned} \tag{6.15}$$

One can then determine the constant w_+ from measurements of the rate, the spectrum, or both. A measurement of w_+ in $K^+ \to \pi^+ e^+ e^-$ has recently been reported [105] (AGS-777). Eq. 6.16 and Fig. 16 give the result of a simultaneous fit of the rate and spectrum shape:

$$\begin{aligned} B(K^+ \to \pi^+ e^+ e^-) &= (2.99 \pm 0.22) \times 10^{-7} \\ w_+ &= 0.89^{+0.24}_{-0.14} \end{aligned} \tag{6.16}$$

Eq. 6.15, which has not been imposed on the fit, is shown as a parabola in Fig. 16. It passes within about 1.5σ of the best fit values. As consistency checks, one can insert these values in turn into Eq. 6.15 yielding:

$$\begin{aligned} B(K^+ \to \pi^+ e^+ e^-) &= (1.30^{+1.24}_{-0.53}) \times 10^{-7} \\ w_+ &= \begin{cases} 1.20 \pm 0.033 & \text{or} \\ -0.62 \pm 0.033 \end{cases} \end{aligned} \tag{6.17}$$

This approach to $K^+ \to \pi^+ e^+ e^-$ seems quite promising, but more data is desirable. A somewhat larger data set with better systematics should be forthcoming from AGS-851. In the longer term, a much larger sample is promised from AGS-865 which is presently under construction.

Some model calculations of w_+ have found: 0.7 [37]; $0.98^{+0.78}_{-0.39}$ [38]; and 1.9 [36]. If we take as a typical number $w_+ = 0.89$ we then predict $B(K^+ \to \pi^+ \mu^+ \mu^-) = 3.07 \times 10^{-8}$. At present there is only an upper limit of $< 2.3 \times 10^{-7}$ on this decay

from AGS-787 [106], but a data set with sensitivity $< 10^{-8}$/ event is presently under analysis by this experiment.

A CP violating imaginary part of the constant w_+ would interfere with the absorptive part generated by the two pion intermediate state (Eq. 6.10), giving rise to a CP odd rate asymmetry [28]:

$$\left|\frac{\Gamma(K^+ \to \pi^+e^+e^-) - \Gamma(K^- \to \pi^-e^+e^-)}{\Gamma(K^+ \to \pi^+e^+e^-) + \Gamma(K^- \to \pi^-e^+e^-)}\right| \approx 0.01 \mathrm{Im} w_+ \approx 3 \times 10^{-5}\eta, \qquad (6.18)$$

where in the last step we have used the estimate of Ref. [28], $\mathrm{Im}w_+ \approx 0.003\eta$. This is too small to see in the near future.

We should comment on a possible parity violating asymmetry for these decays. It was pointed out in Ref. [107] that apart from the one-photon intermediate state, these processes have a short distance contribution from a Z intermediate state or from box diagrams as in Fig. 12. These new operators generate a second possible amplitude in addition to Eq. 6.13:

$$M^{(2)} = \frac{G_F}{\sqrt{2}} V_{us}\alpha\xi\overline{u}(k^-)(\not{k} + \not{p})\gamma_5 v(k^+) \qquad (6.19)$$

where we have used the lowest order χPT result $f_+ = 1$, $f_- = 0$. The constant ξ contains the short distance factors, it is given in Ref. [108]:

$$\xi = -1.4 \times 10^{-4} - \frac{Y(x_t)}{2\pi \sin^2\theta_W} A^2\lambda^4(1 - \rho - i\eta), \qquad (6.20)$$

where $Y(x_t)$ is given in Eq. 6.2. The first term in Eq. 6.20 corresponds to the charm-quark contribution with QCD corrections, and the second term to the top-quark contribution. If we denote by Γ_L, Γ_R, the rates for producing a left-handed (right-handed) μ^+ in $K^+ \to \pi^+\mu^+\mu^-$, then the interference of the two amplitudes generates

the parity violating observable [108]:

$$|\Delta_{LR}| = \left|\frac{\Gamma_R - \Gamma_L}{\Gamma_R + \Gamma_L}\right| \approx 2.3\mathrm{Re}\xi \tag{6.21}$$

A measurement of $|\Delta_{LR}|$ at the tenth of a percent level would provide valuable information on the CKM parameter ρ [108, 109]. Taking for example, $m_t = 140$ GeV, $\rho = -0.51$, Eq. 6.20 yields $|\Delta_{LR}| = 3.7 \times 10^{-3}$.

Finally, the authors of Ref. [110] have proposed some T-odd observables that can be studied in this decay. Unfortunately, in order to extract information on CP violation from this type of observable one must be able to reliably subtract unitarity effects. This usually involves a comparison of the two charge conjugated modes. In Ref. [110] it is found that the unitarity effects are small in asymmetries where the polarization of both the μ^+ and the μ^- are measured. Unfortunately such measurements are extremely difficult, due to the absorption of stopped μ^- before they can decay.

6.5 $K_1^0 \to \pi^0\ell^+\ell^-$

In the limit of CP conservation, the one-photon intermediate state contributes only to $K_1^0(k) \to \pi^0(p)\ell^+(k^+)\ell^-(k^-)$. The decay distributions can be predicted in terms of the constant w_S with Eq. 6.14 simply using:

$$C_1^0(z) = w_S + 2\phi_K(z) \tag{6.22}$$

Ignoring CP violation this results in rates and spectra for the decays $K_S \to \pi^0\ell^+\ell^-$. For the rates one finds [106]:

$$B(K_S \to \pi^0 e^+ e^-) = (3.07 - 18.7 w_S + 28.4 w_S^2) \times 10^{-10}$$

$$B(K_S \to \pi^0\mu^+\mu^-) = (6.29 - 38.9w_S + 60.1w_S^2) \times 10^{-11} \quad (6.23)$$

In general, χPT does not relate w_S to w_+ measured in the charged mode. Without additional input one must first measure w_S in one of the decays and then use it to predict the others. The prediction one finds in the literature is based on an additional assumption. The authors of Ref [28] demanded that the meson Lagrangian transform under $SU(3)_V$ as a pure octet in analogy with the quark electromagnetic penguin operator. That gave them the constraint $w_2 = 4L_9$ which then allowed them to predict:

$$w_S = w_+ + \frac{1}{6}\ln\left(\frac{m_\pi^2}{m_K^2}\right) \quad (6.24)$$

One must remember, however, that Eq. 6.24 is an assumption that goes beyond χPT, and that it is not satisfied in some models [38]. Sample model calculations of w_S yield: 0.3 [37]; $0.98^{+0.98}_{-0.59}$ [38]; and 1.4 [36].

6.6 $K_L \to \pi^0 e^+ e^-$

The decay $K_L \to \pi^0 e^+ e^-$ is significantly more complicated than the others we have been discussing. It has at least three different contributions that could be of the same size. The most interesting one, of course, is the direct CP violation. It originates in the diagrams of Fig. 17. The result has been computed in Refs. [11, 76, 111]. The full result has a complicated form, but Ref. [9] gives an approximate expression:

$$B(K_L \to \pi^0 e^+ e^-) = 0.32 \times 10^{-10}\eta^2 A^4 I(x_t) \quad (6.25)$$

with $I(x_t) \approx 0.73 x_t^{1.18}$. With present day bounds on all the parameters, Ref. [9] finds that this contribution to the rate ranges from about 10^{-12} to 2×10^{-11}.

There is also an indirect CP violating contribution, that is, one that proceeds via

the parameter ϵ in the mass matrix. Its contribution cannot be computed directly at present, and its precise value will only be known after a measurement of $K_S \to \pi^0 e^+ e^-$ is done. However, one can also use Eq. 6.22 to predict the indirect CP violation in the decay $K_L \to \pi^0 \ell^+ \ell^-$:

$$\begin{aligned} B(K_L \to \pi^0 \ell^+ \ell^-)_{ind} &= |\epsilon|^2 \frac{\tau_{K_L}}{\tau_{K_S}} B(K_S \to \pi^0 \ell^+ \ell^-) \\ B(K_L \to \pi^0 e^+ e^-)_{ind} &< 1.27 \times 10^{-12} \end{aligned} \tag{6.26}$$

The last result follows from using $w_+ = 0.89^{+0.24}_{-0.14}$, and Eq. 6.24 to obtain $w_S = 0.47^{+0.24}_{-0.14}$. With this range for w_S, the rate Eq. 6.26 varies by more than three orders of magnitude! In fact, for $w_S = 0.33$, Eq. 6.23 is not sufficiently accurate to calculate the rate. Given this large sensitivity to w_S, and the fact that we rely on Eq. 6.24, this result must be viewed with caution.

Finally, we can use the result for $K_L \to \pi^0 \gamma\gamma$, Eq. 5.9, to estimate the rate for the CP conserving part of the $K_L \to \pi^0 e^+ e^-$ amplitude. As usual [112], we will simply give the contribution from the absorptive part of the two photon intermediate state, depicted in Fig. 18. The contribution from $A(z,\nu)$ is suppressed by m_e and can be neglected. Using Eq. 5.9 we find a simple result if $B(z,\nu)$ is constant or if it depends only on z. We find [69]:

$$A_{abs}(K_L(p) \to \pi^0 e^+(k') e^-(k)) = -\frac{2\alpha^2}{3\pi} a_V \frac{G_8}{m_K^2} p \cdot (k - k') \overline{u} \not{p} v \tag{6.27}$$

After squaring and integrating over phase space, this gives a lower limit for the branching ratio from the CP conserving amplitude. With $-0.32 < a_V < 0.19$, Eq. 5.12, Ref. [70] quotes:

$$B_{CP}(K_L \to \pi^0 e^+ e^-) \leq 4.5 \times 10^{-13} \tag{6.28}$$

However, we must remember that this is only the absorptive part of the amplitude, so that the number is not really an upper bound. However, it is sufficiently smaller than the direct CP-violating component, that it will probably not impede efforts to extract the latter.

The fact that the direct CP-violating contribution to this decay is comparable or greater than the competing contributions, has sparked a good deal of experimental interest, including a number of dedicated searches. The present situation is summarized in Table 4.

Table 4: Summary of $K_L \to \pi^0 e^+ e^-$ Experiments

Experiment	Result	Status	Comments
NA31	$< 4 \times 10^{-8}$ [113]	finished	
FNAL-731	$< 7.5 \times 10^{-9}$ [114]	finished	
AGS-845	$< 5.5 \times 10^{-9}$ [115]	finished	
FNAL-799		analyzing	aims for $10^{-10} - 10^{-9}$ sensitivity
KEK-162		running	aims for 10^{-10} sensitivity
FNAL-799II		under construction	aims for $< 10^{-10}$ sensitivity

Although this decay has a good kinematic signature and its all-electromagnetic final state can be exploited in the design of experiments, it has unfortunately been found to suffer from the complication of a very difficult background. This stems from the processes shown in Fig. 19, i.e. radiative corrections to $K_L \to e^+e^-\gamma$, resulting in $K_L \to e^+e^-\gamma\gamma$. This was first observed by AGS-845 [116] in the course of their search for $K_L \to \pi^0 e^+ e^-$ [115]. The branching ratio was measured to be $(6.6 \pm 3.2) \times 10^{-7}$. The potency of this process as a background to $K_L \to \pi^0 e^+ e^-$, which had not previously been appreciated, was explicated by Greenlee [117]. Although there is no particular enhancement near $m_{\gamma\gamma} = m_{\pi^0}$, he found that the rate is sufficient

to make the extraction of a $K_L \to \pi^0 e^+ e^-$ signal at the 10^{-11} level problematic. For example, assuming an acceptance interval $\Delta m_{\gamma\gamma} = 5$ MeV, with highly optimized kinematic cuts that accept half the $K_L \to \pi^0 e^+ e^-$ events, the background enters at an equivalent branching ratio of 10^{-10}. If the cuts are further tightened to include only 10% of the signal events, the background is reduced by only about a factor 3. Further progress can be made if the resolution in $m_{\gamma\gamma}$ can be improved beyond the already very optimistic assumption used by Greenlee. Another approach to coping with this background is to attempt to subtract it, capitalizing on its smooth dependence upon $m_{\gamma\gamma}$. Of course this requires high statistics, which are not easy to come by at the required level of sensitivity.

6.7 $K_L \to \pi^0 \mu^+ \mu^-$

This decay mode, unlike the previous one, receives a substantial contribution from the two photon amplitude at $\mathcal{O}(p^4)$ since the muon mass is not negligible. This results in the possibility of substantial interference between the CP conserving and violating amplitudes. The amplitude can be written as:

$$M = \frac{\alpha}{4\pi} \mathrm{Re} G_8 \overline{u}(k^-)[i m_\mu h(z) - (\not{k} + \not{p}) g(z)] v(k^+) \tag{6.29}$$

The CP violating form factor is

$$g(z) = \epsilon[\mathrm{Re} w_S + 2\phi_K(z)] + i \mathrm{Im} w_S \tag{6.30}$$

whereas the CP conserving form factor is given by [28]:

$$h(z) = \frac{\alpha}{\beta z} \ln\left(\frac{1-\beta}{1+\beta}\right)\left[(z - r_\pi^2) F\left(\frac{z}{r_\pi^2}\right) - (z - 1 - r_\pi^2) F(z)\right] \tag{6.31}$$

where $\beta = \sqrt{1-4r_\mu^2/z}$. An interference between the two amplitudes generates a CP violating muon polarization. Taking for example $\mathrm{Re}w_S = 0.73$ and $\mathrm{Im}w_S = 0.001$ Ref. [28] finds an average transverse muon polarization $< \xi >= -0.37$ and a branching ratio $B(K_L \to \pi^0\mu^+\mu^-) = 6.3 \times 10^{-12}$. At present there is a preliminary limit $B(K_L \to \pi^0\mu^+\mu^-) < 1.7 \times 10^{-8}$ from FNAL-799 [80].

7 The experiments

In this section recent and current experiments are described and their results summarized. We exclude those results not directly related to the subject of this review (e.g. ϵ'/ϵ, rare π decay). We also discuss briefly new experiments now under construction.

Although these experiments span a range from 0 to greater than 100 GeV/c in beam momentum, they have certain important features in common. In each case the source of the kaons is the interaction of protons from a synchrotron with a fixed target. An intense secondary beam is created and transmitted to a decay region viewed by a detector. In most cases the kaons in the beam are outnumbered by other species of particles. These, along with the kaons which don't decay, have to either be transmitted through insensitive regions of the detector or somehow absorbed without doing irreparable mischief. All but one of the experiments use magnetic spectrometers to measure the momenta of the charged decay products. The neutrals are measured in calorimeters of various types. Scintillator hodoscopes and particle identification devices such as atmospheric Čerenkov counters and muon filters provide triggering capability.

The experiments all exploit common K decay modes for calibration and normalization. Very often the same modes used in this way are sources of the backgrounds that have to be confronted. These backgrounds must be fought both at the trigger and analysis level. Particle identification, timing, geometrical, and kinematic selection reduce the large data samples collected to manageable size. Except in one case, the signal events are completely reconstructed. Typically the last stage of the analysis is a two-dimensional plot of effective mass of the final state particles versus a variable which reflects their direction. The signal is sought in the region of the K mass and

small angle with respect to the beam (see e.g. Fig 1).

All the experiments study at least one "tune up" process on which to demonstrate their ability to detect rare decays. This is a decay topologically similar to the primary object of the experiment, but somewhat more copious. These are often of considerable interest in themselves. For experiments seeking $K_L \to \mu e$ there is $K_L \to \mu^+\mu^-$; for $K^+ \to \pi^+\mu^+e^-$ there is $K^+ \to \pi^+e^+e^-$; for $K^+ \to \pi^+\nu\bar{\nu}$ there is $K^+ \to \pi^+\gamma\gamma$; for $K_L \to \pi^0e^+e^-$ there is $K_L \to \pi^0\gamma\gamma$ or $K_L \to \gamma\gamma ee$.

7.1 AGS-845

Fig. 20 is a plan view of the apparatus designed by a BNL-Yale collaboration to perform the world's first dedicated $K_L \to \pi^0e^+e^-$ experiment, AGS-845. It was optimized to detect all-electromagnetic K_L decays (the lead filter and hodoscope at the rear were used to veto penetrating particles). Several million K_L (along with $\sim 3 \times 10^8$ neutrons) entered the 6-meter evacuated decay region during each 1-second AGS spill. A single-magnet drift chamber spectrometer measured $e^\pm$ momenta and a lead glass Čerenkov array detected γs. The latter also served to measure the $e^\pm$ energy. Comparing this energy with the $e^\pm$ momentum distinguishes these particles from pions and muons. A 2-m long atmospheric hydrogen Čerenkov counter completed the particle identification.

The expected potential backgrounds to $K_L \to \pi^0e^+e^-$ were $K_L \to 2\pi^0$ or $3\pi^0$ in which two of the π^0 undergo Dalitz decays, and accidental coincidences of 2 γs with $Ke3$ decays wherein the π is mistaken for an electron. AGS-845 was able to eliminate all background and set a 90% c.l. limit of $B(K_L \to \pi^0e^+e^-) < 5.5 \times 10^{-9}$. This represents a large improvement in our knowledge of this process, but falls short by at least two orders of magnitude of the Standard Model prediction for this CP-violating

decay. However, as discussed in subsection 6.6 , in the process of setting this limit, AGS-845 discovered a background which may prevent this process from ever fulfilling its potential in the study of CP-violation, i.e. $K_L \to e^+e^-\gamma\gamma$.

AGS-845 also made major contributions to the study of $K_L \to e^+e^-\gamma$ and $K_L \to e^+e^-e^+e^-$. This experiment is now completed. Its results are summarized in Table 5

Table 5: Results of AGS-845

Mode	Result	Comments
$K_L \to \pi^0 e^+e^-$	$< 5.5 \times 10^{-9}$ [115]	search for new scalars non-S.M. CP-violation future: S.M. CP-violation
$K_L \to e^+e^-\gamma$	$(9.1 \pm 0.4^{+0.6}_{-0.5}) \times 10^{-6}$ [78] $\alpha_{K^*} = -0.28 \pm 0.083^{+0.054}_{-0.034}$	c.f. $(9.6 \pm 0.4) \times 10^{-6}$ (theory) i.e. something besides ρ needed
$K_L \to e^+e^-\gamma\gamma$	$(6.6 \pm 3.2) \times 10^{-7}$ [116]	c.f. 5.8×10^{-7} for $k^* > 5$MeV background to $K_L \to \pi^0 ee$
$K_L \to e^+e^-e^+e^-$	$(3.04 \pm 1.24 \pm 0.26) \times 10^{-8}$ [85]	c.f. 3.6×10^{-8} background to $K_L \to e^+e^-$

7.2 KEK-162

KEK-162, shown in Fig. 21, has been built by a KEK-Kyoto collaboration to pursue $K_L \to \pi^0 e^+e^-$ to $\sim 10^{-10}$ [118]. It is quite similar in concept to AGS-845, with adaptations to the lower beam energy such as a more compressed layout, nitrogen rather than hydrogen in the Čerenkovs, etc. The main innovation is the electromagnetic calorimeter constructed of undoped CsI, a fast, bright scintillating crystal with excellent resolution. This calorimeter is designed to achieve 2% rms at 1 GeV. Most

of the light in pure CsI is emitted with decay time < 30 nsec. Fast time response is crucial since the proponents of KEK-162 plan to expose their detector to an order of magnitude higher K_L flux than was seen by AGS-845. The daunting rates also motivate the design of drift chambers which feature small cells, fast gas and custom TDCs.

This experiment is currently setting up.

7.3 FNAL-731/799

FNAL-731 was originally built to measure ϵ'/ϵ in $K^0 \to 2\pi$ decays. In spite of being highly optimized for this purpose, it has produced several estimable rare decay results. The apparatus, built by a Chicago/Elmhurst/FNAL/Princeton/Saclay group, is shown in Fig. 22. Two nearly parallel K_L beams entered a 37m long evacuated decay region. A B_4C regenerator was shuttled between the beams on a pulse to pulse basis to provide K_S decays. A plane of thin trigger scintillators was situated approximately halfway down the vacuum decay vessel. Following the downstream decay region was a 4-station drift chamber dipole spectrometer, additional trigger hodoscope planes and an 804-element lead glass Čerenkov array. Downstream of this were photon vetoes, a 3m thick steel muon filter and, finally, muon veto hodoscopes. An extensive photon veto system bordered the acceptance.

A comparison with detectors designed for lower energy beams is instructive. The FNAL-731 spectrometer was relatively more compact than the typical BNL or KEK detector and so had larger acceptance at the cost of worse charged track momentum resolution. Conversely, the resolution for photons was better for the higher energy experiment because of the $1/\sqrt{E}$ behavior of the stochastic resolution term in lead glass. In FNAL-731, the decay region was shorter relative to the mean K_L decay

length, diluting to some extent the advantage in acceptance. One major advantage of FNAL-731 was the clean beam in which the neutrons were of the same order as the K_L instead of ten or fifty times more numerous. This kept the detector rates relatively low.

A number of rare decay results were obtained from the seven-month 1987-88 run. Subsequently, the detector was reconfigured for the first stage of FNAL-799, a dedicated rare decay experiment. These changes included the removal of the regenerator, an upstream absorber, and the trigger scintillator plane in the vacuum decay vessel. These resulted in a large gain in sensitivity/ incident proton. The number of incident protons/spill was also increased, so that the overall sensitivity/spill increased by more than an order of magnitude. Other modifications were an additional muon hodoscope plane and the development of an online processor which allowed the use of drift chamber information in the second level trigger. For a small portion of this run, a pre-shower detector was installed upstrcam of the lead glass array in order to improve the sensitivity to $K_L \to \pi^0\gamma\gamma$. The collaboration was also modified to consist of Chicago, Elmhurst, FNAL, Illinois, Colorado, UCLA, Rutgers, and Osaka. The experiment ran for 10 weeks in late 1991 and early 1992.

The results of FNAL-731/799 on rare K decays thus far are summarized in Table 6. The last three (preliminary) results come from the first stage of FNAL-799. This run is also expected to yield new results on $K_L \to \pi^0 e^+e^-$, $K_L \to \pi^0\nu\overline{\nu}$, and $K_L \to \pi^0\gamma\gamma$, as well as the first results of this program on $K_L \to e^+e^-\gamma$, $K_L \to \pi\pi ee$, $K_L \to \mu\mu ee$, $K_L \to ee\gamma\gamma$, $K_L \to \pi^0\mu e$ and other rare decays.

The second stage of FNAL-799 is expected to begin taking data in 1994 or 1995. The experiment will be moved and a new beam line will be built which should allow higher primary intensity. The lead glass array will be replaced with one consisting

Table 6: Results of FNAL-731/799

Mode	Result	Comments
$K_L \to \pi^0 e^+ e^-$	$< 7.5 \times 10^{-9}$ [114]	search for new scalars, CP viol.
$K_S \to \pi^0 e^+ e^-$	$< 4.5 \times 10^{-5}$ [119]	needed for interpreting $K_L \to \pi^0 ee$
$K_L \to \pi^+ \pi^- \gamma$	$(3.19 \pm 0.16) \times 10^{-5}$ [92]	direct emission, $k^* > 20$MeV
$K_L \to \pi^0 \gamma\gamma$	$(1.86 \pm 0.60 \pm 0.60) \times 10^{-6}$ [71]	spectrum agrees with χPT
$K_L \to \pi^0 \nu\overline{\nu}$	$< 2.2 \times 10^{-4}$ [63]	CP-violating
$K_L \to \pi^0 \mu^+ \mu^-$	$< 1.7 \times 10^{-8}$ [80]	preliminary
$K_L \to e^+ e^- e^+ e^-$	$(4.17 \pm 0.83) \times 10^{-8}$ [87]	28 events
$K_L \to \mu^+ \mu^- \gamma$	$(3.88 \pm 0.32) \times 10^{-7}$ [80]	167 events

of undoped CsI. The trigger planes and photon vetoes will also be upgraded. With these improvements, the experiment expects to obtain sensitivities $\leq 10^{-10}$ for many rare decays.

7.4 NA31

NA31, although taking an approach to measuring ϵ'/ϵ which is radically different from that of FNAL-731, has had similar success in the pursuit of rare K decay modes. The detector, shown in Fig. 23 was built by a collaboration of CERN, Dortmund, Edinburgh, Mainz, Orsay, Pisa, and Seigen. The most striking difference of this detector from the others described in this section is the absence of a magnet. Charged particle trajectories are determined by two planes of drift chambers, but their energies are measured by electromagnetic and hadronic calorimeters. The electromagnetic calorimeter, which is of the lead/liquid Argon type, has extremely good energy and position resolution. It is finely granulated and can distinguish two photons from one if

they are separated by more than 1 cm. This configuration results in good acceptance for many rare decays, good energy resolution for electromagnetic particles, but relatively poor energy resolution for pions (e.g. the fractional resolution on a 50 GeV/c pion is $\sim$ 9%). Other disadvantages of this configuration, such as the difficulty of distinguishing final state particles which are close in direction, are somewhat mitigated by the fine segmentation of the electromagnetic calorimeter. Similarly the lack of an energy/momentum comparison for distinguishing electrons from heavier particles was partially alleviated by the longitudinal segmentation of the electromagnetic calorimeter and the by presence of the hadronic calorimeter. In addition there were dedicated particle identification systems such as a transient radiation detector and a muon filter. Completing the apparatus were triggering hodoscopes and photon veto counters.

NA31 took data in 1986, 1988, and 1989. The rare decay results it obtained are summarized in Table 7.

Table 7: Results of CERN NA31

Mode	Result	Comments
$K_L \to \pi^0 e^+ e^-$	$< 4 \times 10^{-8}$ [113]	search for new scalars
$K_L \to \pi^0 \gamma\gamma$	$(1.7 \pm 0.3) \times 10^{-6}$ [70]	spectrum agrees with χPT
$K_S \to \gamma\gamma$	$(2.4 \pm 1.2) \times 10^{-6}$ [68]	rate agrees with χPT
$K_L \to e^+ e^- \gamma$	$(9.2 \pm 0.5 \pm 0.5) \times 10^{-6}$ [79]	cf. theory at $(9.1 - 9.5) \times 10^{-6}$
	$\alpha_K = -0.28 \pm 0.13$	i.e. something beyond ρ needed
$K_L \to e^+ e^- e^+ e^-$	$(4 \pm 3) \times 10^{-8}$ [84]	First observation, 2 events
$K^+ \to \pi^+ X^0$; $X^0 \to e^+ e^-$	$< 6 \times 10^{-7}$ to $< 10^{-8}$ [120]	limits depend on m_X and τ_X

NA48, a successor to NA31, is now under construction. It features a fast liquid Krypton-based electromagnetic calorimeter and a magnetic spectrometer for charged

particle momentum measurement. It should have an order of magnitude better sensitivity than NA31 to most rare decays.

7.5 AGS-777/851

Fig. 24 shows the apparatus employed by a BNL/PSI/Washington/Yale group in AGS Experiments 777 and 851. The primary objects of these were respectively a search for $K^+ \to \pi^+\mu^+e^-$ and a study of $K^+ \to \pi^+e^+e^-$. Other processes sought or studied in these experiments were $\pi^0 \to \mu^+e^-$, $\pi^0 \to e^+e^-$, and $A^0 \to e^+e^-$ (where A^0 is a new light particle).

A 6 GeV/c positive beam containing about 10^7 K^+/AGS pulse impinged on a 5m evacuated tank, wherein about 10% of the K^+ decayed. As the beam was unseparated, K^+ constituted only $\sim$ 5% of the flux, the majority consisting of a roughly equal mixture of π^+ and protons. The first element of the detector was a dipole run at a p_T kick of 155 MeV/c. This served to remove the daughter products from the hot beam region and to separate them according to their charge. The beam then passed through holes and deadened regions in subsequent detector elements. Downstream of the first dipole was an MWPC spectrometer with four measuring stations. Two preceded and two followed a dipole run at $\Delta p_T \sim 150$ MeV/c with sense opposite that of the first dipole. Situated between each pair of measuring planes was an atmospheric gas Čerenkov counter. Downstream of the spectrometer were triggering hodoscopes, a lead-scintillator sandwich electromagnetic shower detector, and an iron/proportional tube chamber muon identifier.

Since positive muons only were sought, the muon identifier needed to cover only the right (+) side. This was one of several optimizations made possible by confining the experiment to the $\pi^+\mu^+e^-$ charge combination. On the left, where electron purity

was more important than efficiency, H_2 was used as $\check{C}$ counter gas; whereas on on the right, where positrons had to be efficiently vetoed, CO_2 was used instead. The choice of final state was also of great benefit to the trigger, since e^- are far less common in K^+ decay than are e^+ (the most copious source of e^+ in K^+ decay is $K^+ \to \pi^0 e^+ \nu$ with branching ratio 0.0482; the most copious source of e^- is $K^+ \to \pi^+\pi^0; \pi^0 \to e^+e^-\gamma$ with product branching ratio 2.54×10^{-3}).

The most dangerous backgrounds to $K^+ \to \pi^+\mu^+e^-$ stem from $K^+ \to \pi^+\pi^+\pi^-$ and $K^+ \to \pi^+\pi^0$; $\pi^0 \to \gamma e^+e^-$ decays. In the former, this can occur through various combinations of pion decay and misidentification. There are also several ways in which the latter process can mimic $K^+ \to \pi^+\mu^+e^-$, the worst being the case where the π^+ is mistaken for a μ^+, and the e^+ for a π^+. Since in this instance, a pion mass is misattributed to the e^+, the measured 3-body effective mass can exceed M_{K^+}. Thus the usefulness of kinematic rejection is limited, so that powerful particle identification techniques are required.

$K^+ \to \pi^+\pi^+\pi^-$ and $K^+ \to \pi^+\pi^0$; $\pi^0 \to \gamma e^+e^-$ decays were not totally inimical to this experiment: they also served to calibrate and normalize it. The former process was used to evaluate the performance of the particle identification systems, design the geometrical reconstruction and kinematic fitting procedures, etc.

For AGS-851, the $\check{C}$ gas on the right side was changed from CO_2 to H_2. The $K^+ \to \pi^+\mu^+e^-$ trigger was dropped, and the requirement that the π^+ be detected on the right was lifted.

This program finished taking data in 1989. The AGS-777 data analysis is now complete, that of AGS-851 continues. The results of these experiments thus far on rare K decay are summarized in Table 8.

Subsequent to the completion of this program, the AGS Booster came on line, and

Table 8: Results of AGS-777/851

Mode	Result	Comments
$K^+ \to \pi^+ e^- \mu^+$	$< 2.1 \times 10^{-10}$ [52]	$M_H > 57$ TeV
$K^+ \to \pi^+ e^+ e^-$	$(2.75 \pm 0.23 \pm 0.13) \times 10^{-7}$ [105]	500 events
	$\lambda = 0.105 \pm 0.035 \pm 0.015$	suggests $K_S \to \pi^0 e^+ e^-$ small
$K^+ \to \pi^+ X^0$; $X^0 \to e^+ e^-$	$< 1.1 \times 10^{-8}$ [105]	$150 < m_{ee} < 340$MeV
	$< 4.5 \times 10^{-7}$ [121]	$100\text{MeV} < m_{ee}$
		for $\tau_X < 10^{-13}$ sec.

the prospect of much greater available K^+ flux motivated the proposal of a successor experiment, AGS-865. The institutions collaborating are BNL, INR-Moscow, Dubna, New Mexico, PSI, Basel, Pittsburgh, Tbilisi, Yale, and Zurich. Since AGS-777 was limited primarily by beam-associated background, a new beam has been designed to yield seven times more K^+ with no greater random rates than those of its predecessor. The detector, shown in Fig. 25, is very similar to that of AGS-777. The geometrical acceptance has been increased by about a factor three with respect to that of the earlier detector, however, and the muon identifier covers both sides of the apparatus. Improvements to the background rejection power of the experiment include a fourth PWC plane at each measuring station, the use of aluminum HV wires to reduce multiple scattering, an upgraded electromagnetic calorimeter, finer longitudinal sampling in the muon identifier, etc.

The increases in the K^+ flux, the geometric acceptance, the triggering and reconstruction efficiencies and in running time are expected to yield a factor 70 improvement in the sensitivity of AGS-865 over that of AGS-777/851. This would allow a $K^+ \to \pi^+ \mu^+ e$ sensitivity of 1.3×10^{-12}/event for example. At the same time samples of tens of thousands of decays such as $K^+ \to \pi^+ e^+ e^-$, $\pi^+ \mu^+ \mu^-$ and $\pi^+ \gamma\gamma$ should

be accumulated. There are also a number of other interesting processes which could be studied with special runs and/or modest upgrades to the detector. These include CP-violating asymmetries in $K^{\pm} \to \pi^{\pm}\pi^{+}\pi^{-}$, T-violating polarization in $K^{+}_{\mu 3}$ decay, and parity-violating μ^{+} polarization asymmetry in $K^{+} \to \pi^{+}\mu^{+}\mu^{-}$.

7.6 KEK-137

KEK-137, a Tohoku/Tokyo/Kyoto/KEK collaboration, is one of the two most recent $K_L \to$ 2-lepton experiments. These experiments have had to meet very significant challenges to achieve sensitivities significantly better than 10^{-10}/event. The fraction of K_L that decay and can be accepted in a practical sized apparatus is typically $\sim 1 - 2 \times 10^{-3}$. To get enough K_L, the experiments have to work in the forward or near-forward direction where the neutron flux is $10 - 100$ times higher than the K_L. This translates into neutral beam fluxes of order 10^9 per spill. Chamber and trigger plane rates are typically many MHz, and yet they must perform extremely well because to reject background, searches for $K_L \to \mu e$ must have excellent kinematic resolution. Since the primary background, K_{e3} decay followed by $\pi \to \mu$ via decay or misidentification, occurs at the few % level and is topologically identical to the signal, particle identification power is of limited value. Most of the background rejection comes from kinematic and geometrical cuts. One exploits the fact that in the absence of measuring errors, the e "μ" pairs have effective masses less than $M_K - 8.4$ MeV. Both recent experiments kinematically and geometrically over-constrain their events. The momentum of each track is measured twice spectrometrically and in the case of muon candidates, once more via range.

Here again, the background decays (K_{e3} and for the $K_L \to \mu^{+}\mu^{-}$ case, $K_{\mu 3}$) are not all bad. In this case they serve to calibrate the particle identification devices.

The relatively copious $K_L \to \pi^+\pi^-$ are used to normalize the experiments as well as to calibrate the spectrometers.

The double-arm spectrometer used by KEK-137 to search for $K_L \to \mu e$, $K_L \to e^+e^-$, $K_L \to \mu^+\mu^-$, and other rare decay modes is shown in Fig. 26. A beam of $\sim 10^7$ K_L/pulse was made by directing a $1 - 2 \times 10^{12}$ proton beam from the KEK PS onto a 12 cm-long Cu target. The beam passed through a number of collimators and sweeping magnets into a 10m-long evacuated decay volume. About 8% of the K_L between 2 and 8 GeV decayed in this volume. The rest of the neutral beam, which included about 10^9 neutrons and γs per spill, was conducted in vacuum between the two spectrometer arms. The p_T kick on each arm was 238 MeV/c, divided equally between the two dipoles. Daughter tracks in the Jacobean peak of the desired two-body reactions were consequently bent approximately parallel to the arm axes. Imposing a parallelism requirement greatly reduced the relative number of three-body decays accepted by the trigger. The resolution of this spectrometer for the calibration $K_L \to \pi^+\pi^-$ decays was 1.3 MeV/c^2. As mentioned above, there were separate momentum measurements by the front and rear sections of the spectrometer and a third, coarse, measurement via a muon range array. The multiple measurements were primarily aimed at rejecting pions which decayed to muons in the detector. These were more dangerous than punch-through pions since the decay could disturb the momentum measurement as well as the particle identification. Electrons were identified via atmospheric Čerenkovs filled with atmosphere, and with planes of lead-scintillator shower counters.

This experiment ran for a period of about $2\frac{1}{2}$ years, finishing data-taking in May, 1990. The results are summarized in Table 9.

Table 9: Results of KEK-137

Mode	Result	Comments
$K_L \to \mu e$	9.7×10^{-11} [41]	
$K_L \to e^+e^-$	1.6×10^{-10} [41]	one event in signal region
$K_L \to \mu^+\mu^-$	$(7.9 \pm 0.6 \pm 0.3) \times 10^{-9}$ [100]	178 events
$K_L \to e^+e^-e^+e^-$	$(6 \pm 2 \pm 1) \times 10^{-8}$ [86]	partial reconstruction

7.7 AGS-791

The second of the two-lepton experiments was AGS-791, a collaboration of UC-Irvine, UCLA, LANL, U of Pennsylvania, Stanford, Temple, and William & Mary. The detector, shown in Fig. 27, had many similarities to that of KEK-137: a double arm - double measuring spectrometer, electron ID via atmospheric Č counter plus electromagnetic shower counter, muon range array, etc. However there were significant differences. The primary beam was about twice that of the KEK accelerator, and the daughter tracks entering the apparatus were roughly twice as stiff as those of KEK-137. Thus the muon identifier was considerably thicker and the Čerenkov needed to be filled with a gas of lower index of refraction (He-Ne mixture vs air). In E791, the arms shared their spectrometer magnets, and these were set to opposite polarities (the p_T kick of each was $\sim$ 300 MeV/c). Other differences from KEK-137 included a shorter decay volume but larger geometrical acceptance, lead glass instead of lead-scintillator sandwich counters, finer sampling in the muon identifier, etc. The K_L flux impinging on the detector ($\sim 5 \times 10^7$/ 1-second-spill) was the highest yet used in a K_L decay experiment, and put severe requirements on the triggering and data acquisition systems.

The analysis flow was also similar to that of their KEK competitors. Normaliza-

tion and spectrometer calibration was done with $K_L \to \pi^+\pi^-$ decays, calibration of particle identification devices via K_{e3} decays.

In the course of analyzing the experiment, an unanticipated potential background to $K_L \to \mu e$ was discovered. This was $K_L \to \pi^\pm e^\mp \nu$ decay in which both charged daughters were misidentified (π as e, e as μ). Since a much higher mass is attributed to the electron, the reconstructed two-body effective mass can span the region of the signal. Fortunately the particle identification power of the experiment was sufficient to reduce this background to $\leq 10^{-12}$.

The data was taken in three runs over the period 1988-1990. The sensitivities reached were the highest ever attained in a K decay experiment. The results are summarized in Table 10.

Table 10: Results of E791

Mode	Result	Comments
$K_L \to \mu e$	3.3×10^{-11} [42]	Most sensitive K experiment yet
$K_L \to e^+e^-$	4.7×10^{-11} [42]	
$K_L \to \mu^+\mu^-$	$(7.0 \pm 0.5) \times 10^{-9}$ [122]	718 events

After the completion of data taking on AGS-791, a collaboration of UC-Irvine, Stanford, Temple, Texas, and William & Mary proposed a successor experiment, AGS-871. A schematic of their detector is show in Fig. 28. Although many of the elements of the previous experiment will be reused, there are important differences in the design. The most striking of these is that instead of allowing the beam to pass unimpeded between the arms of the detector as in AGS-791, here it is stopped by a plug in the first spectrometer magnet. This allows larger geometric acceptance and lower rates in the downstream chambers and particle identification devices, at the expense of some increase in rates in the chambers near the plug. To help cope

with this, the forward drift chambers will be replaced by high-rate straw trackers. A second important change is an adjustment in the spectrometer magnet fields so that there is a net Δp_T of 220MeV/c, to bend the two-body decay daughter tracks parallel to the beam, allowing a faster, more effective first level trigger and simpler Čerenkov optics. The over-bend (Δp_T = 440 - 220MeV/c) also leads to about a 20% improvement in the two-body effective mass resolution. Other changes include a longer decay volume, increased chamber redundancy, the use of H_2 in the Čerenkov, better muon range resolution, and upgraded triggering and data acquisition systems. The K_L beam line will be lengthened to allow improved collimation.

Assuming a four-fold increase in the available AGS intensity, the overall improvement in sensitivity expected is about a factor 20. This implies single event sensitivities better than 10^{-12}. Thus a sample of over 10,000 $K_L \to \mu^+\mu^-$ will be accumulated as well as a few examples of $K_L \to e^+e^-$.

7.8 AGS-787

The apparatus built by a BNL/Princeton/TRIUMF collaboration to carry out the first stage of AGS-787 is shown in Fig. 29. The solenoidal configuration, unique among the detectors described in this section, was mandated by the problematic signature of $K^+ \to \pi^+\nu\overline{\nu}$. A π^+ is hardly a novelty in the final state of a K^+ decay and since it alone of the three daughters is detectable, one has only the weak kinematic constraint $p_\pi \leq (M_K^2 - M_\pi^2)/2M_K$. What makes the experiment possible is the good signature of the *backgrounds*. The leading K^+ decays by far are $K_{\pi 2}$ and $K_{\mu 2}$, each of which features a single charged track of unique cm momentum (205 MeV/c and 236 MeV/c respectively). Thus with good kinematic resolution one can reject the two-body backgrounds by a large factor. In addition one can veto on the photons from

$K_{\pi 2}$ and on the identity of the muon in $K_{\mu 2}$. Other potential sources of background (e.g. $K^+ \to \mu^+ \nu\gamma$, $K_{\mu 3}$, $K_{\pi 3}$, etc.) are less copious and all have combinations of at least two of the three 'handles' mentioned above: kinematic signature, detectable extra tracks, and charged daughter $\neq \pi^+$.

Like all previous searches for $K^+ \to \pi^+ \nu\bar{\nu}$, AGS-787 employs a stopping K^+ beam. This allows direct access to the kinematic features of signal and background. Other advantages are the feasibility of large geometric acceptance and veto hermiticity, the powerful particle identification techniques available at low energy, and the very good ratio of useful K^+ decays to unwanted beam particles. The latter results from the pure separated beams which are practical at low energies and the fact that one can stop a relatively large fraction of a low energy K^+ beam. This is quite important in an experiment in which the signature is a single unaccompanied π^+.

In the design of AGS-787, great efforts were made to minimize the presence of "dead" material. Energy deposited or interactions undergone in such material can compromise the veto or confound the particle identification. For example, a π^+ whose scatter in the stopping target goes undetected can defeat the kinematic rejection of $K_{\pi 2}$, if the π^0 decay photons are also missed.

The background due to such "down-shifted" $K_{\pi 2}$ decays led the experimenters initially to concentrate on the kinematic region with $p_{\pi^+} > 205$ MeV/c where the only sources of π^+ more copious than the signal are are $K^+ \to \pi^+ e^+ e^-$ and $K^+ \to \pi^+ \gamma\gamma$. These have branching ratios of $\sim 3 \times 10^{-7}$ and $< 10^{-6}$ respectively. The rejection of electromagnetic particles is extremely good in AGS-787 (e.g. only 1 or 2 of 10^6 π^0 are missed), so that these do not constitute a significant problem. In fact in this region, the most difficult backgrounds have proved to be $K^+ \to \mu^+ \nu$ with muons which interact or enter the dead regions of the detector before making their range.

Thus far, AGS-787 has operated at K^+ stopping rates up to $\sim 300,000/$ beam spill. To obtain this rate, about $1.5M$ 800 MeV/c K^+ from the LESB1 were directed onto a BeO degrader 54cm in length. The K^+ were accompanied by an approximately equal number of protons and by about $3M$ π^+. The K^+ emerged from the degrader with about 100 MeV of energy and came to rest in a highly segmented scintillating fiber target [123]. K^+ were required to decay at least 2 nsec after stopping to be accepted. Charged daughters which leave the target within about 30^0 of the plane transverse to the beam were tracked a cylindrical drift chamber onto which a field of 1T was imposed. These then entered a cylindrical array of plastic scintillation counters and PWCs (range stack) which served to measure their residual energy and range. The range stack was read out on both upstream and downstream ends so that the detected particles could be localized in three dimensions. The counters were instrumented with 500 MHz transient recorders which recorded all scintillation light over an interval of about 10 μsec. This allowed the characteristic $\pi \rightarrow \mu \rightarrow e$ sequence to be observed in the stopping counter. This is a powerful signature for π^+, which was defeated in < 1 out of 10^5 cases. Comparisons among range, energy, and momentum of the daughter track also constitute a very effective particle identification technique. Surrounding the range stack was a cylindrical array of lead-scintillator sandwich counters (barrel veto) which veto gammas in the central region. The gamma veto was completed by lead-scintillator sandwich end-cap counters.

Calibration and normalization of the experiment was done primarily via $K_{\pi 2}$ and $K_{\mu 2}$.

The results of AGS-787 are summarized in Table 11. These results are based on data collected in an 1988 engineering run and in the first major physics run (1989). There were runs of about equal sensitivity in 1990 and 1991. During the 1989 run it

Table 11: Results of E787

Mode	Result	Comments
$K^+ \to \pi^+ X^0$	$< 1.7 \times 10^{-9}$ [59]	familon, etc. search;
$K^+ \to \pi^+ \nu\bar{\nu}$	$< 5.2 \times 10^{-9}$ [59, 60]	constrains new physics
$K^+ \to \pi^+ \mu^+ \mu^-$	$< 2.3 \times 10^{-7}$ [106]	should be discovered in '89-'91 data
$K^+ \to \mu^+ \nu \mu^+ \mu^-$.	$< 4.1 \times 10^{-7}$ [106]	Higgs hunting ground
$K^+ \to \pi^+ \gamma\gamma$	$< 10^{-6}$ [75]	should be discovered in '89-'91 data
$K^+ \to \pi^+ X^0$; $X^0 \to \gamma\gamma$	$\leq 10^{-7}$ [75]	$m_{X^0} \leq 90$ MeV/c^2

was found that the instrumentation of the experiment was sufficient to reject background in the kinematic region below the $K_{\pi 2}$ as well as above it. Thus far the acceptance in the two kinematic regions has proved to be about equal.

In 1989 a major upgrade of the beam and detector was approved with the aim of reaching the 10^{-10} sensitivity level necessary to probe the Standard Model predictions for $K^+ \to \pi^+ \nu\bar{\nu}$. The collaboration was augmented by groups from INS/Tokyo and KEK. A new low energy separated beam (LESB3) which provides much improved K^+ flux and purity was constructed. This beam was designed to exploit the AGS upgrade to deliver up to 1.5×10^7 800MeV/c K^+ with a K^+/π^+ ratio of 2/1. Extensive detector improvements were also undertaken. These include upgrades to the K^+ and π^+ measuring devices, the photon vetoes, the electronics and data acquisition system. A new, brighter, stopping target was constructed out of close-packed 5mm square cross-section scintillating fibers. A new central drift chamber with only $\frac{1}{5}$ the mass of its predecessor is being constructed. In the range stack, the scintillator read out granularity is being increased and the embedded proportional chambers are being replaced by far less massive straw chambers. Pure CsI end cap vetoes are being built to replace the current lead-scintillator sandwich devices. A pure CsI liner will

be installed inside the current barrel veto. A number of supplementary vetoes will increase the hermiticity of the the detector. Transient recorders will be installed on the target and on all vetoes. Finally, a new trigger and data acquisition system, capable of taking ten times the previous rate is being developed.

8 Conclusions

The study of rare kaon decays continues to be a crucial arena for the testing of electroweak theory. The decays $K \to \pi\nu\overline{\nu}$, can be computed reliably, and their study will yield valuable information on the CKM parameters ρ and η, that will eventually permit us to test the three generation structure of the standard model. Other rare decays that are sensitive to these parameters are $K_L \to \pi^0\ell^+\ell^-$, $K^+ \to \pi^+\ell^+\ell^-$ and perhaps $K_L \to \mu^+\mu^-$ as well. Of course, these modes also constitute ideal candidates to search for new physics in the form of deviations from the standard model expectations. This is particularly true for CP violation.

The search for the forbidden lepton flavor violating decays constitutes one of the simplest and most cost-effective ways to constrain interactions beyond the minimal standard model. The present level of sensitivity of these experiments is already testing energy scales that we will not be able to probe directly for many years.

In the process of searching for the very rare and forbidden decay modes of the K_L and the $K^\pm$, large samples of other, less rare, decays are being collected. Among them are the radiative decays that are dominated by long distance contributions. Their detailed understanding is crucial in the effort to use modes like $K_L \to \pi^0 e^+ e^-$ or $K_L \to \mu^+\mu^-$ to measure the parameters ρ and η. These radiative decay modes are also interesting in their own right, in that they allow us to test the framework

of chiral perturbation theory, and in that context they provide information on the non-perturbative aspects of the strong interactions.

There are a number of accelerator developments under way to augment the supply of kaons for these studies. The AGS upgrade is well along. It will provide a fourfold increase in what is already the world's most intense source of kaons. Construction has begun on the Fermilab Main Injector which promises to provide a source of comparable intensity at higher energy. Construction of the DAΦNE ϕ storage ring at Frascati is also under way. This facility will provide a somewhat less intense source of kaons, but one in which the initial state of the kaons can be tightly controlled. In the somewhat more distant future, facilities such as TRIUMF Laboratory's proposed KAON complex can provide further large increments in sensitivity.

The field of rare kaon decays has provided many discoveries of the highest importance. From an historical perspective, the reach in sensitivity of the present and near-future experiments is quite large. It would be very surprising if further discoveries did not await these initiatives.

Acknowledgements

We wish to acknowledge useful conversations and other assistance from W. Bardeen, A. Barker, L. Bergstrom, A. Buras, H. Y. Cheng, S. Dawson, J. F. Donoghue, C. Q. Geng, E. Golowich, T. Han, X. G. He, J. Kambor, S. Kettell, A. El-Khadra, H. Ma, W. Marciano, W. Morse, K. Ohl, J. Prades, C. Quigg, E. Ramberg, S. Willenbrock, B. Winstein, T. Yamanaka, and M. Zeller.

This work was supported by the U.S. Department of Energy under contracts DE-AC02-76CH00016 and DE-AC02-76CH03000.

References

[1] D. Bryman, *Int. Jour. of Mod. Phys.* **A4** 79 (1989).

[2] J. Hagelin and L. Littenberg, *Prog. Part. Nucl. Phys.* **23** 1 (1989).

[3] R. Battiston, *et. al.*, *Phys. Rep.* **214** 293 (1992).

[4] J. Ritchie and S. Wojcicki, *Rev. of Mod. Phys.* to appear.

[5] J. Donoghue, B. Holstein and G. Valencia, *Int. Jour. of Mod. Phys.* **A2** 319 (1987).

[6] U. Meissner, BUTP-93/01 to appear in *J. Phys. G: Nucl. Part. Phys.*

[7] W. Marciano, Rare Decay Symposium, Ed. D. Bryman *et. al.*, World Scientific 1 (1988).

[8] B. Winstein and L. Wolfenstein, *Rev. of Mod. Phys.* to appear.

[9] A. Buras and M. Harlander, *Review Volume on Heavy Flavors*, ed. A. Buras and M. Lindner, World Scientific, Singapore (1992).

[10] T. Inami and C. S. Lim, *Prog. Theo. Phys.* **65** 297 (1981); E.**65** 1772 (1981).

[11] G. Buchalla, A. Buras and M. Harlander, *Nucl. Phys.* **B349** 1 (1991).

[12] L. Wolfenstein, *Phys. Rev. Lett.* **51** 1945 (1983).

[13] H. Leutwyler and M. Roos, *Z. Phys.* **C25** 91 (1984).

[14] M. Neubert, *Phys. Lett.* **B264** 455 (1991); G. Burdman, *Phys. Lett.* **B284** 133 (1992).

[15] D. Cassel,talk at DPF meeting FNAL Nov. 1992.

[16] S. Weinberg, *Physica* **96A** 327 (1979).

[17] J. Gasser and H. Leutwyler, *Ann. Phys.* **158** 142 (1984); J. Gasser and H. Leutwyler, *Nucl. Phys.* **B250** 465 (1985).

[18] H. Georgi, *Weak Interactions and Modern Particle Physics* Benjamin, New York, (1984).

[19] J. Donoghue, E. Golowich and B. Holstein, *Dynamics of the Standard Model* Univ. Press, Cambridge UK (1992).

[20] J. Bijnens, G. Ecker and J. Gasser, CERN-TH-6625/92 and references therein.

[21] B. Holstein, *Phys. Lett.* **244B** 83 (1990).

[22] J. Wess and B. Zumino, *Phys. Lett.* **37B** 95 (1971); E. Witten, *Nucl. Phys.* **B223** 422 (1983).

[23] J. A. Cronin, *Phys. Rev.* **161** 1483 (1967).

[24] J. Donoghue, E. Golowich and B. Holstein, *Phys. Rep.* **131** 319 (1986).

[25] T. J. Devlin and J. O. Dickey, *Rev. of Mod. Phys.* **51** 237 (1979).

[26] J. Kambor, J. Missimer and D. Wyler, *Nucl. Phys.* **B346** 17 (1990).

[27] G. Ecker, A. Pich and E. de Rafael, *Nucl. Phys.* **B291** 692 (1987).

[28] G. Ecker, A. Pich and E. de Rafael, *Nucl. Phys.* **B303** 665 (1988).

[29] H. Y. Cheng, *Phys. Rev.* **D42** 72 (1990).

[30] J. Bijnens, G. Ecker and A. Pich, *Phys. Lett.* **286B** 341 (1992).

[31] W. Bardeen, A. Buras and J. Gerard, *Phys. Lett.* **180B** 133 (1986); **211B** (1988) 343; *Nucl. Phys.* **B293** 787 (1987).

[32] A. Pich and E. de Rafael, *Nucl. Phys.* **B358** 311 (1991).

[33] J. Donoghue, C. Ramirez and G. Valencia, *Phys. Rev.* **D39** 1947 (1989); G. Ecker, *et. al.*, *Nucl. Phys.* **B321** 311 (1989).

[34] J. Bijnens, C. Bruno and E. de Rafael, CERN-TH-6521/92, and references therein.

[35] J. Donoghue and B. Holstein, *Phys. Rev.* **D40** 2378 (1989); *ibid.* 3700; and references therein.

[36] G. Ecker, A. Pich and E. de Rafael, *Phys. Lett.* **237B** 481 (1990).

[37] H. Y. Cheng, *Phys. Rev.* **D42** 3850 (1990); *Phys. Lett.* **238B** 399 (1990).

[38] C. Bruno and J. Prades, CPT-92/P 2795 (1992).

[39] W. Buchmüller and D. Wyler, *Nucl. Phys.* **B268** 621 (1986).

[40] Particle Data Group 1992, *Phys. Rev.* **D45** No.11 part II.

[41] T. Akagi *et. al.*, *Phys. Rev. Lett.* **67** 2614 (1991).

[42] K. Arisaka *et. al.*, *Phys. Rev. Lett.* **70** 1049 (1993).

[43] R. Cahn and H. Harari, *Nucl. Phys.* **B176** 135 (1980).

[44] J. Pati and H. Stemnitzer, *Phys. Lett.* **172B** 441 (1986).

[45] O. Shanker, *Nucl. Phys.* **B206** 253 (1982).

[46] R. Bolton, *et. al.*, *Phys. Rev.* **D38** 2121 (1988).

[47] A. Acker and S. Pakvasa, *Mod. Phys. Lett.* **A7** 1219 (1992).

[48] W. Marciano and A. Sanda, *Phys. Rev. Lett.* **38** 1512 (1977); W. Marciano, *Phys. Rev.* **D45** R721 (1992).

[49] A. Barroso, G. Branco and M. Bento, *Phys. Lett.* **134B** 123 (1984).

[50] P. Langacker, S. Uma Sankar and K. Schilcher, *Phys. Rev.* **D38** 2841 (1988).

[51] S. Dawson and G. Valencia, Fermilab-Pub-93/024-T.

[52] A. M Lee, *et. al.*, *Phys. Rev. Lett.* **64** 165 (1990).

[53] A. Diamant-Berger, *et. al.*, *Phys. Lett.* **62B** 485 (1976).

[54] SUSY: B. Campbell, *Phys. Rev.* **D28** 209 (1983); Technicolor: E. Eichten, *et. al.*, *Phys. Rev* **D34** 1547 (1986); Leptoquarks: L. Hall and L. Randall, *Nucl. Phys.* **B274** 157 (1986); Horizontal interactions: W. S. Hou and A. Soni, *Phys. Rev.* **D35** 2776 (1987); Multiscalar models: H. Haber and Y. Nir, *Nucl. Phys.* **B335** 363 (1990); G. Bélanger, C. Q. Geng and P. Turcotte, *Phys. Rev.* **D46** 2950 (1992); A. Antaramian, L. Hall and A. Rasin, *Phys. Rev. Lett.* **69** 1871 (1992). A recent review with more references is P. Langacker in 1990 Snowmass proceedings.

[55] I. Bigi and F. Gabbiani, *Nucl. Phys.* **B367** 3 (1991).

[56] S. Weinberg, *Phys. Rev. Lett.* **40** 223 (1978); F. Wilczek, *Phys. Rev. Lett.* **40** 279 (1978); T. Goldman and C.M. Hoffman, *Phys. Rev. Lett.* **40** 220 (1978); J.M. Frére, et al., *Phys. Lett.* **B103** 129 (1981).

[57] F. Wilczek, *Phys. Rev. Lett.* **49** 1549 (1982).

[58] M. Suzuki, *Phys. Rev. Lett.* **56** 1339 (1986); S.H. Aronson, et al., *Phys. Rev. Lett.* **56** 1342 (1986); C. Bouchiat and J. Iliopoulos, *Phys. Lett.* **169B** 447 (1986).

[59] M.S. Atiya, et al., BNL48066, submitted to *Phys. Rev. Lett.* ; M.S. Atiya, et al., *Phys. Rev. Lett.* **64** 21 (1990).

[60] M.S. Atiya, et al., BNL48091, submitted to *Phys. Rev. Lett.* .

[61] L. Littenberg, *Phys. Rev.* **D39** 3322 (1989).

[62] G. Buchalla and A. Buras, MPI-PTh 2-93.

[63] G. E. Graham, *et al.*, EFI-92-20 Apr. 1992.

[64] K. Arisaka, *et al.*, FNAL Jun. 1991.

[65] T. Inagaki, T. Sato, and T. Shinkawa, *Experiment to search for the Decay* $K_L^0 \to \pi^0\nu\bar{\nu}$ *at KEK 12 GeV Proton Synchrotron*, 30 November 1991.

[66] G. Ecker, A. Pich and E. de Rafael, *Phys. Lett.* **189B** 363 (1987); L. Cappiello and G. D'Ambrosio. *Nuov. Cim.* **99A** 153 (1988).

[67] G. D'Ambrosio and D. Espriu, *Phys. Lett.* **175B** 237 (1986); J. Goity, *Zeit. Phys.* **C34** 341 (1987).

[68] H. Burkhardt *et. al.*, *Phys. Lett.* 199B 139 (1987).

[69] J. Bijnens, S. Dawson and G. Valencia, *Phys. Rev.* **D44** 3555 (1991).

[70] G. D. Barr, *et. al.*, *Phys. Lett.* **242B** 523 (1990);G. D. Barr, *et, al.*, *Phys. Lett.* **284B** 440 (1992).

[71] V. Papadimitriou *et. al.*, *Phys. Rev.* **D44** R573 (1991).

[72] L. M. Sehgal, *Phys. Rev.* **D41** 161 (1990); P. Ko, *Phys. Rev.* **D41** 1531 (1990).

[73] J. Donoghue, B. Holstein and Y. C. Lin, *Nucl. Phys.* **B277** 651 (1986).

[74] L. Cappiello, G. D'Ambrosio, and M. Miragliuolo, *Phys. Lett.* **298B** 423 (1993).

[75] M. S. Atiya, *et. al.*, *Phys. Rev. Lett.* **65** 1188 (1990).

[76] F. Gilman and M. Wise, *Phys. Rev.* **D21** 3150 (1980).

[77] G. Shore and G. Veneziano, *Nucl. Phys.* **B381** 3 (1992).

[78] K.E. Ohl, et al., *Phys. Rev. Lett.* **65**, 1407 (1990).

[79] G. D. Barr, *et. al.*, *Phys. Lett.* **240B** 283 (1990)

[80] R. Tschirhart, talk at DPF Meeting at FNAL, Nov. 1992.

[81] L. Bergström, E. Massó, P. Singer, *Phys. Lett.* **131B** 229 (1983); L. Bergström, *et. al.*, *Phys. Lett.* **134B** 373 (1984).

[82] C. Quigg and J. D. Jackson, UCRL-18487 unpublished (1968).

[83] N. Kroll and W. Wada, *Phys. Rev.* **98** 1355 (1955).

[84] G. D. Barr, *et. al.*, *Phys. Lett.* **259B** 389 (1991).

[85] M.R. Vagins, *et. al.*, YAUG-A-93/1, Jan. 1993, submitted to *Phys. Rev. Lett.*

[86] T. Akagi, et al., *KEK Preprint 92-35*, May 1992.

[87] Ping Gu, talk at DPF Meeting at FNAL, Nov. 1992.

[88] T. Miyazaki and E. Takasugi, *Phys. Rev.* **D8** 2051 (1973).

[89] C. S. Lai, and B. L. Young, *Nuov. Cim.* **52A** 83 (1967); L. Sehgal and L. Wolfenstein, *Phys. Rev.* **162** 1362 (1967); D. Beder, *Nucl. Phys.* **B47** 286 (1972).

[90] G. Costa and P. Kabir, *Il Nuov. Cim.* **LI A** N.2 564 (1967).

[91] A. S. Carroll, *et. al.*, *Phys. Rev. Lett.* **44** 529 (1980); E**44** 1026 (1980).

[92] G. J. Bock, *et. al.*, FNAL 92/384-E;E. Ramberg, *et al.*, FNAL 92/385-E

[93] Y. C. Lin and G. Valencia, *Phys. Rev.* **D37** 143 (1988).

[94] C. Picciotto, *Phys. Rev.* **D45** 1569 (1992).

[95] G. Ecker, H. Neufeld and A. Pich, *Phys. Lett.* **278B** 337 (1992).

[96] L. Sehgal and M. Wanninger, *Phys. Rev.* **D46** 1035 (1992); E **D46** 5209 (1992).

[97] P. Herczeg, *Phys. Rev.* **D27** 1512 (1983).

[98] G. Ecker and A. Pich, *Nucl. Phys.* **B366** 189 (1991).

[99] F. Botella and C. S. Lim, *Phys. Rev. Lett.* **56** 1651 (1986).

[100] T. Akagi, et al., *Phys. Rev. Lett.* **67** 2618 (1991).

[101] A. J. Schwartz, Princeton/hep/92-15.

[102] M. Savage, M. Luke and M. Wise, *Phys. Lett.* **291B** 481 (1992).

[103] C. Quigg, private communication.

[104] G. Bélanger and C. Q. Geng, *Phys. Rev.* **D43** 140 (1991); P. Ko, *Phys. Rev.* **D45** 174 (1992).

[105] C. Alliegro *et. al*, *Phys. Rev. Lett.* **68** 278 (1992).

[106] M. S. Atiya, *et. al.*, *Phys. Rev. Lett.* **63** 2177 (1989).

[107] M. Savage and M. Wise, *Phys. Lett.* **250B** 151 (1990).

[108] M. Lu, M. Wise and M. Savage, *Phys. Rev.* **D46** 5026 (1992).

[109] G. Bélanger, C. Q. Geng and P. Turcotte, UdeM-LPN-TH-90.

[110] P. Agrawal *et. al.*, *Phys. Rev. Lett.* **67** 537 (1991); *Phys. Rev.* **D45** 2383 (1992).

[111] C. Dib, I. Dunietz, and F.J. Gilman, *Phys. Rev.* **D39** 2639 (1989); C. Dib, I. Dunietz, and F.J. Gilman *Phys. Lett.* **218B** 487 (1989); J.M. Flynn, *Nucl. Phys.* **B13** 474 (1990); J.M. Flynn and L. Randall, *Nucl. Phys.* **B326** 31 (1989), E.-*ibid.* **B334** 580 (1990).

[112] J. Donoghue, B. Holstein and G. Valencia, *Phys. Rev.* **D35** 2769 (1987); L. M. Sehgal, *Phys. Rev.* **D38** 808 (1988); J. Flynn and L. Randall, *Phys. Lett.* **216B** 221 (1989).

[113] G.D. Barr, et al., *Phys. Lett.* **B214** 303 (1988).

[114] A. Barker, et al., *Phys. Rev.* **D41** 3546 (1990).

[115] K.E. Ohl, et al.. *Phys. Rev. Lett.* **64**, 2755 (1990).

[116] W.M. Morse, et al., *Phys. Rev.* **D65**, 36 (1992).

[117] H.B. Greenlee, *Phys. Rev.* **D42** 3724 (1992).

[118] K. Miyake, et al.,*Measurement of CP-violating direct amplitude in* $K_L \to \pi^0 e^+ e^-$ *decay*, Aug. 1988.

[119] L. K. Gibbons, et al., *Phys. Rev. Lett.* **61** 2661 (1988).

[120] G. D. Barr, *et. al.*, *Phys. Lett.* **235B** 356 (1990)

[121] N.J. Baker, et al., *Phys. Rev. Lett.* **59** 2832 (1987).

[122] A. Schwartz., in *Fourth Conference on the Intersections between Particle and Nuclear Physics*, Tucson, Arizona, AIP Conference proceedings No 243, ed. W. T. H. Van Oers (AIP, New York), p. 609.

[123] M.S. Atiya, et al., *NIM.* **A321** 129 (1992).

List of Tables

Figure Captions

Fig. 1: Results from recent searches for lepton flavor violation in K decay. a) $m(\mu e)$ vs θ^2_{lineup} for $K_L \to \mu e$ candidates from KEK-137; b) $m(\mu e)$ vs p_T^2 for $K_L \to \mu e$ candidates from AGS-791; c) $m(\pi\mu e)$ vs vertex quality variable for $K^+ \to \pi^+\mu^+e^-$ candidates from AGS-777.

Fig. 2: Box diagrams giving rise to $K_L \to \mu^\pm e^\mp$ and $K \to \pi\mu^\pm e^\mp$ in models with massive neutrinos.

Fig. 3: Short distance contributions to $K \to \pi\nu\bar{\nu}$. The full circle represents the effective one-loop sdZ coupling.

Fig. 4: Potential long distance contributions to $K^+ \to \pi^+\nu\bar{\nu}$.

Fig. 5: Search regions for $K^+ \to \pi^+\nu\bar{\nu}$ from AGS 787. a) $p_{\pi^+} > p_{K\pi 2}$ and b) $p_{\pi^+} < p_{K\pi 2}$.

Fig. 6: Loop diagrams that give rise to $K_L \to \pi^0\gamma\gamma$ at order $\mathcal{O}(p^4)$. The same diagrams without the π^0 line give rise to $K_S \to \gamma\gamma$. The **X** represents a vertex from Eq. 2.9.

Fig. 7: Examples of $\mathcal{O}(p^6)$ contributions to $K_L \to \pi^0\gamma\gamma$ in VMD models. a) Pole diagrams and b) Direct weak counter-terms. In both cases the **X** represents a weak transition, but in (b) it is $\mathcal{O}(p^6)$.

Fig. 8: Rate for $K_L \to \pi^0\gamma\gamma$. a) Theoretical spectra. The solid line is the $\mathcal{O}(p^4)$ χPT ($\alpha_V = 0$) result, and the dashed and dotted lines show the range for the values of α_V given in the text. Phase space and pure VMD spectra are also shown; b) Data from Ref. [70] (solid histogram), compared with $\mathcal{O}(p^4)$ result

(dotted histogram). The latter has been multiplied by the experimental acceptance (shown as crosses). Dashed histogram is calculated background.

Fig. 9: Pole diagrams that give rise to $C(z,\nu)$ in $K^{\pm} \to \pi^{\pm}\gamma\gamma$.

Fig. 10: Pole diagrams contributing to $K_L \to \gamma\gamma$

Fig. 11: Pole diagrams contributing to the direct emission in $K_L \to \pi^+\pi^-\gamma$.

Fig. 12: Short distance diagrams giving rise to $K_L \to \ell^+\ell^-$ and $K^+ \to \pi^+\ell^+\ell^-$. The full circle represents the effective one-loop sdZ vertex.

Fig. 13: Dominant long distance contribution to $K_L \to \ell^+\ell^-$. The vertical dashed line represents the cut to obtain the absorptive part.

Fig. 14: Diagrams contributing to $K \to \pi\gamma^*$ at $\mathcal{O}(p^4)$. The full circle represents a vertex from Eq. 2.7, whereas the full box represents a vertex from Eq. 2.12. The **X** is a $\mathcal{O}(p^2)$ weak transition from Eq. 2.9.

Fig. 15: Calculated decay distribution for $K^+ \to \pi^+e^+e^-$, for values of w_+ mentioned in the text.

Fig. 16: Fit of $K^+ \to \pi^+e^+e^-$ spectrum and branching ratio to predictions of χPT. From Ref. [105].

Fig. 17: Short distance contributions to the direct CP violation in $K_L \to \pi^0e^+e^-$. Again, the full circle represents effective one-loop couplings.

Fig. 18: Two photon contribution to the CP conserving absorptive part of $K_L \to \pi^0e^+e^-$.

Fig. 19: Background to the process $K_L \to \pi^0e^+e^-$.

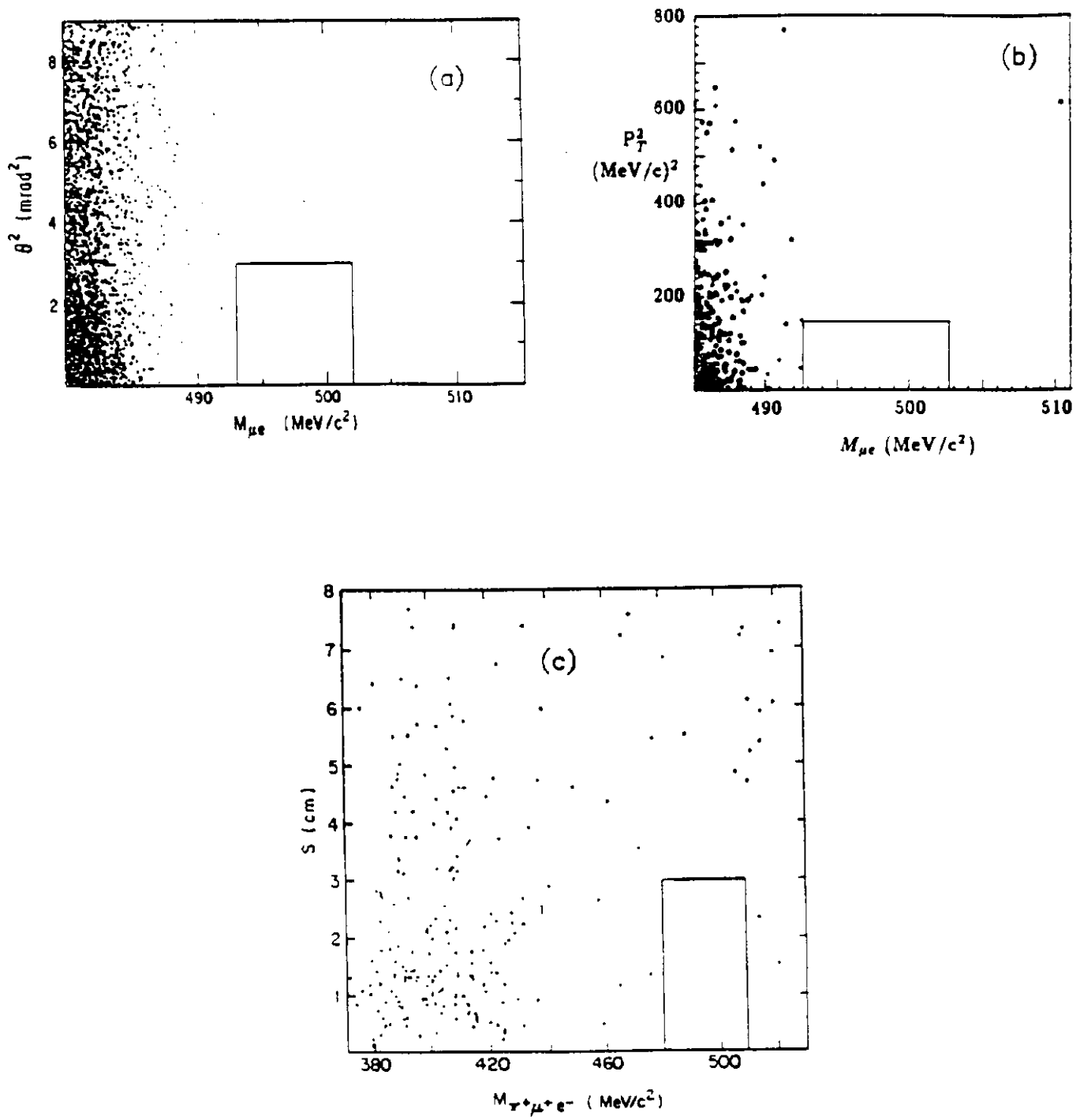
(a)
θ^2 (mrad^2)
$M_{\mu e}$ (MeV/c^2)
(b)
P_T^2 (MeV/c)^2
$M_{\mu e}$ (MeV/c^2)
(c)
S (cm)
$M_{\pi^+\mu^+e^-}$ (MeV/c^2)

FIGURE 1.

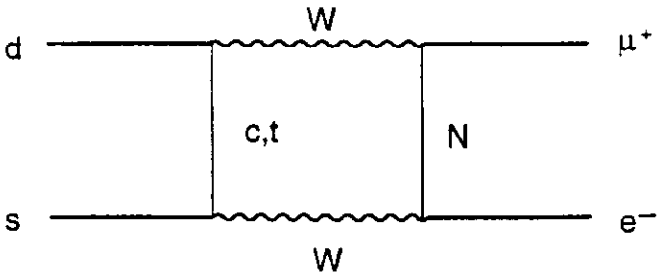

FIGURE 2.

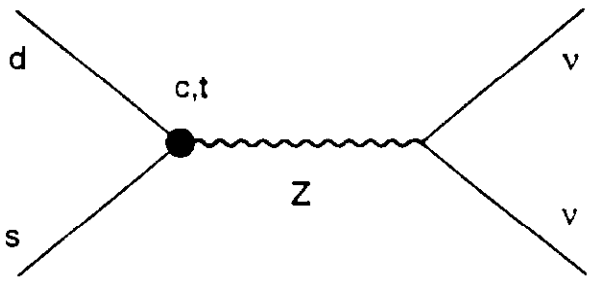

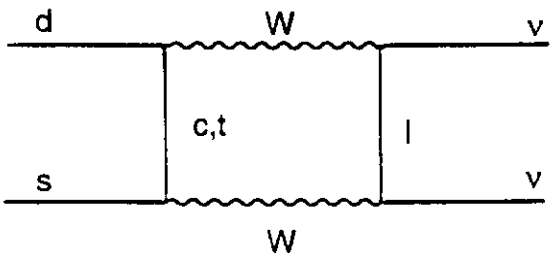

FIGURE 3.

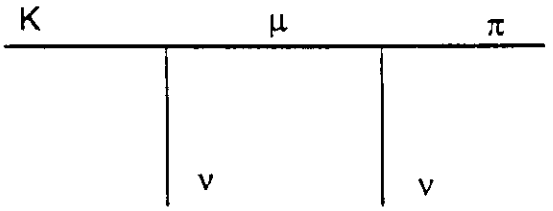

FIGURE 4.

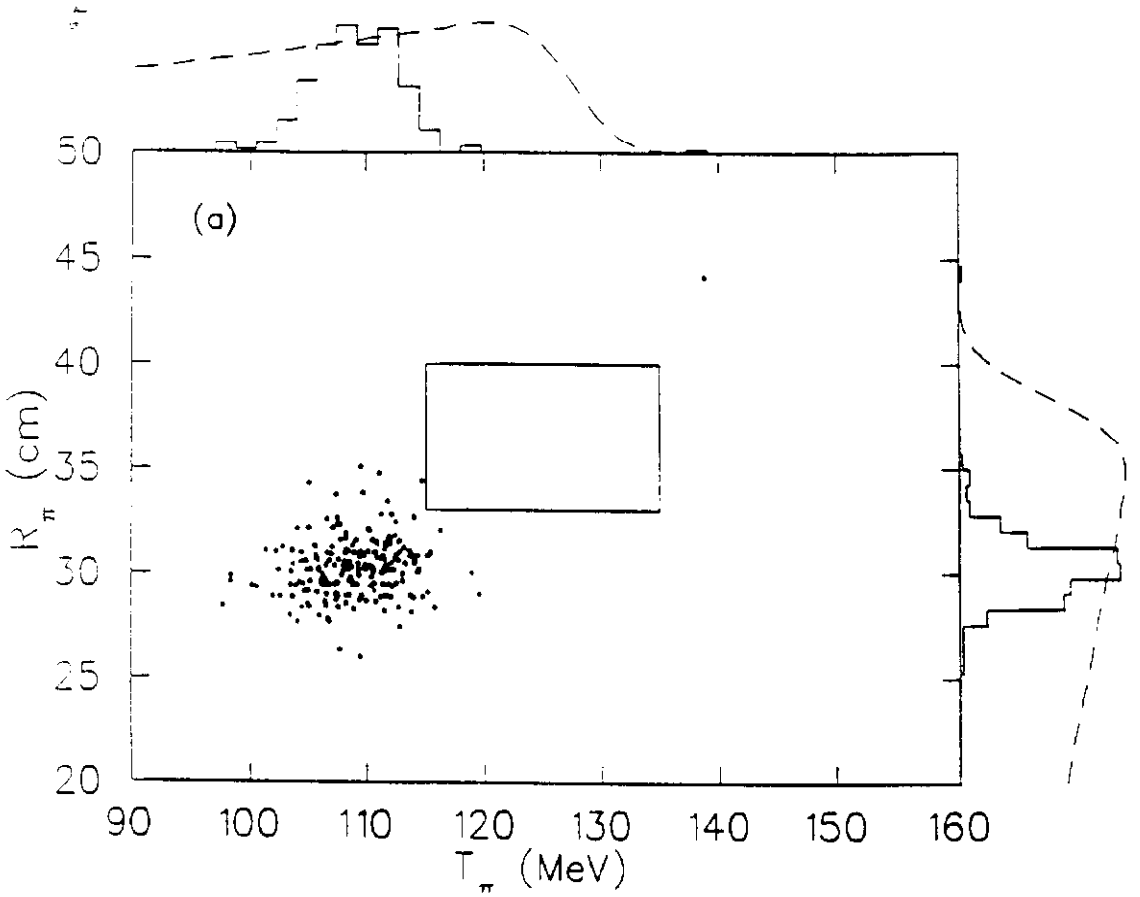
(a)
50
45
40
35
30
25
20
R_π (cm)
90
100
110
120
130
140
150
160
T_π (MeV)

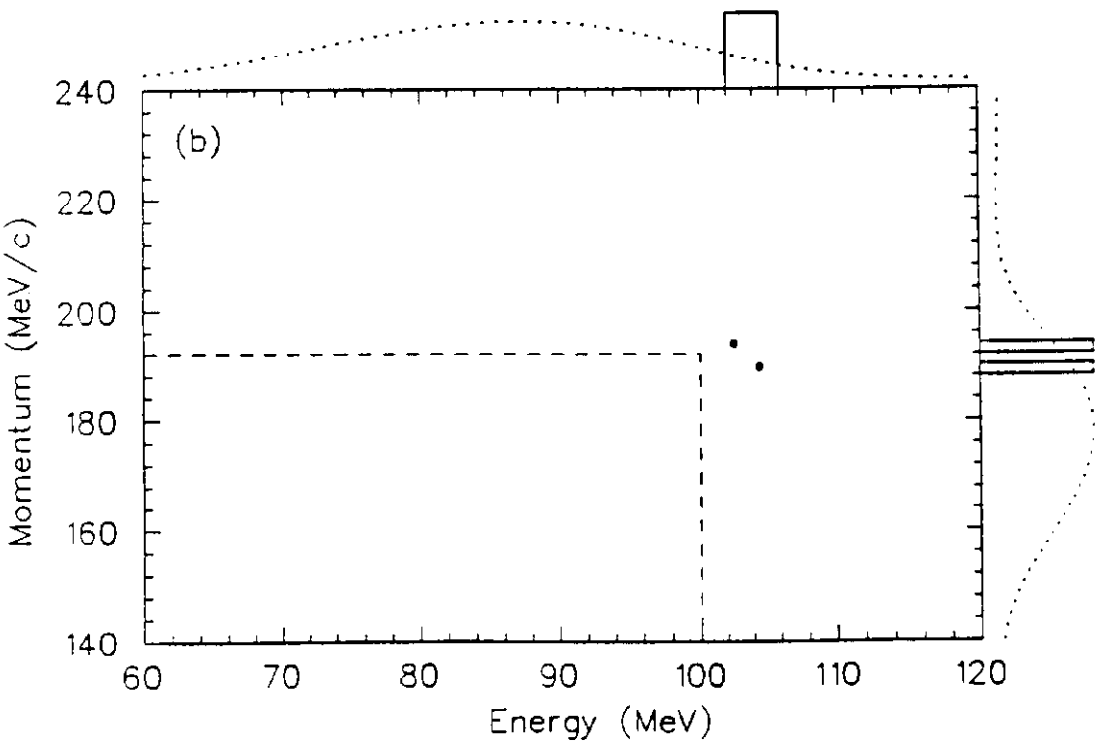
(b)
240
220
200
180
160
140
Momentum (MeV/c)
60
70
80
90
100
110
120
Energy (MeV)

FIGURE 5.

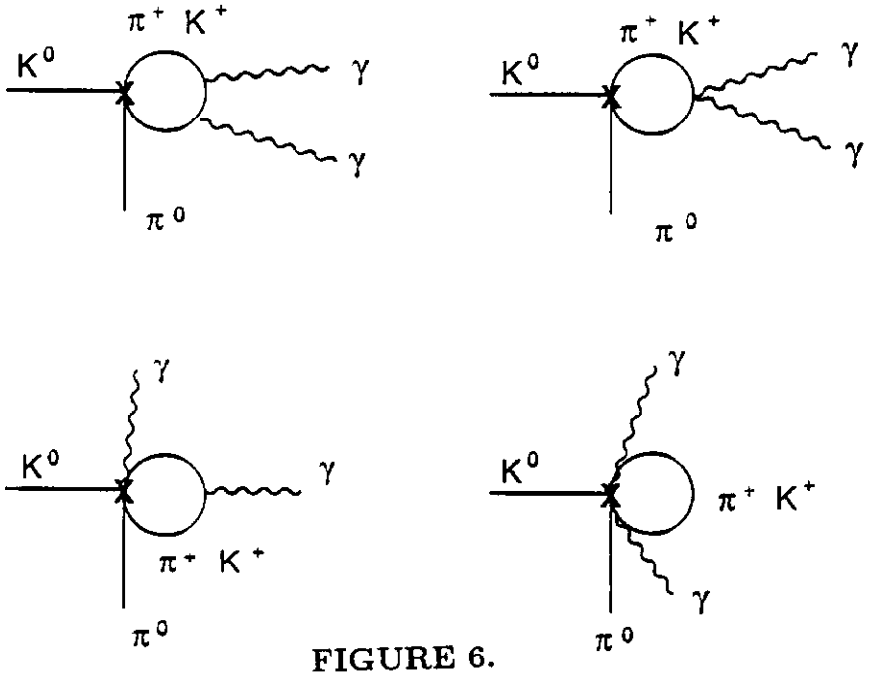

FIGURE 6.

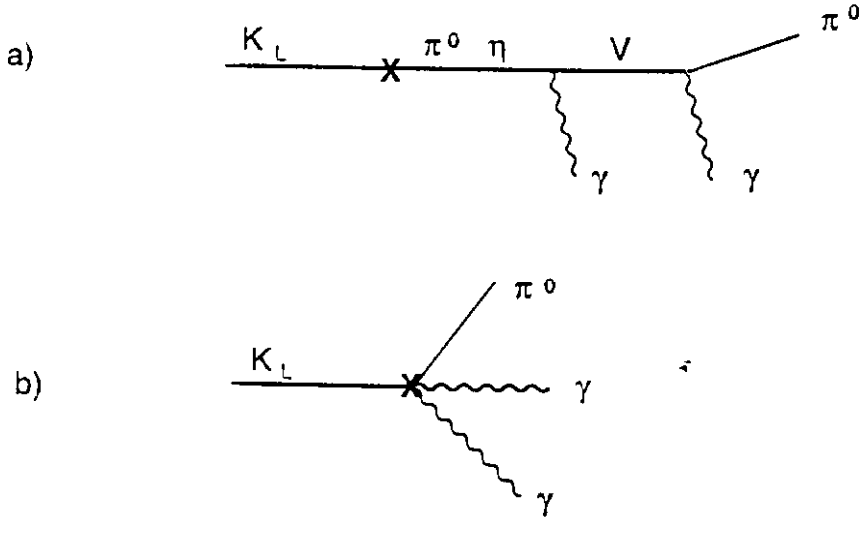

FIGURE 7.

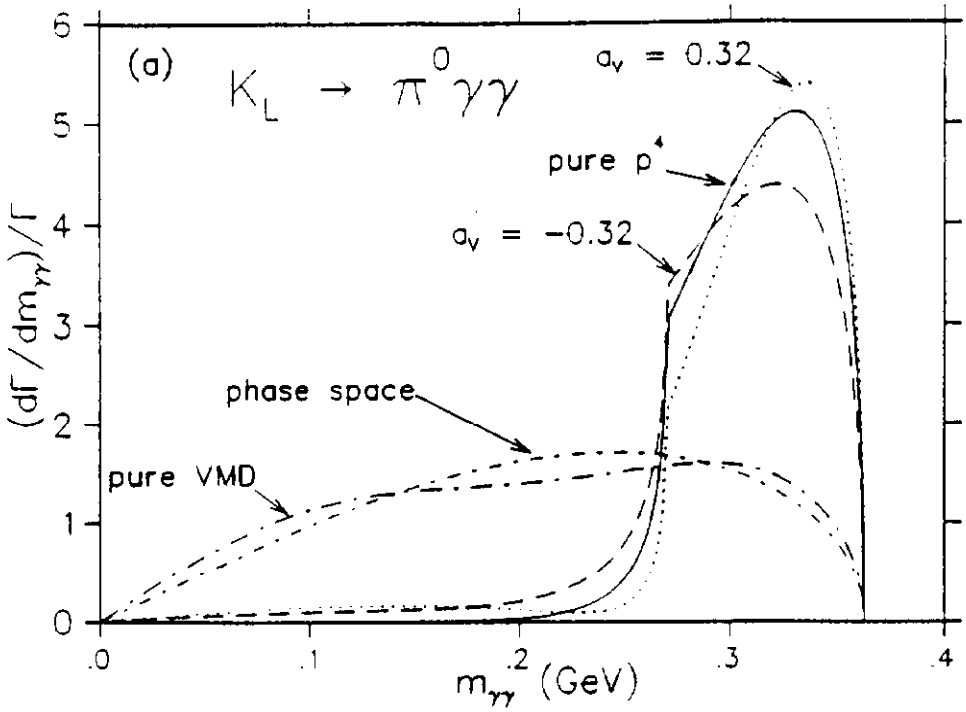
(a)
$K_L \rightarrow \pi^0\gamma\gamma$
$a_v = 0.32$
pure p^4
$a_v = -0.32$
phase space
pure VMD
$(d\Gamma/dm_{\gamma\gamma})/\Gamma$
$m_{\gamma\gamma}^2$ (GeV)

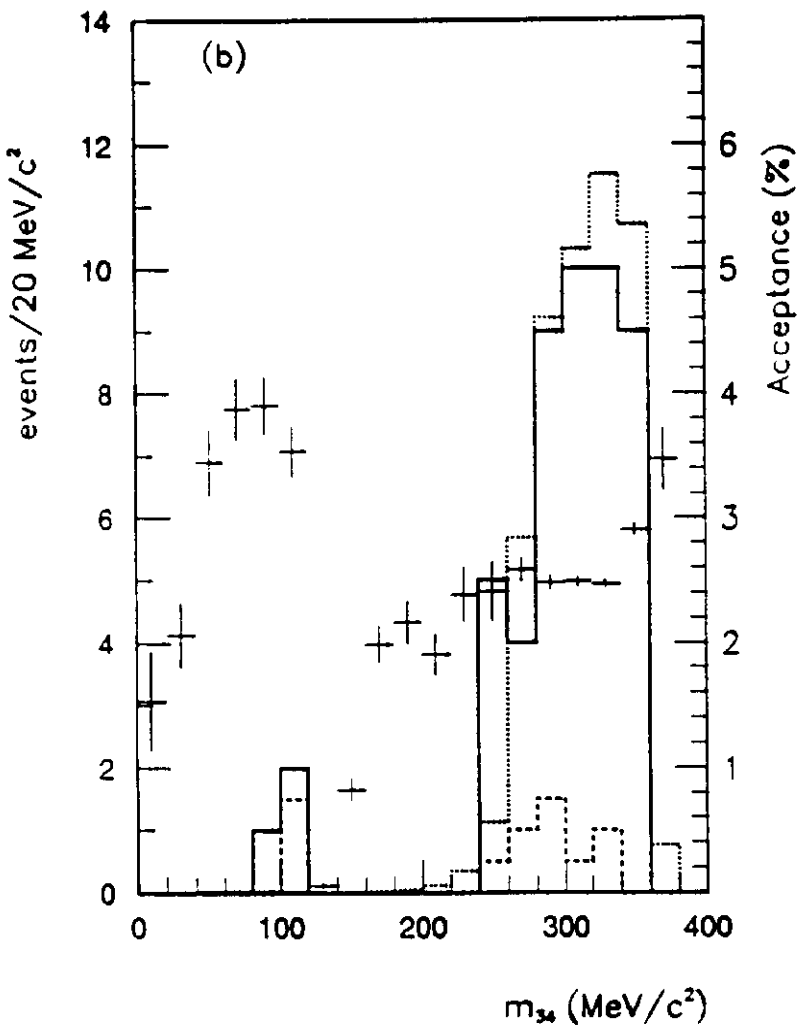
(b)
events/20 MeV/c^2
Acceptance (%)
m_{34} (MeV/c^2)

FIGURE 8.

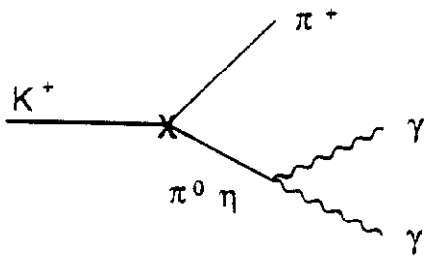

FIGURE 9.

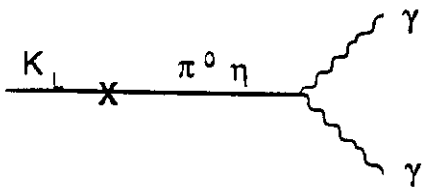

FIGURE 10.

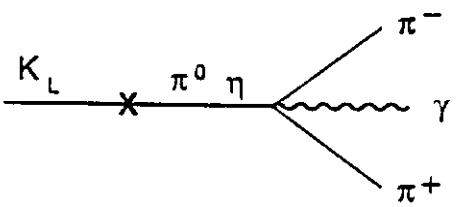

FIGURE 11.

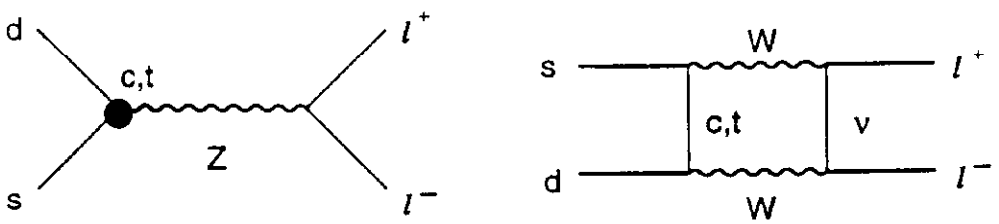

FIGURE 12.

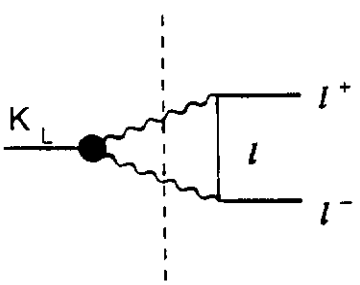

FIGURE 13.

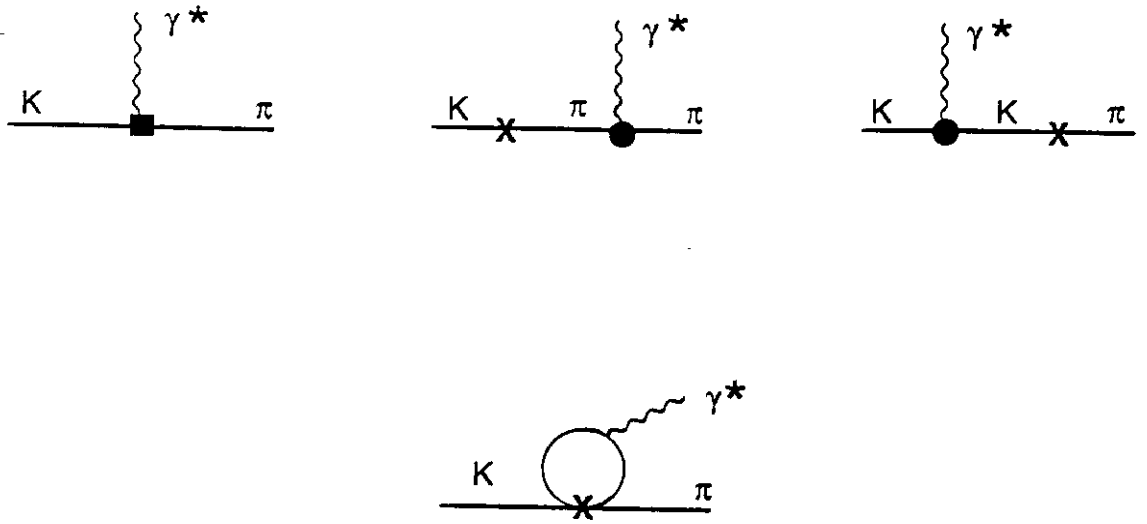

FIGURE 14.

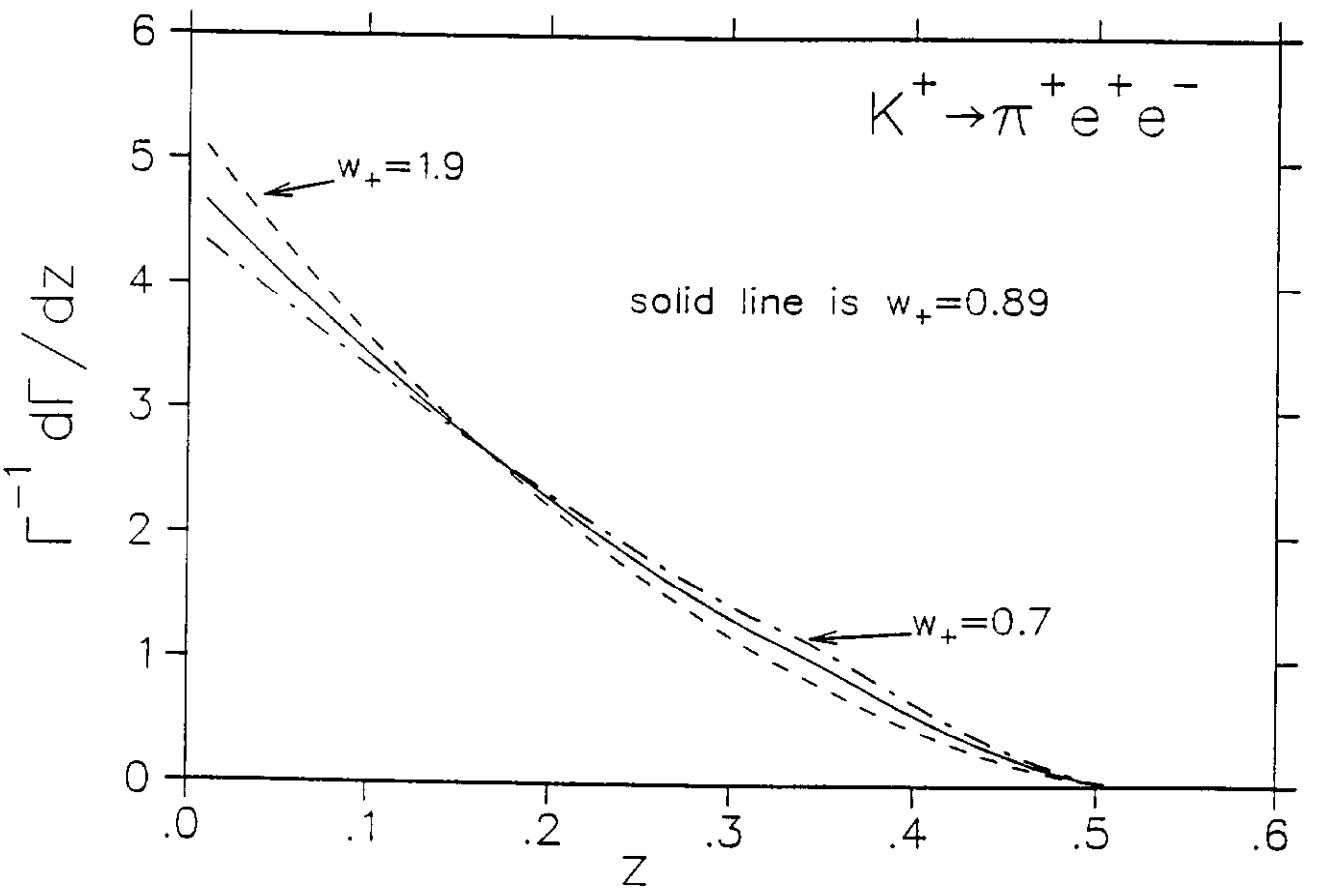

FIGURE 15.

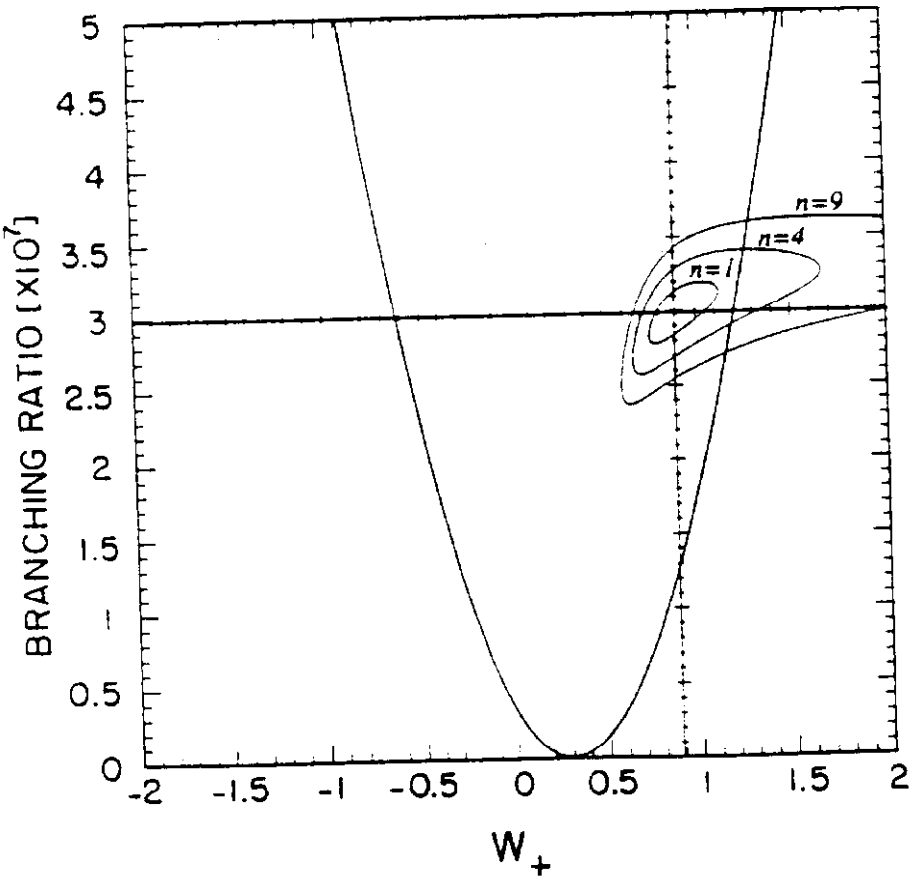
BRANCHING RATIO [X10^{-7}]
5
4.5
4
3.5
3
2.5
2
1.5
1
0.5
0
-2
-1.5
-1
-0.5
0
0.5
1
1.5
2
W_+
n=9
n=4
n=1

FIGURE 16.

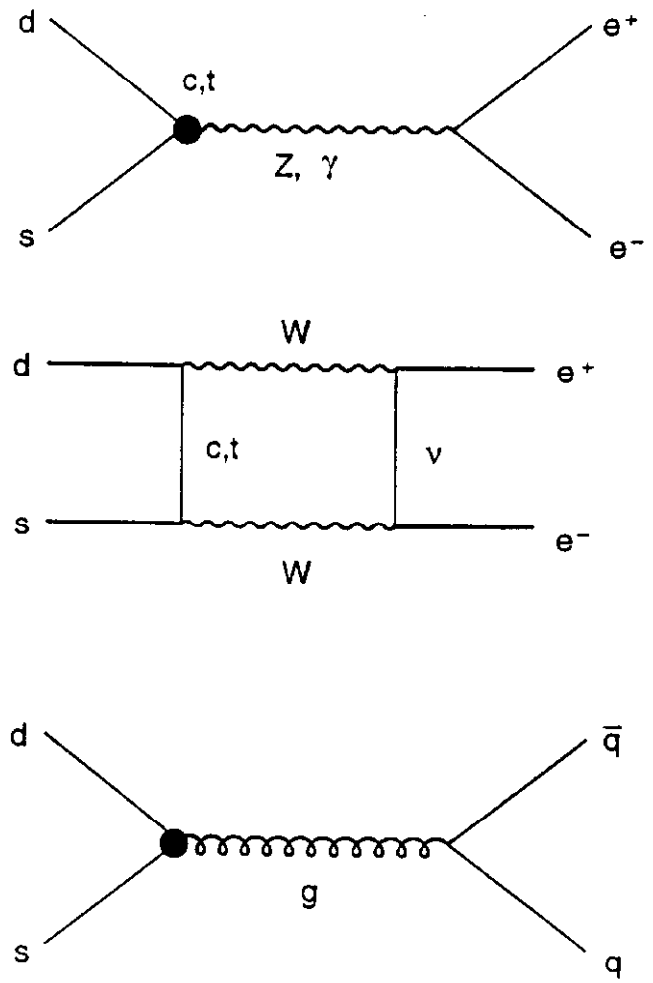

FIGURE 17.

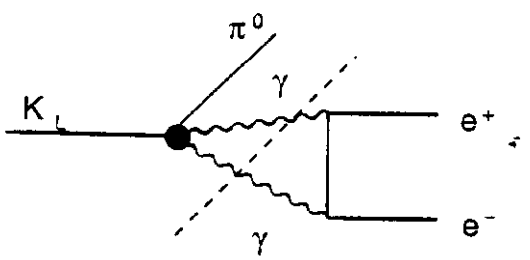

FIGURE 18.

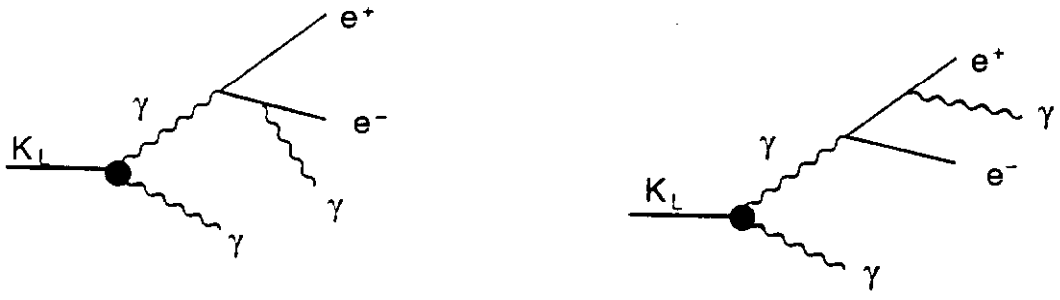

FIGURE 19.

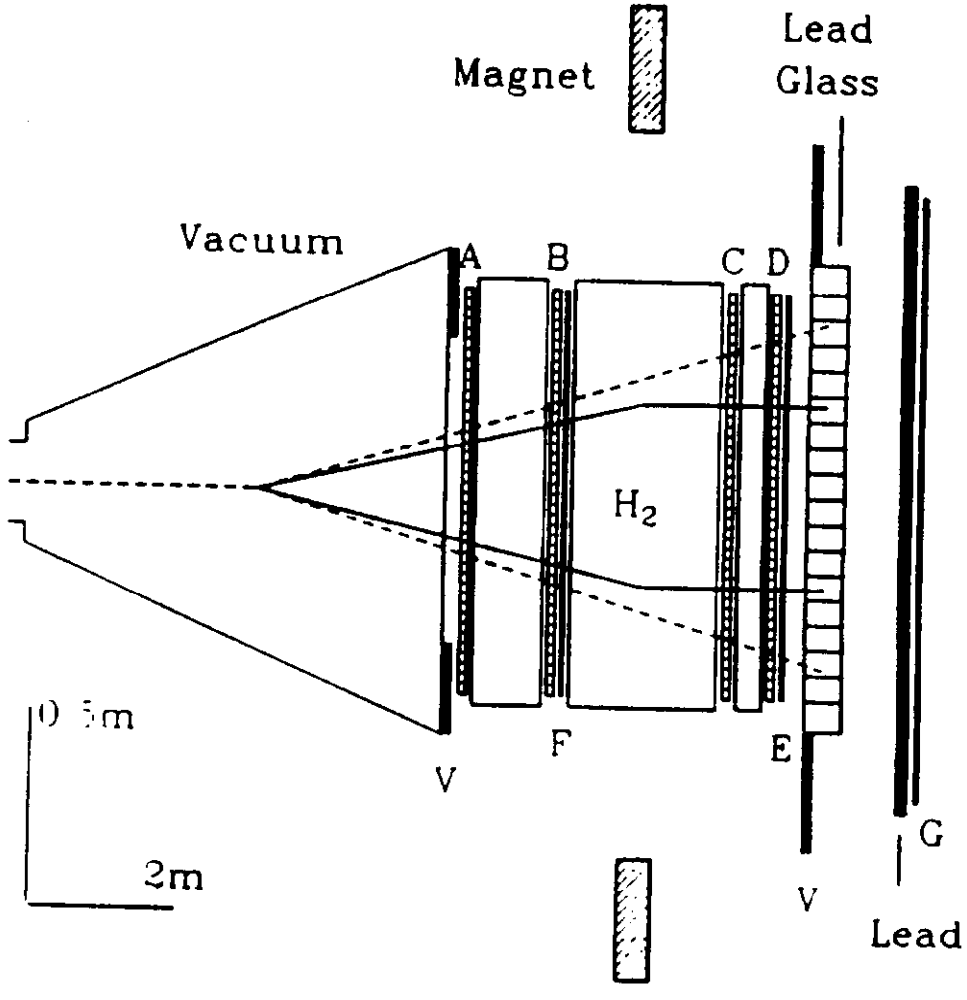

FIGURE 20.

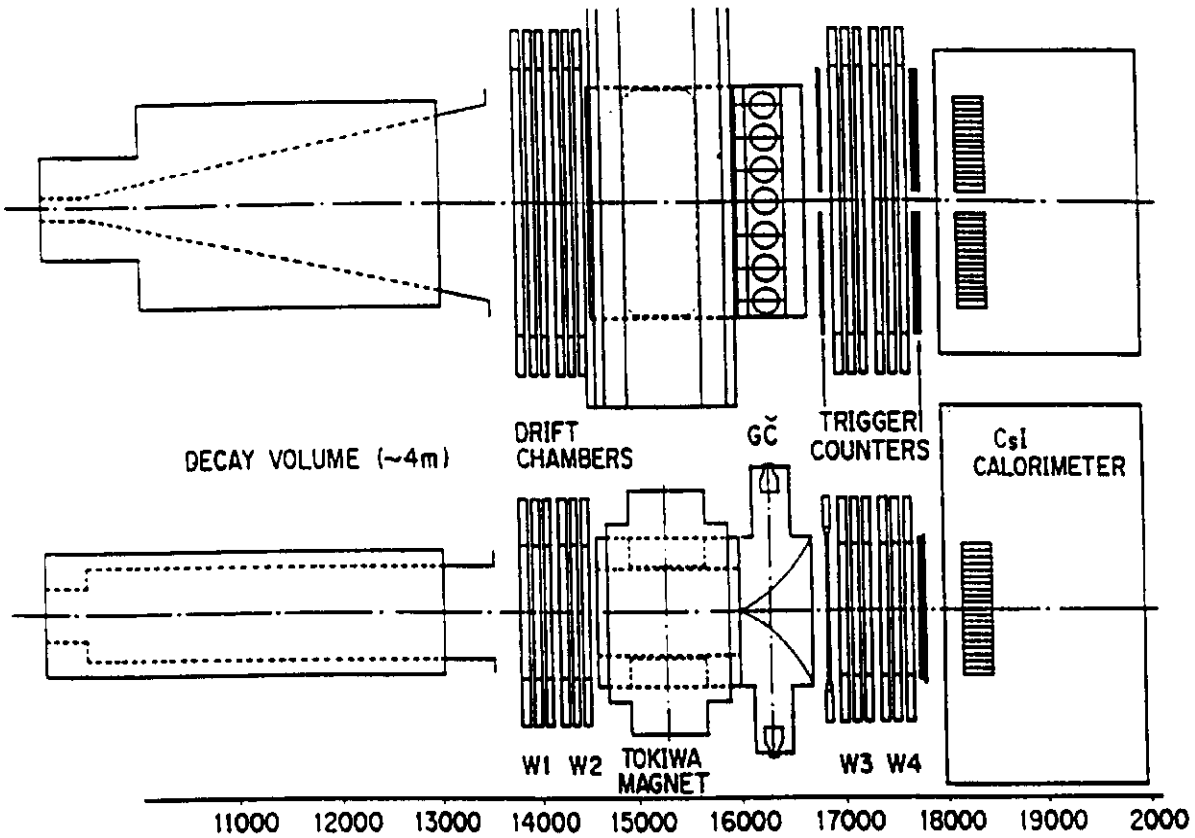

FIGURE 21.

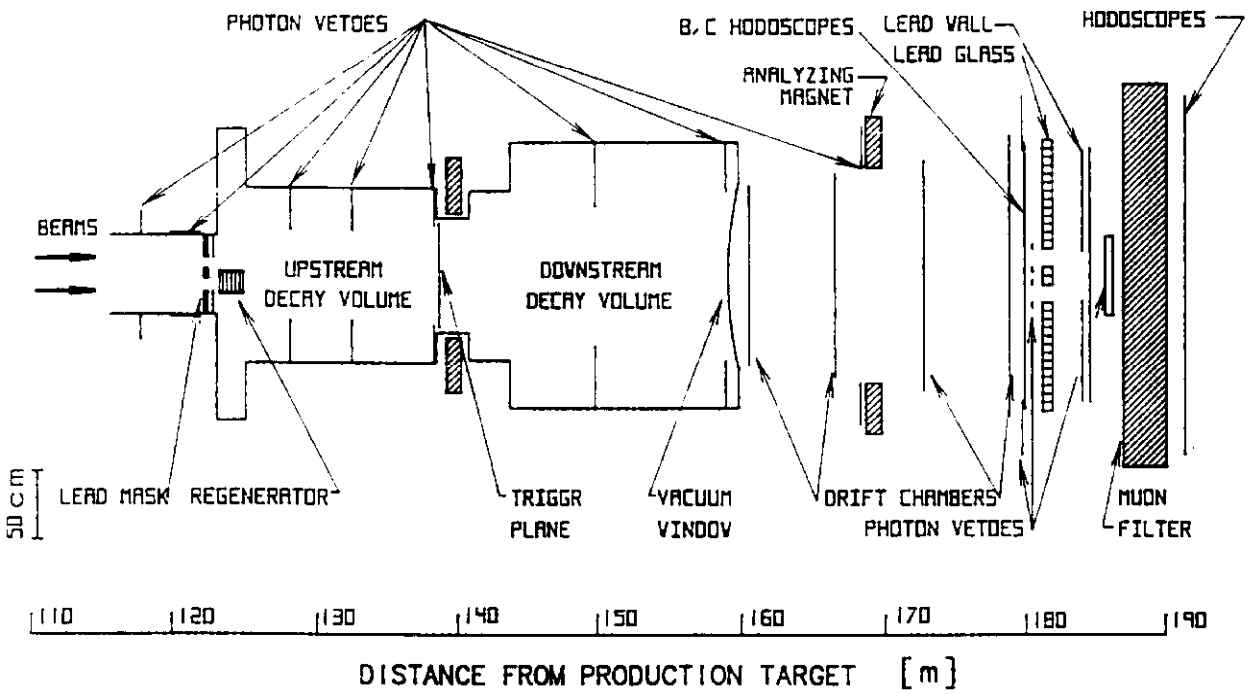

FIGURE 22.

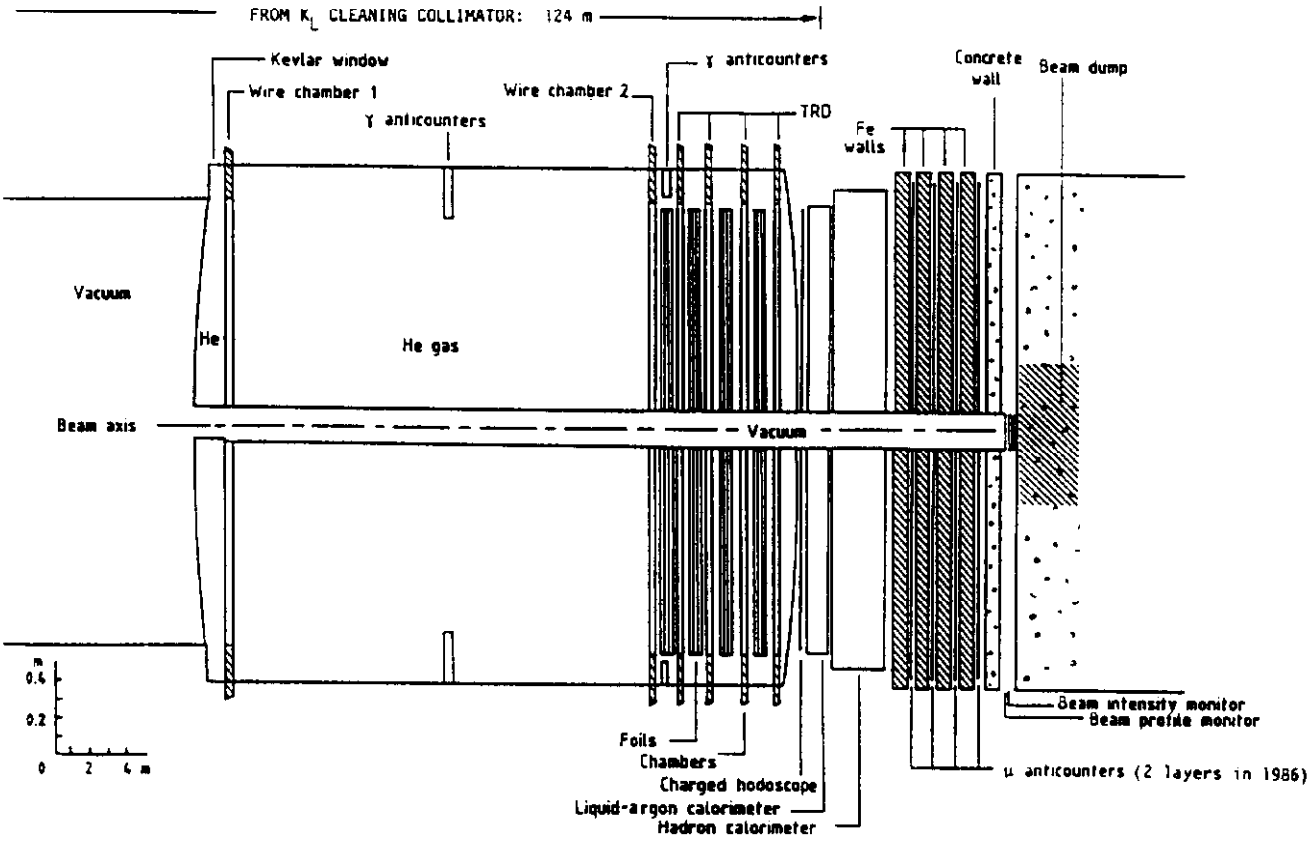
FROM K_L CLEANING COLLIMATOR: 124 m
Kevlar window
Wire chamber 1
Y anticounters
Wire chamber 2
γ anticounters
TRD
Fe walls
Concrete wall
Beam dump
Vacuum
He
He gas
Beam axis
Vacuum
m
0.6
0.2
0
2
4 m
Beam intensity monitor
Beam profile monitor
Foils
Chambers
Charged hodoscope
Liquid-argon calorimeter
Hadron calorimeter
μ anticounters (2 layers in 1986)

FIGURE 23.

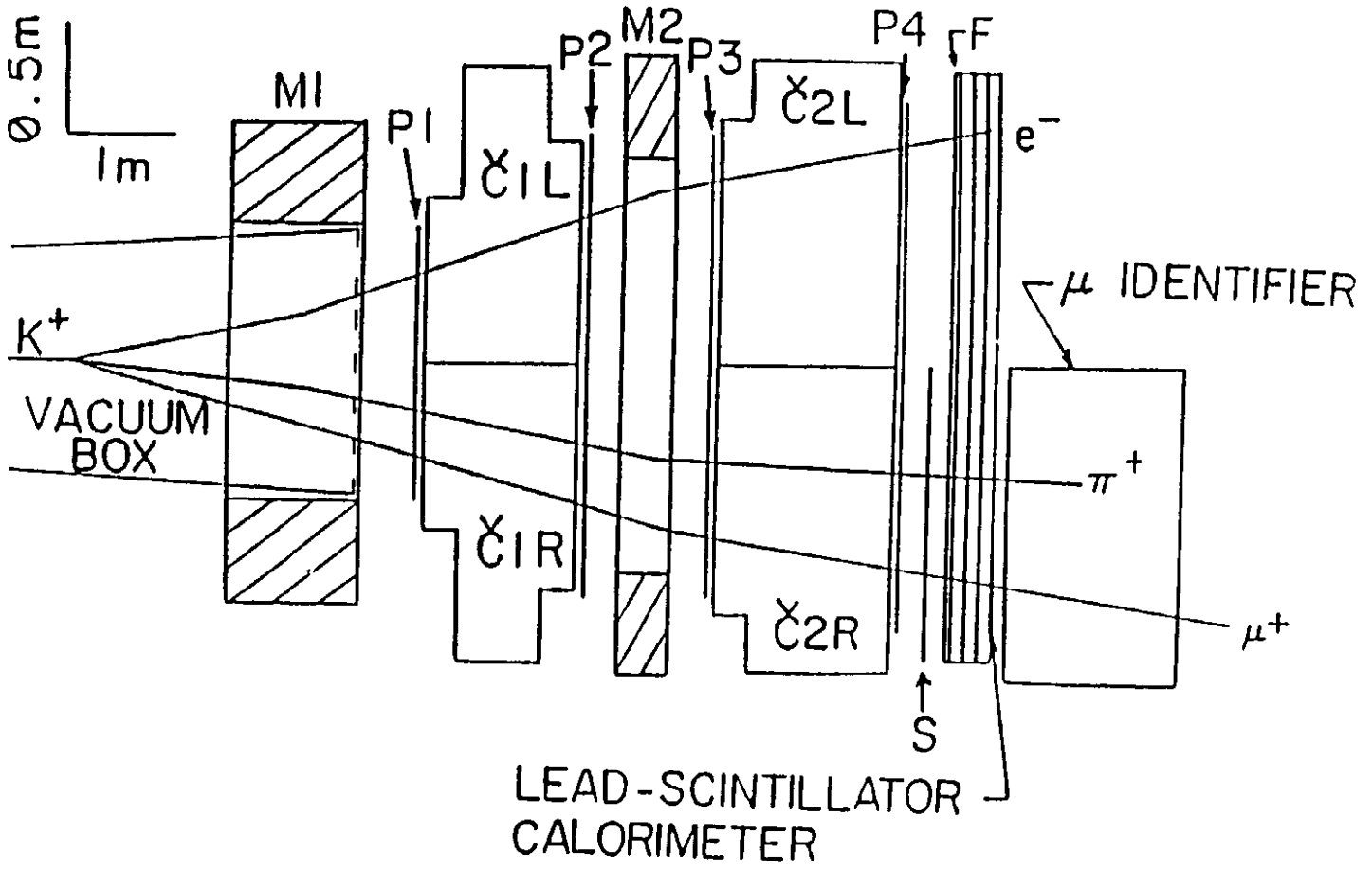
LEFT SIDE
0.5m
1m
M1
P1
P2
M2
P3
P4
F
čIL
čIR
č2L
č2R
e⁻
μ IDENTIFIER
K⁺
VACUUM BOX
π⁺
μ⁺
S
LEAD-SCINTILLATOR CALORIMETER
RIGHT SIDE

FIGURE 24.

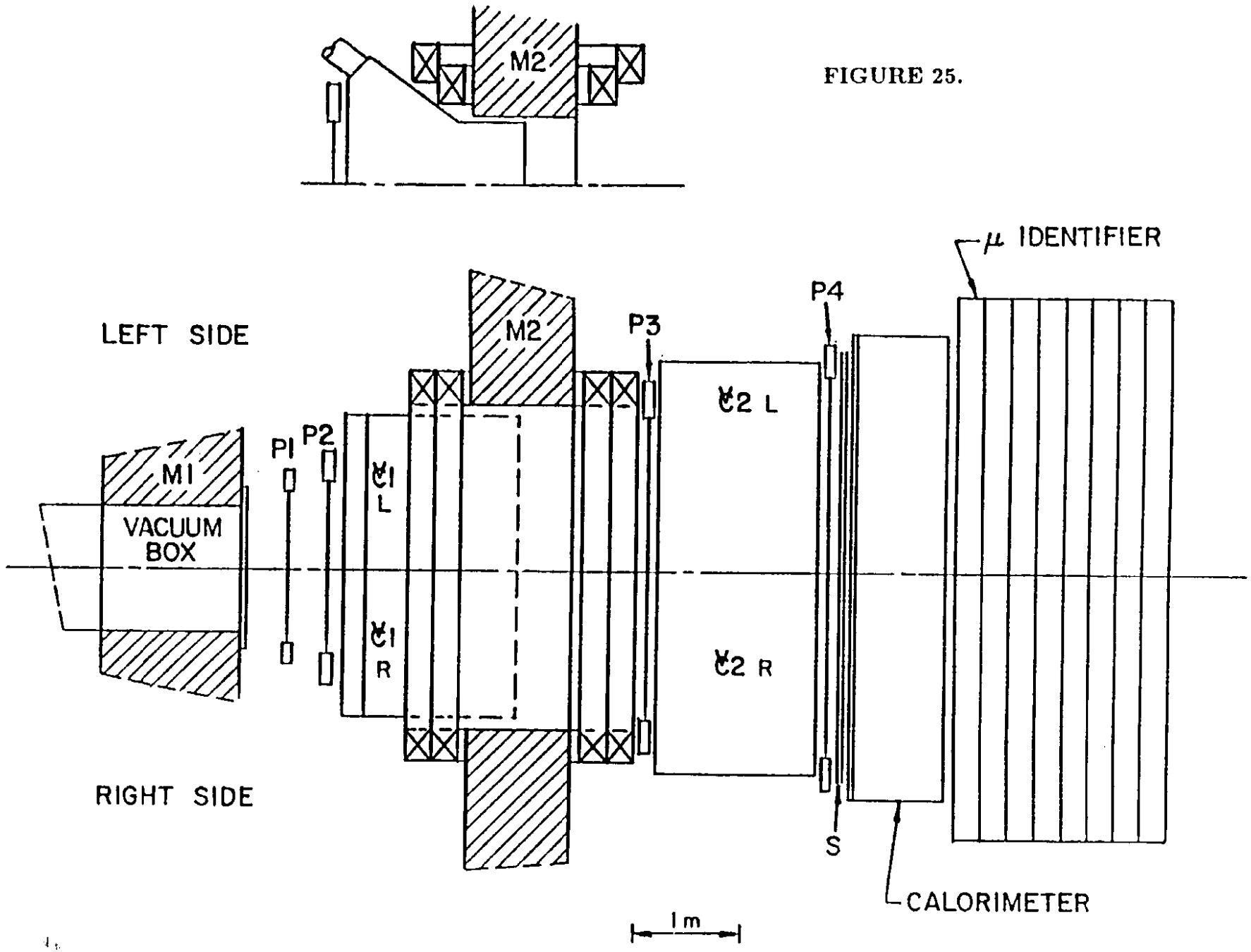
M2
LEFT SIDE
M2
P3
P4
μ IDENTIFIER
C2 L
M1
VACUUM
BOX
P1
P2
C1
L
C1
R
C2 R
RIGHT SIDE
S
CALORIMETER
1 m

FIGURE 25.

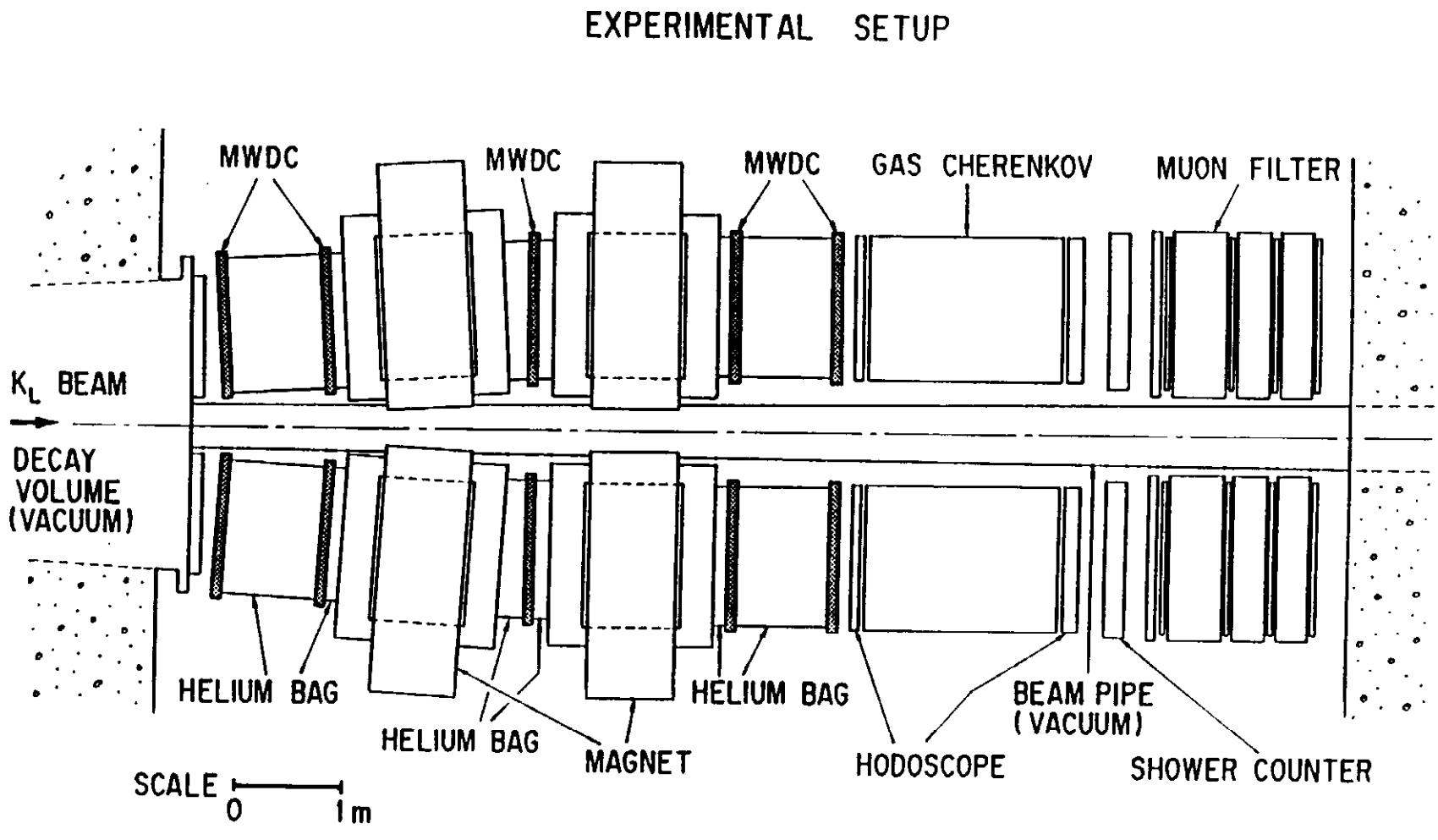
EXPERIMENTAL SETUP
MWDC
MWDC
MWDC
GAS CHERENKOV
MUON FILTER
K_L BEAM
DECAY VOLUME (VACUUM)
HELIUM BAG
HELIUM BAG
MAGNET
HELIUM BAG
BEAM PIPE (VACUUM)
HODOSCOPE
SHOWER COUNTER
SCALE 0 1 m

FIGURE 26.

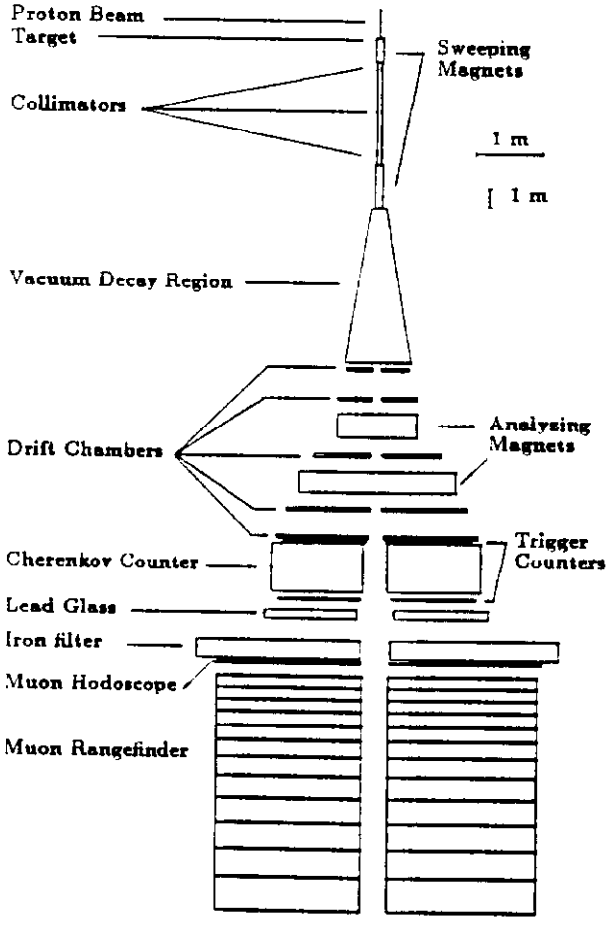
Proton Beam
Target
Collimators
Sweeping Magnets
1 m
1 m
Vacuum Decay Region
Drift Chambers
Analysing Magnets
Cherenkov Counter
Trigger Counters
Lead Glass
Iron filter
Muon Hodoscope
Muon Rangefinder

FIGURE 27.

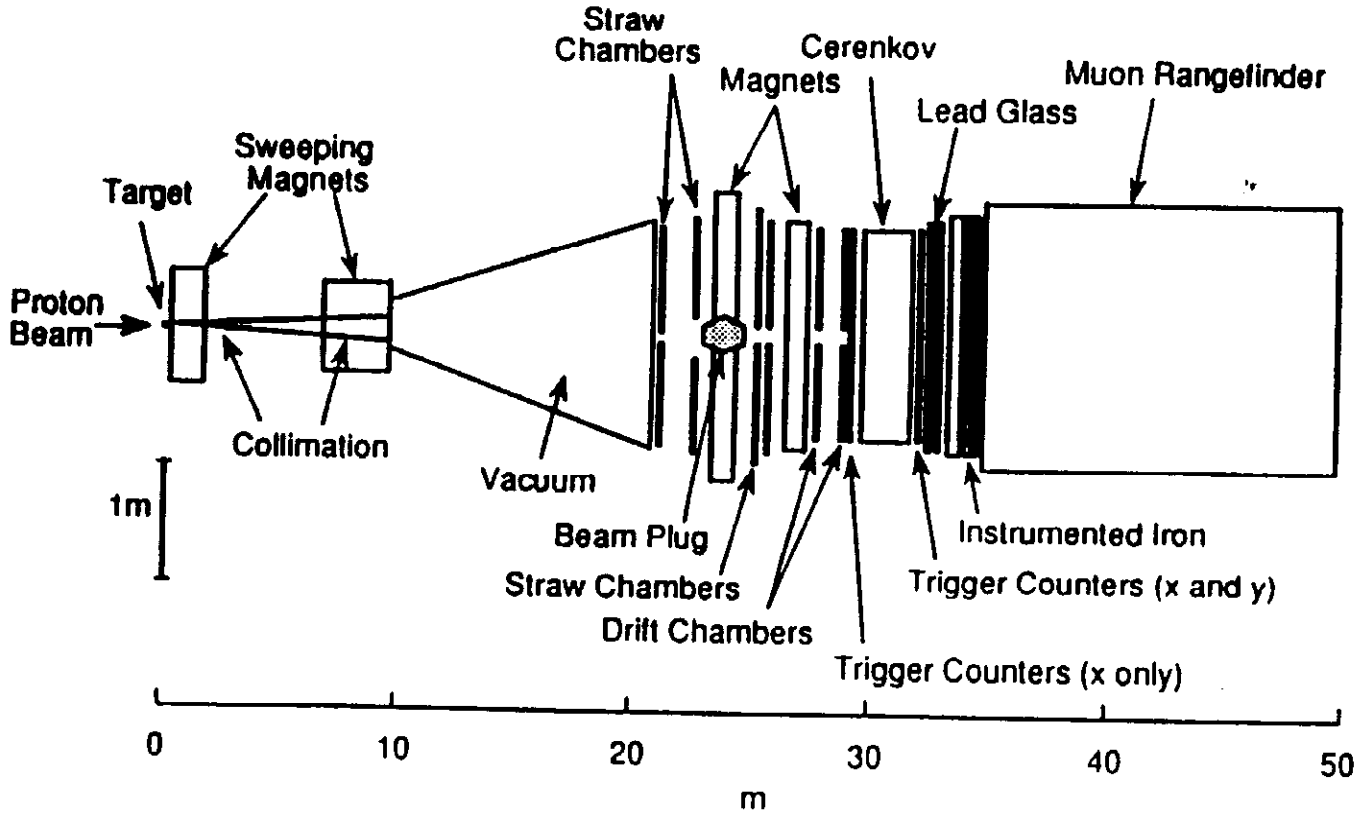
Straw
Chambers
Cerenkov
Magnets
Muon Rangefinder
Lead Glass
Sweeping
Magnets
Target
Proton
Beam
Collimation
Vacuum
1m
Beam Plug
Straw Chambers
Drift Chambers
Trigger Counters (x only)
Instrumented Iron
Trigger Counters (x and y)
0
10
20
30
40
50
m

FIGURE 28.

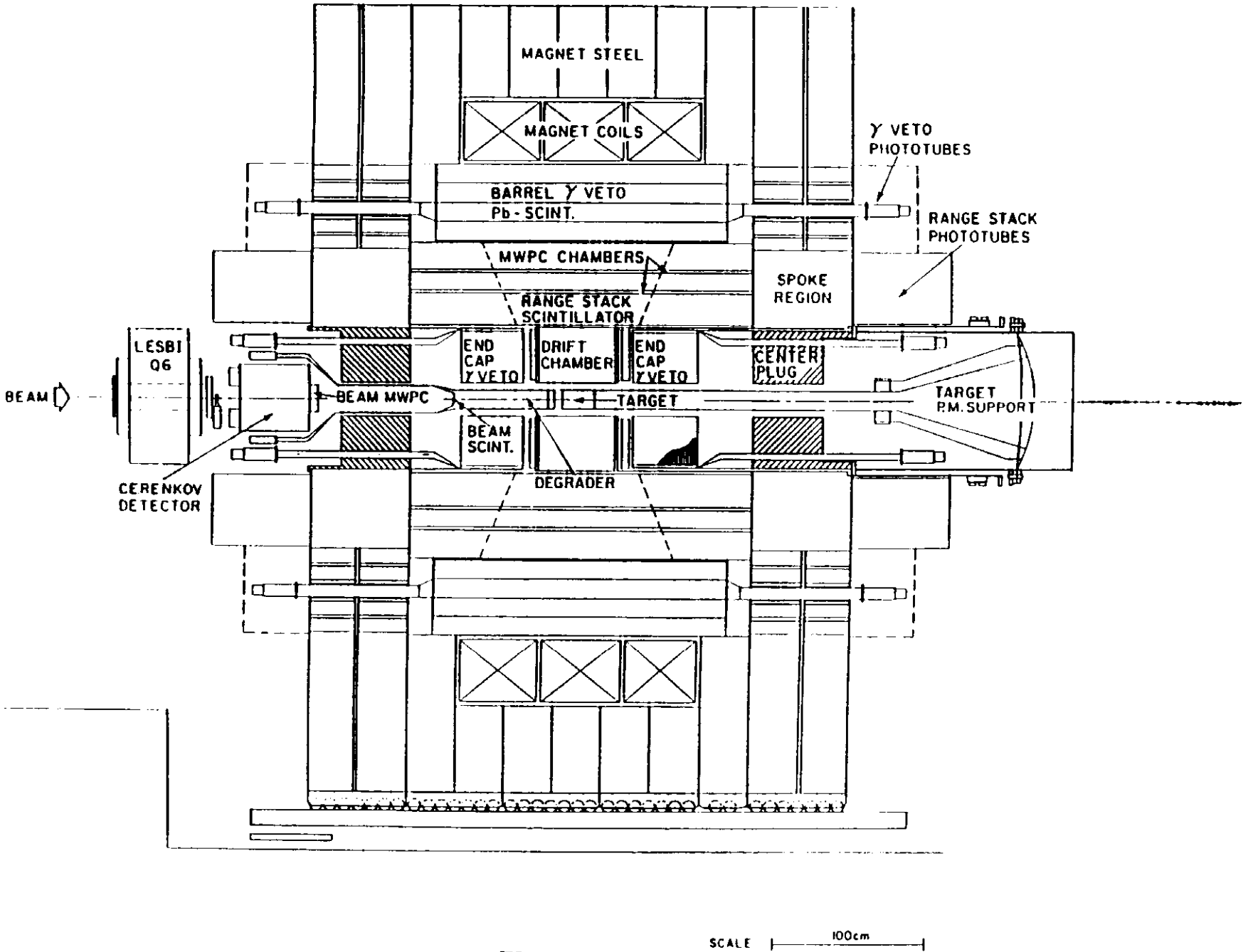
MAGNET STEEL
MAGNET COILS
γ VETO PHOTOTUBES
BARREL γ VETO Pb - SCINT.
RANGE STACK PHOTOTUBES
MWPC CHAMBERS
SPOKE REGION
RANGE STACK SCINTILLATOR
LESBI Q6
END CAP γ VETO
DRIFT CHAMBER
END CAP γ VETO
CENTER PLUG
BEAM
BEAM MWPC
TARGET
TARGET P.M. SUPPORT
BEAM SCINT.
CERENKOV DETECTOR
DEGRADER
SCALE
100cm

FIGURE 29.